

STRUCTURAL INSIGHTS INTO ION SELECTIVITY AND CALCIUM
BLOCKAGE OF CYCLIC NUCLEOTIDE-GATED CHANNELS

APPROVED BY ADVISORY COMMITTEE

Youxing Jiang, PhD

Ege Kavalali, PhD

Johann Deisenhofer, PhD

Philip J. Thomas, PhD

To my family, Asegedech Kassie, Yonatan, Hana and Natnael Getahun, for all your patience and support.

STRUCTURAL INSIGHT INTO THE ION SELECTIVITY AND CALCIUM
BLOCKAGE IN CYCLIC NUCLEOTIDE-GATED CHANNELS

by

MEHABAW GETAHUN DEREBE

DISSERTATION

Presented to the Faculty of the Graduate School of Biomedical Sciences

The University of Texas Southwestern Medical Center at Dallas

In Partial Fulfillment of the Requirements

For the degree of

DOCTOR OF PHILOSOPHY

The University of Texas Southwestern Medical Center at Dallas

Dallas, Texas

January, 2010

Copyright

by

MEHABAW GETAHUN DEREBE

All Rights Reserved

Acknowledgements

I am grateful to UT Southwestern Graduate School for giving me the opportunity to study my doctoral degree. Despite the ups and downs of a scientific endeavor, my stay here at UT Southwestern has been uniquely enriching. I would like to take this opportunity to thank many people who contributed to make my stay here a possibility. The list of people whom I want to thank both inside and outside of UT Southwestern is very long to ever fully document. So, to everyone who has helped me along this journey, I am enormously grateful and if I forgot to mention by name it is only for space reasons.

The first person I would like to acknowledge is my mentor Youxing Jiang. Your captivating presentation during my first year inspired me about ion channels that led me to be your first rotation student and eventually join your lab. Thank you for giving me the opportunity to study in your lab and making the lab atmosphere relatively friendly. I am grateful for letting me work with a group of people most of whom are not only talented but also respectable human beings. Above all, thank you for helping me sail through the ups and downs of my study in the last five years. Without a doubt, the last five years in the lab have been the most extraordinary of my life in so many ways. Certainly, the mentor plays the grandest role in determining a student's success from instilling an inquisitive way of thinking to helping maneuver through the training process.

I am also grateful for a number of people in the lab. Thank you Ning Shi for teaching me much of what I know during my rotation and my work with you in the prokaryotic sodium channel project. Even-though the project has yet to bear fruit and claimed two years of my graduate school time without any useful result, through it I learned many of the lab's experimental repertoires. Thank you is also for Jun Liao with whom I had many insightful discussions. You are a resourceful person and I am very grateful for several thoughts we shared together. I am grateful to Liping Chen who has been very helpful in many ways throughout my stay. The smooth functioning of the lab depended on you and you have delivered; thank you for being so thoughtful and dependable. Thanks also goes to David Sauer for many insightful discussions. Thank you David for being very understanding, helpful and having such a positive personality. The other lab person I would like to acknowledge is WeiZhong Zeng for help in electrophysiological experiments. Every other member of the lab contributed to or affected my graduate career in one or another way. So, I would like to acknowledge the following people for helping me or not and making my stay in the lab the way it was: Yunkun Wu, Yang Li, Sheng Ye, Changkeun Lee, Yi Yang, Chunguang Kong, Michael Dorwart, Amer Alam.

My gratitude outside the Jiang lab goes to my dissertation committee members- Johann Deisenhofer, Ege Kavalali, Mischa Machius and Philip Thomas. Thank you all for guiding me through this long process and for being so

patient with me all along. My thanks also goes to Biophysics Program Chair Kevin Gardner for helping through these years, especially for role in my two year training grant.

Last, but certainly not least, I would like to acknowledge my dearest family- Asegedech Kassie, Yonatan, Hana and Natnael Getahun- for all your love, support and patience over the past six long years. Graduate school has always been my goal after college but I had no idea it could be so demanding. Thank you for sticking for so long and weathering the ups and downs with me. Your support and encouragement was the major factor in this accomplishment. Yoni, Hana and Nati- I am especially grateful for your patience through all the inconveniences. Above anything, I hope my accomplishment has taught you that patience and perseverance are important virtues to achieve anything in life. I love you all more than anything.

STRUCTURAL INSIGHT INTO THE ION SELECTIVITY AND CALCIUM
BLOCKAGE IN CYCLIC NUCLEOTIDE-GATED CHANNELS

MEHABAW GETAHUN DEREBE, Ph.D.

The University of Texas Southwestern Medical Center at Dallas, 2010

YOUXING JIANG, Ph.D.

Cyclic nucleotides-gated (CNG) channels play an essential role in the visual and olfactory sensory systems and are ubiquitously expressed in a variety of neuronal and non neuronal cells. Details of their underlying ion selectivity properties are still not fully understood and a matter of debate in the absence of high resolution structures. Presented in this study are high resolution (1.58-1.95Å)

crystal structures and functional analyses of engineered mimics of CNG channels by duplicating their selectivity filter sequences in the background of the bacterial non-selective NaK channel. Mimics share several striking functional similarities in ion selectivity with eukaryotic CNG channels: they are non-selective and permeate Na^+ and K^+ equally well; externally added Ca^{2+} serves as a permeating blocker, with the conserved acidic residue in the filter mediating Ca^{2+} binding. Structures reveal a hitherto unseen selectivity filter architecture that suggests that CNG channel selectivity filters likely comprise three contiguous ion binding sites. The high resolution structures also allow for a thorough characterization of monovalent and divalent ion permeation which, in combination with electrophysiological recordings, offers structural insight into CNG channel function at an unprecedented level of detail.

Table of Contents

Dedication	ii
Acknowledgements	v
Abstract	viii
Table of contents	x
List of prior publications	xiii
List of figures	xiv
List of tables	xviii
List of abbreviations	xix
Chapter 1: Introduction	1
Chapter 2: Literature review	5
Introduction.....	5
Ion channels.....	9
Ion selectivity.....	18
Potassium channels and the structural basis of ion selectivity.....	26
NaK channel and non-selectivity.....	38
Cyclic Nucleotide-Gated (CNG) channels.....	44
<i>Calcium permeation and block in CNG channels</i>	53
<i>CNG channelopathies</i>	56

	xi
Chapter 3: Methodology	57
Generation of NaK mutants that mimic CNG channel pores.....	61
Protein expression and purification.....	63
Crystallization and soaking experiments.....	64
Data collection and structure determination.....	65
Functional Studies.....	66
<i>Liposome preparation</i>	67
<i>Protein reconstitution</i>	69
<i>Radioactive tracer uptake assay</i>	71
<i>Electrophysiological analyses</i>	74
Chapter 4: Results	79
Ion selectivity studies of CNG-mimicking NaK mutants...	79
<i>Functional analyses- CNG mimicking NaK mutants are non-selective</i>	82
<i>Structural determination of CNG-mimicking NaK mutants</i>	90
<i>Monovalent cation binding in the selectivity filter</i>	100

Divalent cation binding/blockage in CNG-mimicking NaK mutants.....	104
<i>Functional Analyses</i>	105
<i>Structural basis of divalent cation blockage in CNG-mimicking NaK mutants</i>	111
Viability of CNG-mimicking NaK mutants.....	116
Chapter 5: Discussion	122
Chapter 6: Future directions	133
References	142

Prior Publications

F. Capitelli, **M. Derebe**, Single crystal X-ray diffraction study of a pure natrolite sample, *J. Chem. Crystallography*, Springer, 2007, 37(8), 583-586.

M. G. Derebe, N. Retta, A.G.G. Moliterni, F. Capitelli, Synthesis and crystal structure of diaquabis(diketohydrindene-diketohydrindamine)manganese(II), *Zeitschrift für Kristallographie*, 2003, Volume 218, Issue 01, p. 062.

M. G. Derebe, V. J. T. Raju and N. Retta, Synthesis and Characterization of some metal complexes of a Schiff base derived from ninhydrin and alanine. *Bull. Chem. Soc. Ethiop.* 2002, 16(1), 53-64.

List of Figures

Figure 2.1	Ion transport proteins.....	8
Figure 2.2	A hypothetical cartoon of ion channels showing the closed and open states.....	10
Figure 2.3	The neuron and propagation of the nerve impulse.....	10
Figure 2.4	Predicted topology of main channel forming subunits of common pore loop ion channels.....	16
Figure 2.5	Mullins cylindrical pore theory.....	22
Figure 2.6	An oversimplified representation of Bezanilla and Armstrong's view of selectivity in K^+ pores.....	24
Figure 2.7	Topology of tetrameric K^+ channels with six or two transmembrane segments- monomer and tetramer.....	28
Figure 2.8	Different views of the KcsA potassium channel structure.....	30
Figure 2.9	High resolution structure of the KcsA potassium channel showing coordination of K^+ ions in the selectivity filter.....	33

Figure 2.10	Structure of the KcsA K^+ channel selectivity filter in high and low K^+ concentration.....	35
Figure 2.11	The snug-fit model of ion selectivity.....	35
Figure 2.12	Structure of the NaK channel in comparison to that of KcsA.....	40
Figure 2.13	K^+ and Na^+ coordination in the NaK channel.....	42
Figure 2.14	Simplified cartoon comparing mode of action of CNG channels in photo and olfactory transduction.....	46
Figure 2.15	Topology of CNG channels.....	50
Figure 3.1	Partial sequence alignment between NaK, K^+ channels and CNG channels from different organisms.....	60
Figure 3.2	Depiction of the radioactive tracer uptake and its slightly modified competition assays.....	72
Figure 3.3	Liposome preparation and generation of the giant liposome single channel patch clamping.....	76
Figure 4.1	Single channel traces and I-V curves of NaK-ETPP, NaK-DTPP and NaK-NTPP.....	84
Figure 4.2	$^{86}Rb^+$ flux into NaK-DTPS, NaK-ETPP and control proteoliposomes.....	89

Figure 4.3	Comparison of structures of NaK mutants using NaK-DTPP as an example with those of wild type NaKΔ19 and KcsA.....	93
Figure 4.4	Superimposition of the selectivity filter of NaK-DTPP with those of KcsA and wild type NaK.....	94
Figure 4.5	Ordered water molecules and funnel shaped external entryway in selectivity filter of NaK-DTPP.....	95
Figure 4.6	Protein packing around the selectivity filters of CNG-mimicking mutants.....	98
Figure 4.7	Protein packing around residue 66 in the selectivity filters of CNG-mimicking mutants.....	99
Figure 4.8	K⁺ and Na⁺ binding in the selectivity filter of NaK mutants.....	101
Figure 4.9	Structural alignment of NaK-ETPP and NaK-DTPP.....	103
Figure 4.10	Ca²⁺ competition in NaK mutants.....	107
Figure 4.11	Ca²⁺ blockage and permeation in NaK mutants.....	109
Figure 4.12	Ca²⁺ current in NaK-ETPP.....	110
Figure 4.13	Divalent cation binding in the selectivity filter of NaK mutants.....	113

Figure 4.14	Divalent cation binding in the extracellular entryway.....	115
Figure 4.15	Structure based mutagenesis of bovine CNGA1 channel- Properties of E363T/T357E swap mutation.....	118
Figure 4.16	Structure based mutagenesis of NaK-ETPP (I)- Properties of NaK-ETPP(T60E/E66T).....	119
Figure 4.17	Structure based mutagenesis of NaK-ETPP (II)- Properties of NaK-ETPP(T60V).....	120
Figure 5.1	Coordination of K^+ and Na^+ in the NaK mutants.....	125
Figure 5.2	Summary of mono- and divalent cation binding in the selectivity filters of NaK mutants.....	127
Figure 6.1	Structure of the selectivity filter of NaK-ETPT.....	136
Figure 6.2	Selectivity filter structure of NaK-QTPP and its alignment with that of NaK-ETPP.....	139

List of Tables

Table I	Ionic radii (Pauling) and standard enthalpies of hydration at 25⁰C for some group I, II cations, the proton and chloride ions.....	20
Table II	Standardized nomenclature of cyclic nucleotide-gated ion channels.....	48
Table III	Ion permeability ratio of different CNG channels.....	52
Table IV	Data collection and refinement statistics for NaK-DTPP, NaK-NTPP and NaK-ETPP in K⁺ and K⁺/Na⁺.....	92

List of Abbreviations

AC	Adenylate cyclase
ADP	Adenosine 5'-DiPhosphate
ATP	Adenosine 5'-TriPhosphate
BK	Big conductance K⁺ channel
Ca_v	Voltage-gated Ca²⁺ channels
CFTR	Cystic Fibrosis Transmembrane Conductance regulator
cAMP	Cyclic Adenosine 5'-MonoPhosphate
cGMP	Cyclic Guanosine 5'-MonoPhosphate
CNG	<u>C</u>yclic <u>N</u>ucleotide-<u>G</u>ated channels
DM	n-decyl-β-D-maltopyranoside
Fab	Fragment, antigen binding
GTP	Guanosine 5'-TriPhosphate
HEPES	4-(2-hydroxyethyl)-1-piperazineethanesulfonic acid
ΔH°	Standard enthalpy change
IPTG	Isopropyl-β-D-thiogalactopyranoside
Kcal	Kilo-calories
KcsA	Potassium channel from <i>Streptomyces lividans</i>
K_i	Inhibition constant

Kir	Inward rectifier potassium channels
KirBac	Bacterial inward rectifier potassium channels
K_v	Voltage-gated K⁺ channels
KvAP	Potassium channel from <i>Aeropyrum pernix</i>
Kv1.2	Mammalian <i>Shaker</i> family potassium channel
LMV	Large, multi-lamellar vesicle
MPD	(±)-2-Methyl-2,4-pentandiol
MthK	Potassium channel from <i>Methanobacterium thermoautotrophicum</i>
NaK	Na⁺, K⁺ conducting channel from <i>Bacillus cereus</i>
Na_v	Voltage-gated Na⁺ channels
NMG	N-Methyl-D-Glucamine
OSN	<u>O</u>lfactory <u>S</u>ensory <u>N</u>eurons
POPE	1-palmitoyl-2-oleoyl-phosphatidylethanolamine
POPG	1-palmitoyl-2-oleoyl-phosphatidylglycerol
RM	Rod Monochromacy
SUV	Small, uni-lamellar vesicles
TM	Transmembrane
TPeA	Tetrapentyl ammonium
TRP	<u>T</u>ransient <u>R</u>eceptor <u>P</u>otential channels

CHAPTER ONE

Introduction

Ion channels are a diverse group of membrane proteins upon which life depends. They exist to provide a hydrophilic medium within the hydrophobic cellular enclosure (the lipid bilayer) to help ions traverse from one aqueous media to another, the cytoplasm of a cell to the extracellular medium or vice versa. They are characterized by two properties: selective permeation of one or a group of ions and a method of gating.

Ion channels exhibit selective ion transport, the extent of which vary widely and is generally correlated with their biological function. Some ion channels can discriminate between similar ions while others can discriminate cations over anions but not as well among cations. An example of the former are the voltage-gated K^+ channels that exhibit high selectivity for K^+ and cyclic nucleotide-gated (CNG) channels are good examples of the later group because almost all common cations can permeate these channels but not anions.

Ion channels are regulated pores and as such have a mechanism by which they are opened or closed in response to a stimulus-- a process called gating. Common stimuli include changes in membrane potential, temperature and membrane tension or binding of a ligand. Among channels that transport the same or similar ion(s), the gating mechanism usually underlies their variation. The

focus of this work is however related to mechanism of ion selectivity and permeation.

Deeper mechanistic understanding of channel function generally requires high resolution structural information. For instance, a detailed understanding of K^+ channel biology is made possible by the recent wave of high resolution structures of many K^+ channels. However, structures are not available for other ion channels, including CNG channels. The present study focuses on getting such structural information for CNG channels, especially as it relates to their ion selectivity and permeation properties.

CNG channels are a physiologically essential class of proteins whose functional significance in higher animals, especially in photo and olfactory signal transduction, is generally well understood. They belong to the tetrameric cation channel family that includes the voltage-gated K^+ , Na^+ , Ca^{2+} channels. However, despite having a voltage sensor domain similar to the other members, CNG channels are gated by binding of a cyclic nucleotide to their c-terminal ligand binding domain. In addition, unlike the other members, which exhibit highly selective permeation of their respective ions, CNG channels are permeable to group IA and some group IIA cations. A detailed molecular picture, especially as it relates to their ion permeation and selectivity properties, has been lacking due to absence of high resolution structural information. The present study is thus aimed

to provide structural insights into the ion selectivity and permeation properties of CNG channels.

To achieve the above stated goal many approaches can be envisioned. Ideally, one would like to crystallize and determine the structure of the eukaryotic CNG channel. However, this is technically difficult and may require several years of work. Instead, the present work centered on modifying a bacterial non-selective cation channel, NaK, to contain selectivity filters identical in sequence to those found in majority of CNG channels. These mutants are amenable to high resolution structure determination. The studies described in this dissertation will focus on functional characterization of NaK mutants that mimic the selectivity filters of most CNG channels and detailed structural analysis of their selectivity filters. The methodology of mutant design, functional and structural analyses is described in Chapter Three. Chapter Four presents the structural and functional data. The first part of Chapter Four describes monovalent cation selectivity studies of mutants using electrophysiological and radioactive $^{86}\text{Rb}^+$ tracer uptake methods, structural analysis of the selectivity filters of the mutants and their monovalent cation binding properties. In the second part, the divalent cation binding/blockage studies are presented. Ca^{2+} permeation and subsequent blockage of monovalent current has special significance to the function of CNG channels. This property is investigated in CNG-mimicking NaK mutants. Specifically, single channel electrophysiological and radioactive $^{86}\text{Rb}^+$ tracer uptake results are

provided for the NaK mutants. Also, a detailed structural analysis of Ca^{2+} and Ba^{2+} binding in the selectivity filters of the NaK mutants is presented. The last part of Chapter Four examines the viability of the NaK mutants as a structural model for CNG channel pores by employing structure based mutagenesis study. Based on the structure of a NaK mutant, mutations were designed on a eukaryotic CNG channel and the NaK mutant to investigate the role of key residues. Chapter Five summarizes the key findings of the study and discusses their significance in relation to the stated goal. The last chapter deals with potentially useful studies that can be pursued in light of findings of the present work.

CHAPTER TWO

Literature Review

INTRODUCTION

The plasma membrane is a physical enclosure that demarcates the boundary of cells separating the internal milieu from the external environment. Its main building blocks, the lipids, are generally amphipathic with a typically long lipophilic (or hydrophobic) group and a hydrophilic head group, which self associate spontaneously into a two-dimensional fluid bilayer as a result of interactions with the hydrophilic water molecules of the surrounding aqueous medium thereby effectively creating a physical boundary. This means that polar, charged or bulky groups, which are necessary for the survival of the cell, cannot freely cross the non-polar bilayer into the cytoplasm or vice versa, creating a need for transport mechanisms for these entities. As a result, the plasma membrane contains, in addition to the lipids that make up the main components, transport proteins and other molecules that modify its property. Membrane transport proteins are critical components of the plasma membrane because they mediate the transport of ions, solutes or other molecules into and out of the cell, thereby providing food and nutrients and export waste, all necessary for the survival of the individual cell and ultimately the animal or plant (Alberts, 2002).

Transport proteins can be classified into two groups- ion channels and transporters (Figure 2-1). Ion channels are passive devices that selectively transport ions down their electrochemical gradient. Their functions underlie some of the fundamental cellular processes, like the nerve impulse, the beating of the heart, hearing and sensation. These channels have gates that open or close in response to an external stimulus. When the gate is opened ions pass through these proteins at rates close to the diffusion limit, in the order of several thousand ions per millisecond. Ion channels exhibit specificity as to the type of ion(s) they let through. Some are highly selective while others are less so. Their ion selectivity and gating properties underlie the physiological function of these proteins.

Transporters on the other hand are responsible for transporting numerous solutes and ions and accordingly there is significantly greater diversity among these proteins. They form strong complexes with their substrates in a highly specific fashion and as a result require several milliseconds to transport their substrate(s). Transporters can be subdivided into two groups, depending on their energy requirement, as passive and active (Figure 2-1) (Siegel, 1999). Passive transporters, also called facilitators or uncoupled transporters, provide highly selective pathways for their substrates, such as D-glucose, but are not coupled to energy sources and, therefore, cannot concentrate their substrates. Active transporters on the other hand are coupled to energy sources that can alter the steady-state distribution of their substrate(s). One type of active transporters,

called primary transporters, couple a chemical reaction to protein conformational transitions, which supply energy to generate concentration gradients of one or more substrates across cell membranes. Secondary transporters derive energy from existing ion gradients to transport a second ion or solute in a direction that is either the same as (symport) or opposite to (antiport) that of the energizing ion.

Ion channels and transporters are complimentary in their function. Transporters generate and maintain ionic concentration gradients across the plasma membrane. This concentration gradient is then exploited by ion channels to generate electrical signals and other cellular functions.

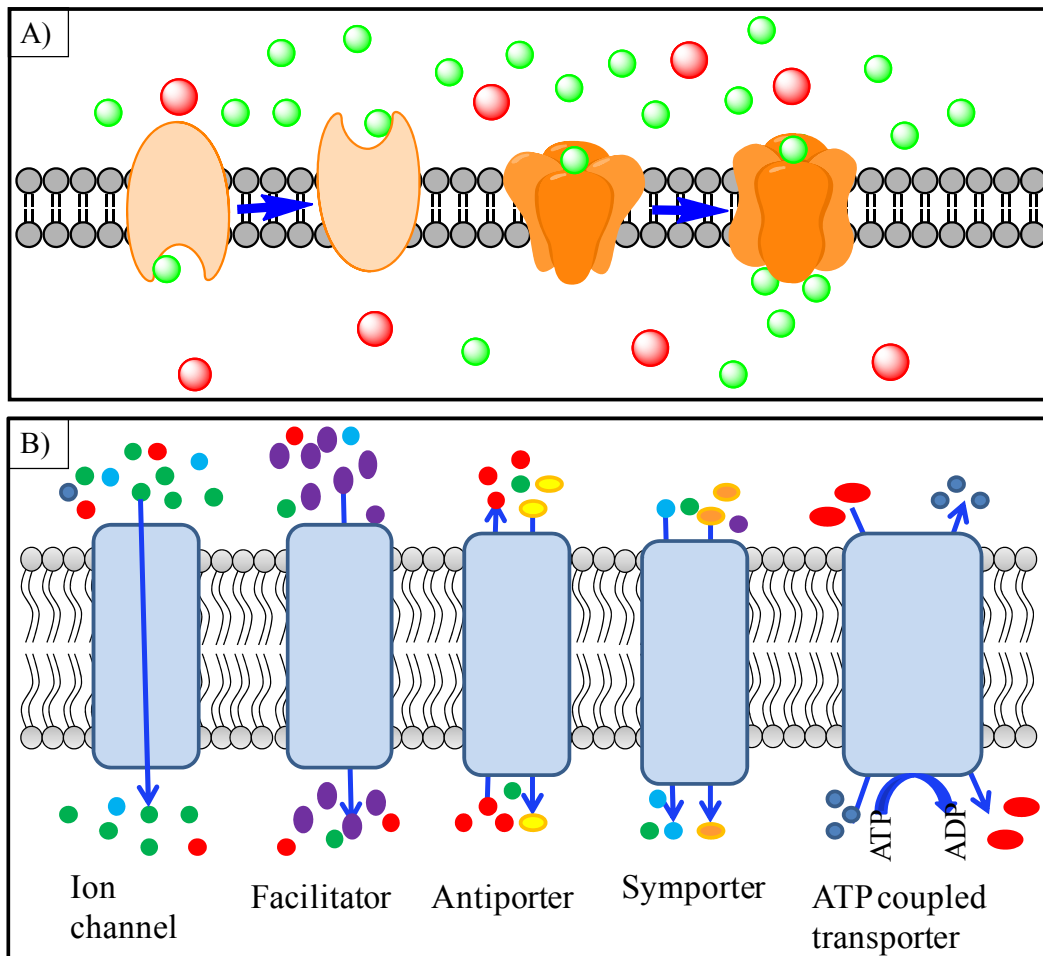


Figure 2-1 - Ion transport proteins. Panel (A) shows a comparison between a transporter, in which the ion binds at a site and a conformational change transports the ion across the plasma membrane, and an ion channel where the ions simply diffuse through the pore when the gate is opened following their concentration gradient. The green spheres represent the ions being transported. Panel (B) shows a cartoon of the varieties of transport proteins. Colored circles and ellipses represent ions or solute molecules transported and arrows show the direction of flow.

ION CHANNELS

Many vital biological processes, like the beating of the heart, neuronal information flow, muscular movement, taste, hearing, learning and memory require the flow of ions across the plasma membrane. However, ions are charged/polar particles, which exist as hydrated complexes in aqueous solution or in cells and cannot cross the hydrophobic lipid membrane unassisted. Ion transport proteins, channels among them, fulfill this requirement.

Ion channels are a diverse group of proteins that form aqueous pathways or pores in the plasma membrane. Embedded in the membrane they control the flow of ions into and out of the cell, each ion moving down their own concentration gradient. These proteins are intrinsically passive devices that allow the free down-hill transport of ions when opened without any energy requirement (Figure 2-2). Opening and closing happens in response to stimuli like a change in membrane potential, membrane tension or temperature, or binding of a ligand.

Over the years these group of proteins have been shown to be indispensable to life in higher organisms. For instance, the generation and propagation of the action potential in the nervous system, a crucial biological process, is highly dependent on the proper functioning of ion channels. In more detail, the action potential (or the nerve impulse) is an alteration of the membrane potential of an excitable membrane that propagates rapidly along the membrane

of an excitable cell making rapid signaling and communication possible (Figure 2-3) (Alberts, 2002; Hille, 2001). A related critical function of ion channels occurs in the heart. The heart harbors many different types of ion channels, each with a specific function in pace-making. The heart beats properly when these channels function normally and coordinated with each other.

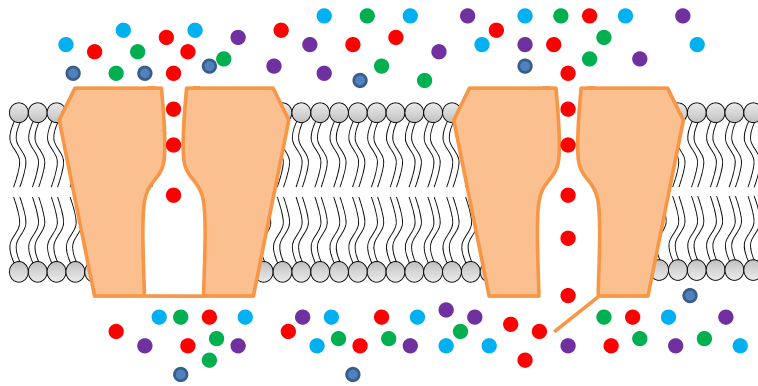


Figure 2-2 – A hypothetical cartoon of ion channels showing the closed and open states. When the gate is closed no ions can cross through the channel pore (left). As soon as the gate opens (right) ions of certain type diffuse through the channel.

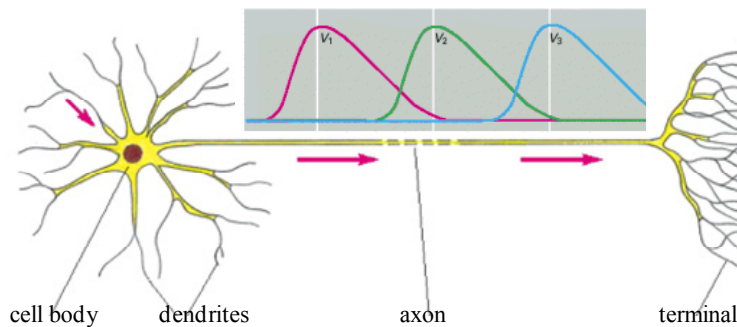


Figure 2-3 – The neuron and propagation of the nerve impulse. A typical mammalian nerve cell and its parts are shown. The nerve impulse flows from the cell body to the nerve terminals, where it is relayed to the receiving cell. Direction of flow is as shown in pink arrows and the associated membrane potential is depicted with the three hypothetical curves as measured at three different points across the axon (modified from Alberts, et al, 2002).

The most notable early work on ion channels is the exquisite description of the generation and propagation of the action potential in the squid giant axon by Hodgkin and Huxley (Hodgkin and Huxley, 1952a, b, c; Hodgkin et al., 1952), for which they were awarded the 1963 Nobel Prize in Physiology or Medicine. They described the changes in the permeability of the membrane for Na^+ and K^+ when the membrane potential is changed. They concluded that there were three components of the membrane current - Na^+ , K^+ , and leak currents and suggested the presence of 'unknown structures' that allow the ions to pass through. These 'unknown structures' of Hodgkin and Huxley later came to be known as Na^+ and K^+ channels. Without specific knowledge of ion channels they were able to correctly describe the basis of membrane excitation as the result of changes in ion permeability of the membrane. Subsequent work by Bertil Hille and Clay Armstrong established most of the concepts behind ion channels that included ions passing through aqueous pores called channels that are proteins, distinction between Na^+ and K^+ channels (including their selectivity), the basic principles of gating or opening and closing of their pores, channel blockers as molecules that physically block the pores, etc (Armstrong, 1971; Hille, 1970, 1973). Most of these concepts were subsequently proven by exquisite electrophysiological experiments using new methods developed by Sakmann and Neher (Hamill et al., 1981; Neher et al., 1978). Since then, many ion channel or ion-coupled transporter proteins have been identified, characterized, cloned and some crystallized and

their high-resolution structures determined. Of unique significance to ion channel studies was the crystal structure of the bacterial KcsA K⁺ channel of MacKinnon (Doyle et al., 1998) that supported some of the earlier thoughts about channel function and structure.

Ion channels have been conserved throughout evolution. Advances in molecular cloning and genome sequencing projects have provided information as about the abundance of ion channels in all kingdoms of life. In the human genome alone there are several hundreds of genes thought to encode for ion channels (Ashcroft, 2006). These ion channels underlie diverse yet critical functions upon which human life depends. They generate the electrical signals necessary for relaying information or performing a task, regulate cell volume, help identify dark from light or distinguish between colors, help smell and hear, and are directly involved in cell proliferation, learning and memory and other cellular processes. Ion channels of lower organisms have also been shown to perform vital functions. However, an important contrast arises with microbial ion channels. In support of the evolutionary ancestry of these proteins, many ion channels have been identified from the microbial genome by sequence homology to eukaryotic ion channels (Kung and Blount, 2004). However, their biological function remains largely unknown. Most of these microbial channels appear to be hypothetical proteins with no known function. Since they have been maintained through evolutionary selection it is reasonable to assume that they serve vital functions for

microbes. Some have been implicated in metabolic control or in responses to sudden environmental changes. Nevertheless, recent advances in the understanding of ion channel molecular mechanisms have been possible due to structural insights from microbial channels, primarily because they are easier to over-express, crystallize and structurally characterize compared to their eukaryotic counterparts. In fact, most ion channel structures determined are microbial ion channels.

As described, ion channels are involved in virtually every physiological process in humans and are found in all forms of life making them one of the most diverse groups of proteins. However, naming of channels has not been systematized until recently and scientists previously gave their own names or acronyms as each was identified. As a result several names for the same channel were not uncommon in the old literature. A systematic nomenclature was subsequently agreed upon, and nowadays, ion channel classification follows guidelines as outlined by the International Union of Pharmacology (IUPHAR). Their classification generally involves the ion they transport and/or their gating mechanism. For instance, channels could be called voltage-gated, ligand-gated or transmitter-gated based on their gating mechanism. Voltage-gated channels, for example, can further be sub-divided as K^+ , Na^+ or Ca^{2+} channels depending on the ion they transport. Each of these families has many members with multiple paralogs and splicing variants. And yet for some channels naming simply follows

the number of pores they have, as in two pore channels, or the duration of response to stimuli, as in transient receptor (TRP) channels.

Ion channels are regulated pores, that is they open or close in response to a stimulus, a process called gating. The stimulus could be a change in membrane potential, membrane tension, temperature or binding of a ligand. The mechanism of sensing the stimulus and relaying that into opening or closing the channel differs among these proteins and in some cases is a heavily debated subject, especially in the case of voltage-gated channels. However, in general terms, stimuli are detected by specific gating domains or module, parts of the protein directly responsible for sensing and responding to the signal. This module then translates that signal into a conformational change that opens or closes the pore of the channel. In voltage-gated potassium (Kv), sodium (Nav) and calcium (Cav) channels, a change in membrane potential is detected by the voltage sensor domain, which then moves to gate the channels. In others, like the cyclic nucleotide-gated (CNG) channel, glutamate receptors, GABA (γ -aminobutyric acid) receptors, a ligand physically binds to the respective ligand-binding domain to open or close the channel. Mechanosensitive channels respond to changes in membrane stretch forces and yet other channels are sensitive to changes in temperature. Most channels have a gate that when closed serves as a physical barrier to ion flow, though it occurs through a number of different mechanisms. Some ion channels have a 'movable' ball-like structure with a small linker

polypeptide segment that swings back and forth to plug the channel depending on the stimulus. In others, the inner transmembrane helices lining the pore have hinges that allow the ion conduction pathway to dilate, restricting or allowing ions to flow. In some channels the selectivity filter itself serves as the gate. In this mechanism a conformational change by some residues in the selectivity filter gates the channel.

Ion channels are also characterized by exhibiting selectivity, the property of selectively passing one ion or a group of ions while discriminating others. This property is central to their function and hence their names- potassium, sodium, calcium, chloride, etc- channels. The extent of discrimination varies from one to another. Some channels, like the voltage-gated K^+ channels, exhibit a very high degree of selectivity while others, like the cyclic nucleotide-gated channels, permit several similar ions at a similar rate. This property will further be elaborated in subsequent sections.

Structurally, ion channels are generally composed of one or more pore-forming principal subunits, often in association with auxiliary subunits that modulate channel activity. The number of transmembrane segments varies among different types of channels. For instance, some channels have two transmembrane segments, like the inward rectifier Kir and the bacterial KcsA potassium channels, while voltage-gated potassium channels comprise six transmembrane segments (Figure 2-4). Nevertheless, most channels conform to a common structural theme

in which a central pore, through which the ions move, is formed by four or five transmembrane spanning α -helices. Most of these channels have pore loops, short polypeptide segments that fall back into the membrane to form the selectivity filter that determines the ion permeation properties of the channel (Figure 2-4).

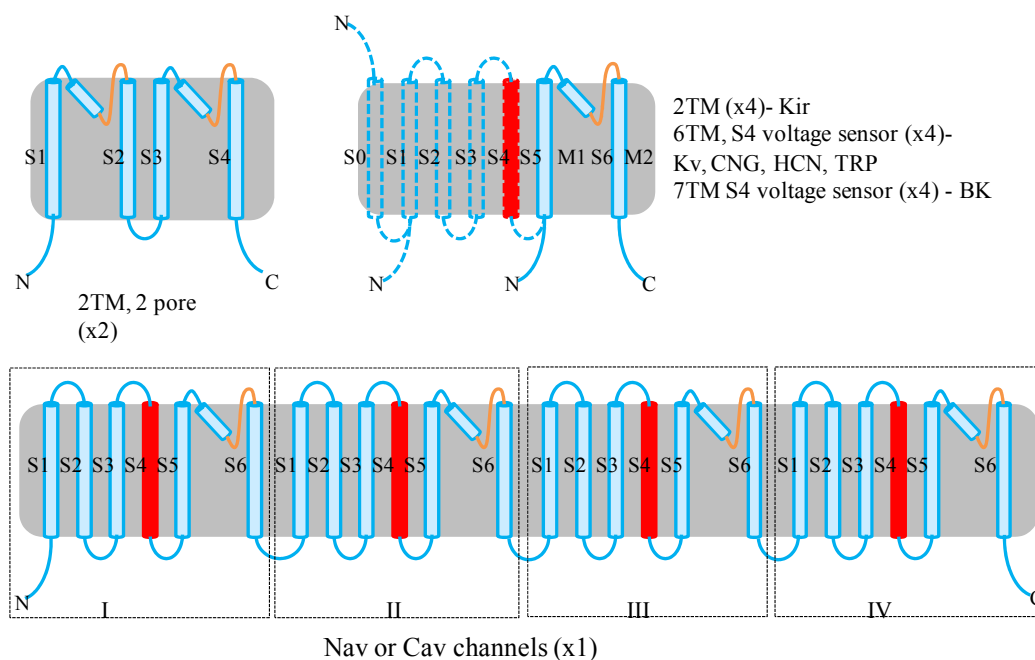


Figure 2-4 – Predicted topology of main channel forming subunits of common pore loop ion channels, auxiliary subunits not shown. Cylinders (labeled S0-S6 or M1, M2) represent transmembrane (TM) segments and numbers in parentheses indicate the number of subunits that form the functional channel. In these channels the ion conduction pathway is created by a re-entrant loop between the last two transmembrane segments (shown in orange). Among these pore-loop channels are the S4 family of ion channels which have a stretch of positively charged residues in their S4 transmembrane segment, shown in red. In most of these the S4 segment is responsible for gating by change in membrane voltage. Abbreviations:- Kir, inwardly rectifying K^+ channel; K_v , Na_v , Ca_v , voltage-gated K^+ Na^+ and Ca^+ channels, respectively; CNG, cyclic-nucleotide-gated channel; BK, big conductance K^+ channel; HCN, hyperpolarization-activated channel; TRP, transient receptor potential channel.

The necessity and ubiquity of ion channels suggests that defects in their molecular structure and/or function will have profound physiological effects. As a result there are many disorders related to channel malfunction. When the cause of the disorder is mutation(s) in the gene encoding for the ion channel or an auxiliary subunit, channel malfunctions are called channelopathies. A plethora of human channelopathies have been identified (Ashcroft, 2006; Camerino et al., 2008). With the exception of cystic fibrosis, a recessive disease that results from mutations on the CFTR (cystic fibrosis transmembrane conductance regulator) gene, inherited channelopathies are rare. The physiological effects of channelopathies can vary from asymptomatic to fatal.

ION SELECTIVITY

A unique feature of ion channels is that they have the ability to selectively pass one ion or a group of ions while excluding all others, a property termed 'ion selectivity'. It is a relative phenomenon that relates the comparative permeability of ions to the channel and thus cannot be exact since there are physico-chemically closely related ions. This is to say that even though ion channels usually have certain preferences for the type or identity of ion(s) they transport, they also allow ions of similar type, the extent of which varies among these proteins. Some channels exhibit a very precise selectivity, such as the voltage-gated K^+ or Na^+ channels, while others are distinctly non-selective, as in the case of cyclic nucleotide-gated (CNG) channels or transient receptor potential (TRP) channels. The former group can discriminate among closest competitor ions in a thousand fold or more ratios, while the later discriminate cations over anions but very poorly among those cations. It is important to note that wide variations in ion selectivities exist even in channels of the same group. The extent of selectivity exhibited by an ion channel frequently underlies its cellular function. The molecular mechanism of such exquisite ion selectivity by these proteins has been a subject of intense study in the last few decades and a discussion is warranted; however first, an analysis of properties of ions as it relates to their natural environment, aqueous media, is imperative.

Ions are charged particles, individual charged atoms or molecules, and as such in aqueous solution they are surrounded by a cluster of water molecules, that is they exist as hydrated complexes due to the ion-dipole interaction forces between the charged ion and ends of dipolar water molecules. Different ions may be hydrated to a different extent. Moreover, cations and anions are hydrated in different fashion, since cations interact with the negative (oxygen) end of the water dipole while anions interact with the positive (hydrogen) end of the dipole. Irrespective of its extent or nature, hydration occurs when dipoles from water molecules orient themselves around the ion forming a layer of water molecules, the hydration shell. Several layers of this shell can be envisioned; however the system is very dynamic, continuously being reorganized due to water molecules pinching off while new water molecules associate on a nanosecond time scale because of competition between the hydration shell and hydrogen bonding within bulk water itself (Hille, 2001). This process of hydration of ions is an electrostatic stabilization process that results in a release of energy, the enthalpy of hydration ($\Delta H^{\circ}_{\text{hydration}}$), the amount of which varies widely depending on the radius and formal charge of the ion (Table I). The amount of this stabilization energy is one of the major factors that affect the selective transport of ions through channel proteins.

Given their inherent charge, ions are naturally unable to partition into a low dielectric environment where no complementary charge is present.

Physiologically this has the consequence of making the hydrophobic core of the lipid membrane a barrier to ion diffusion. The biological solution to this problem is the ion channel. Ion channels exist to provide a hydrophilic medium (the pore) within the hydrophobic cellular enclosure (the lipid bilayer) to help ions traverse from one aqueous media to another, the cytoplasm of a cell to the extracellular medium or vice versa, so that the cells can perform their function.

Table I. Ionic radii (Pauling) and standard enthalpies of hydration at 25⁰C for some group I, II cations, the proton and chloride ions (Hille, 2001).

Ion	H⁺	Li⁺	Na⁺	K⁺	Rb⁺	Cs⁺	Ca²⁺	Ba²⁺	Cl⁻
Radius (Å)	-	0.60	0.95	1.33	1.48	1.69	0.99	1.35	1.81
ΔH⁰_{hydration} (kCal/mol)	-269	-131	-105	-85	-79	-71	-476	-362	-82

While free diffusion through the membrane is extremely slow, ions permeate through their respective channels at a rate near the diffusion limit, on the order of several thousand ions per millisecond. Now, the question becomes how and why these hydrated ions, presumably at their energy minima, pass through the channel protein. Do the ions pass through the protein with their hydration shell intact? If so, how is such a rate attainable, and are the pores large enough to accommodate such large species? Or, does the hydration shell have to be stripped off and if so, to what extent and what compensates for the associated loss of the

hydration energy? How do these proteins manage to conduct their ions at such tremendous rates while exhibiting exquisite selectivity? Many theories have been proposed to explain these phenomena.

One of the earliest theories put forward well before the identification of any ion channels was the 'pore theory', which views biological membranes having tubes with water-liking walls through which hydrated ions can diffuse. Mullins, after careful experiments on the relative rates of 'influx' of different types of ions into the frog muscle and squid axon (Mullins, 1959a, b) proposed the cylindrical pore theory, in which he suggested that ions cross the membrane through narrow cylindrical aqueous pores of specific size and that the ions have to be dehydrated, at least partially (Figure 2-5). He said that for membranes to exhibit such selectivity, the ions should move only through pores that fit the specific ions and that the pores serve to replace the hydration, at least partially, that the ion would assume in aqueous solution (Figure 2-5). As such, he realized the necessity of dehydration of permeant ions and that the loss of hydration energy is the predominant energy barrier for this process. Still a broadly valid concept, Mullins cylindrical pore theory forms the basis of some of the early permeation theories, though some aspects of it were soon challenged.

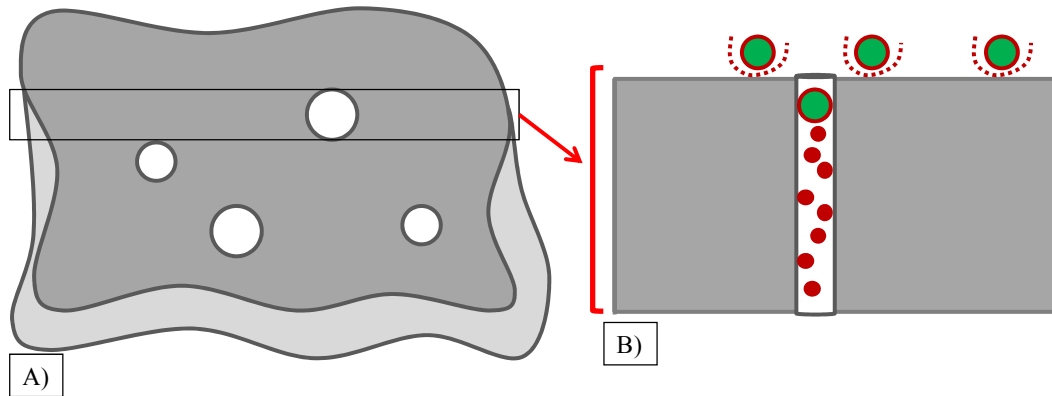


Figure 2-5 – Mullins cylindrical pore theory (Mullins, 1959a). In (A) is representation (top view) of the membrane with different pore sizes for different ions and (B) shows a side view of the membrane around an ion pore (K^+ pore for instance). The ions (green dots) are depicted as passing through the pore of the membrane together with water molecules (small dots) and a layer of their hydration shell (red ring around green ion) while those outside the pore may have additional hydration layers (broken red half rings).

Another early theory of ion selectivity is that of Eisenman's field strength or equilibrium ion selectivity model (Eisenman, 1962; Hille, 2001). Eisenman's work focused on understanding the atomic mechanism of operation of ion specific glass electrodes. His premise was that the electrostatic energy difference associated with the ion exchange, that is partitioning of ions from an aqueous solution to the glass medium, varies for different ions. The sites in the glass were modeled as simple spherical anions in vacuum without any solvent. Depending on the dipole strength, or the electrostatic field strength as he refers to it, of the ion exchange site in the glass he suggested that many ion selectivity sequences of alkali metal ions can be perceived. By simply varying the field strength (dipole strength) of the ion binding site he was able to reproduce experimentally observed

selectivity sequences for different types of glass electrodes. He also suggested that these selectivity sequences can be invoked for biological membranes, with eleven sequences to be of practical importance for selectivity among group I cations (Eisenman, 1962; Hille, 2001). Even though spherical anion models of coordinating ligands in biological membranes may not be accurate, the idea that selectivity resulted from the energy difference between ions of their hydration and site-interaction energies is still important.

An alternative mechanism of ion selectivity called the snug-fit model was put forward by Bezanilla and Armstrong (Armstrong, 2007; Bezanilla and Armstrong, 1972). This model emphasizes structural rigidity of ion channels and the necessity of almost complete dehydration of ions in the pore, in contrast to Mullin's partial dehydration. By analyzing the effect of other ions in the K^+ conduction of the squid axon they suggested that the K^+ pores have a wide ($\sim 8 \text{ \AA}$ diameter) but less selective mouth that can allow passage of Na^+ , Cs^+ , Li^+ and TEA^+ (tetraethyl ammonium ion). The remainder of the pore, the tunnel, was postulated to be much narrower ($2.6 - 3 \text{ \AA}$ in diameter) allowing the passage of only K^+ and Rb^+ ions. The case of Na^+ was puzzling because the K^+ pores allow the larger K^+ ion (1.33 \AA) to pass while discriminating against the smaller ion Na^+ (0.95 \AA). Their explanation was that Na^+ is small enough that it cannot enter the tunnel because it cannot properly fit into the rigid 'coordination cages' provided by the pore as replacements for the water molecules surrounding an ion. In other

words, they viewed K^+ channels as pores or cages with oxygens fixed in position to provide a good fit for a K^+ ion but not others. The distance from Na^+ ion, for instance, to two of the oxygens of the cage is greater than would be the case for Na^+ ion in water, and therefore the coulombic energy of a Na^+ ion in the cage/pore is much higher than in water (Figure 2-6). Because of this relatively high energetic cost, Na^+ ions are unlikely to enter the cage. This model provides useful insight because it introduces structural perspective to ion selectivity. However, in retrospect the assumption that the pores are rigid structural elements may not hold true since we now know that proteins, and hence, ion channels are dynamic and the small (0.38 Å) difference in ionic radius between K^+ and Na^+ may very well be within thermal fluctuation ranges of the coordinating oxygen ligands.

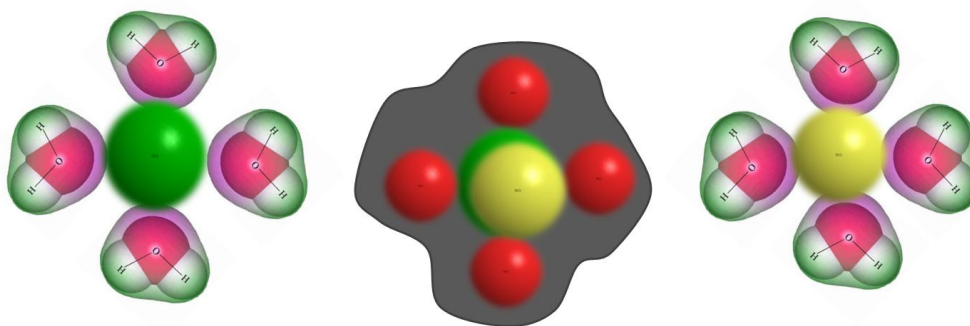


Figure 2-6 – A simplified representation of Bezanilla and Armstrong's view of selectivity in K^+ pores (Bezanilla and Armstrong, 1972). K^+ ions (green spheres) and Na^+ ions (yellow spheres) are shown coordinated with oxygens of water molecules, (left) & (right) respectively, as they exist in solution. In the tunnel of K^+ pores (middle), a Na^+ ion is too small to make stabilizing contacts with the oxygen atoms (red spheres) of a proposed coordination cage, while K^+ has the proper size. Note: The color representation of the water molecules is to show the polarity.

Like for any physicochemical process, free energy optimization is the driving force for ion selectivity. However, proteins are intrinsically dynamic, and thus, the molecular mechanism by which ion channels exhibit exquisite selectivity while maintaining very high rates of conduction is likely more complicated than proposed by any of the above early models. As Bertil Hille summarizes (Hille, 1973), selectivity may arise as a result of geometric, chemical and energetic factors. In essence, early models capture parts of the important contributions that result in ion selectivity but the most accurate description may involve aspects of each.

POTASSIUM CHANNELS AND THE STRUCTURAL BASIS OF ION SELECTIVITY

Potassium channels are probably the most ubiquitous of ion channels. They are found in the most primitive life forms, the unicellular bacterium, to the most sophisticated cellular processes, the nervous system, of the most advanced life forms. As one of the most well studied ion channel families, these channels also act as models for our understanding of the general channel properties. From Hodgkin and Huxley's description of the action potential to the recent X-ray crystal structures, potassium channels played important roles in understanding channel function. Physiologically, they play key roles in a plethora of cellular processes necessary for survival, most notably in nerve and heart function, but also important roles in a number of other basic processes.

The great diversity in their cellular function arises mainly from the mechanism by which these proteins are gated. Their ion permeation properties, however, are largely similar; a manifestation of a common pore domain while there is significant variability in the attached regulatory domains. These channels conduct K^+ ions near diffusion limit while exhibiting more than thousand-fold selectivity over its closest competitor Na^+ with only 0.38\AA difference in their Pauling ionic radii ($K^+ = 1.33\text{\AA}$, $Na^+ = 0.95\text{\AA}$). The molecular basis of this exquisite potassium selectivity has been a subject of intense study. In an elegant

mutational analysis, MacKinnon's group identified a stretch of eight residues (TXXTXGYG) in a region called the selectivity filter that is highly conserved among K^+ channels, responsible for this high K^+ selectivity (Heginbotham et al., 1994). By making point mutations to this sequence within the voltage-gated *Shaker* K^+ channel, which they refer to as the 'signature sequence', and assessing their effect on selectivity they discovered the TTVGYG sequence as the key determinant for K^+ selectivity. Earlier, the same group had found that deletion of two C-terminal residues (YG) from the signature sequence of the *Shaker* K^+ channel rendered the channel non-selective (Heginbotham et al., 1992), similar to cyclic nucleotide-gated channels, asserting that the selectivity difference exhibited among ion channels of the same family arises due to variations of their selectivity filter sequences.

Potassium channels belong to the so called pore-loop tetrameric cation channel superfamily, characterized by a small polypeptide segment of the channel-forming monomeric subunits fall back into the plasma membrane, with an overall four-fold symmetry, forming the ion conduction pathway (Figures 2-4 and 2-7). This pore-loop architecture has long been shown to be a common structural feature of many ion channels in addition to the tetrameric cation channel superfamily (Figure 2-4). The selectivity filter harboring the signature sequence is found in this pore region (Figure 7A). This (pore) region has been shown, by using toxin blockers and through mutagenesis experiments (Mackinnon

and Yellen, 1990; Yellen et al., 1991) to be between the fifth and sixth transmembrane segments of the *Shaker* K⁺ channel. In addition, sequence conservation implicated that all K⁺ channels, both eukaryotic and prokaryotic, share the same selectivity filter structure, a hypothesis later supported by insight gained from high resolution crystal structures.

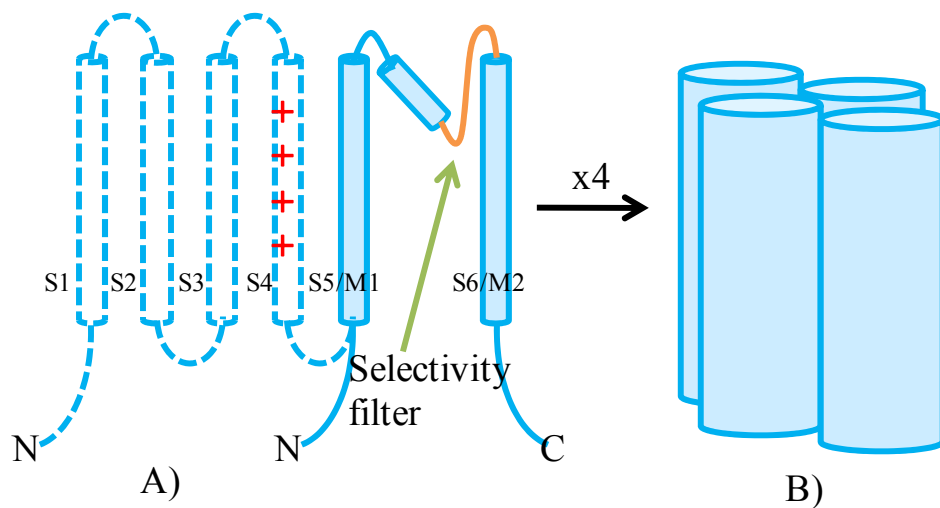


Figure 2-7 – Topology of tetrameric K⁺ channels with six or two transmembrane segments:- monomer (A) and tetramer (B). In (A) transmembrane segments labeled S1-S6 (M1 & M2 in two-transmembrane-segment-only channels) are shown as cylinders, the pore helix is shown as a small cylinder in between the last two transmembrane segments, and the selectivity filter shown in orange. The positively charged residues found in the S4 transmembrane segment of voltage-gated K⁺ channels are depicted as red '+'s. B) is a schematic representation of the tetrameric functional unit.

Prior to 1998, there were converging ideas on the structural views of the selectivity filter but a detailed atomic picture was lacking due mainly to absence of structural information. A huge leap in ion channel studies came when the

MacKinnon group published the X-ray crystal structure of the K^+ channel from the microbe *Streptomyces lividans*, KcsA (Doyle et al., 1998), (Figure 2-8). For his work, Roderick MacKinnon was eventually awarded the 2003 Nobel Prize in Chemistry. This work validated many concepts developed previously, and it provided additional fundamental insights (Figure 2-8). First, it showed the tetrameric nature of the channel with a four-fold symmetry about a central pore (Figure 2-8 A&B). Each subunit in KcsA is made up of two transmembrane segments, the M1-outer and M2-inner helices, with a re-entrant loop between the segments. Four M2 helices forming in a channel tetramer form an inverted teepee, (Figure 2-8C). The re-entrant loop harbors the selectivity filter, the narrowest point in the pore, which was previously shown to determine selectivity. Moreover, there was a large aqueous cavity right beneath the selectivity filter proposed to serve as a rehydration site for K^+ ions exiting the selectivity filter thereby stabilizing the ions in transit. It was also observed that there are negatively charged residues at both intracellular and extracellular entryways and the pore helices are oriented in such a way that, together with the negatively charged residues, generates a cation attractive potential necessary for ions to be dragged inside the pore (Doyle et al., 1998). These observations were invoked in explaining the fundamental question of how a hydrated positively charged ion crosses the lipid bilayer barrier with rates close to the diffusion limit. The selectivity filter was shown to be constructed from a broken-helix part of the pore

loop, where the main chain atoms lining the ion conduction pathway create a highly polar environment (Figure 2-8C). In addition, although the precise orientation of the carbonyl oxygens couldn't be discerned due to resolution limitations, it was proposed that these closely spaced main chain carbonyl groups directed towards the ion conduction pathway account for K^+ ion coordination as it traverses through channel. Na^+ , a smaller ion, couldn't properly fit in the coordination sites, hence the K^+ selectivity, similar to the snug-fit model of selectivity of Armstrong and Bezanilla.

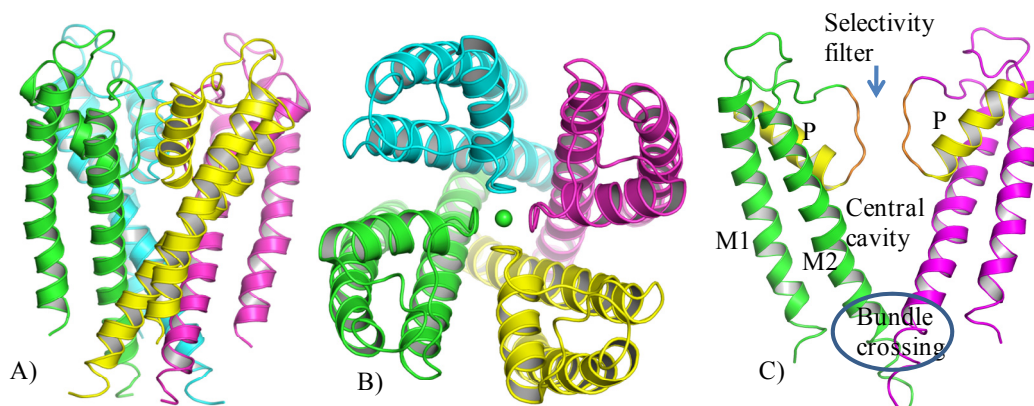


Figure 2-8 – Different views of the KcsA potassium channel structure (PDB ID-1bl8). A) and B) show the side and top views of the tetrameric channel, respectively, each subunit represented with a different color. The ion conduction pathway is clearly visible from B) with the green dot representing the K^+ ions. C) shows two opposite subunits, with the outer (M1) and inner (M2) helices labeled as such. Front and back subunits were removed for clarity. Pore helices (labeled P) are colored yellow while the selectivity filter is shown in orange. The central cavity and bundle crossing are also shown.

A clearer picture of the KcsA selectivity filter came with the high-resolution structure in which the KcsA protein was complexed with an Fab fragment of a monoclonal antibody (Zhou et al., 2001) raised against the tetrameric channel. In the structure, the Fab fragments were attached to the extracellular turret of the channel. The Fab fragment apparently helped in getting a higher resolution structure, presumably due to increased polar contacts of the complex, which improves crystal quality. The high resolution structure clearly showed that carbonyl groups of the signature sequence residues orient themselves toward the ion conduction pathway forming four equivalent K^+ binding sites (Figure 2-9) that mimic the hydration shell of a K^+ ion in aqueous solution. Their orientation and organization are such that K^+ ions can pass through only after complete dehydration. The carbonyl groups thus provide a water-like coordination environment for K^+ ions in transit (Figure 2-9). Each K^+ ion is coordinated by eight carbonyl groups in square-antiprism coordination (Figure 2-9C, D), similar to the first hydration shell of K^+ ions in water. After passing through the selectivity filter, K^+ ions are rehydrated in the central aqueous cavity. These features of the potassium channel, acting in concert, account for the exhibited high K^+ selectivity and permeation rates.

A series of high resolution X-ray structures of other K^+ channels soon followed and showed that they share the same selectivity filter organization as the one described above supporting the idea that most K^+ channels generally have

similar selectivity filters. The structure of another bacterial K^+ channel, MthK, (Jiang et al., 2002) provided the open pore conformation of K^+ channels, in contrast to the closed KcsA structure (Figures 2-8, 2-9). The mechanics of gating is still not well understood, but these two structures provided a perspective of the open and closed conformations in potassium channels. The key insight from comparing the two structures is the relatively unchanged selectivity filter despite the dramatic movement in the inner helices. In addition to KcsA and MthK structures, this is also shown in structures of other K^+ channels- the inward rectifier bacterial K^+ channel KirBac (Kuo et al., 2003), the voltage-gated bacterial K^+ channel KvAP (Jiang et al., 2003) and the eukaryotic voltage-gated Shaker family K^+ channel Kv1.2 (Long et al., 2005). In all of these structures the selectivity filter structure is generally the same and their variety mainly arises from their gating mechanism.

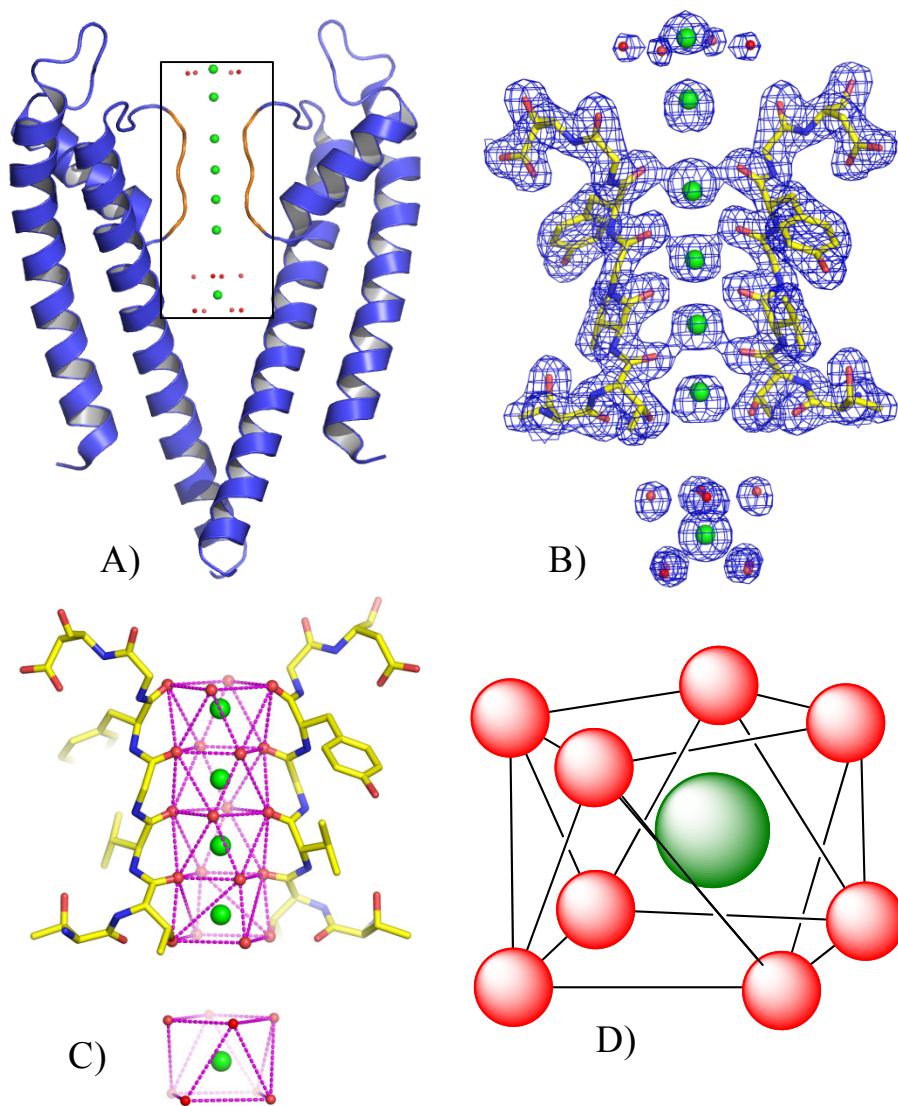


Figure 2-9 – High resolution structure of the KcsA potassium channel showing coordination of K⁺ ions in the selectivity filter. A) shows two subunits of KcsA (PDB ID 1K4C), the selectivity filter (in box), with coordinating water molecules (red spheres) in the extracellular entryway and the central cavity; B) detailed structure and 2Fo-Fc electron density map, contoured at 2 σ , of the selectivity filter; C) is representation of K⁺ coordination by main chain carbonyl groups and D) a geometrical representation of the K⁺ coordination in C).

These structures provided deeper insights into the selectivity filter of the channels at atomic level adding a structural dimension to mechanistic discussions. However, the molecular mechanism of ion selectivity is still a heavily debated subject. Along with the high resolution structure of KcsA-Fab was a comparison of selectivity filter structures in high and low concentrations of K^+ . At high concentrations of K^+ ($\geq 20\text{mM}$) the KcsA selectivity filter contains the four K^+ binding sites (Figure 2-9, 2-10A), coined the ‘conducting’ conformation. In crystallization solutions containing Na^+ and low K^+ ($\sim 3\text{mM}$) the selectivity filter structure changed significantly losing the middle two of the four K^+ binding sites resulting in what the authors called ‘non-conducting’ or ‘collapsed’ conformation (Figure 2-10B) (Zhou et al., 2001). The structural model of selectivity emerged from these structural analyses, emphasizing geometric precision and structural rigidity. Briefly, it argued that the narrow pore is optimized so that K^+ can fit snugly without facing energetic penalty while the smaller Na^+ would face bigger energetic cost because it cannot fit snugly. This structural view of selectivity is similar to Armstrong and Bezanilla’s geometrical snug-fit model (Figure 2-11).

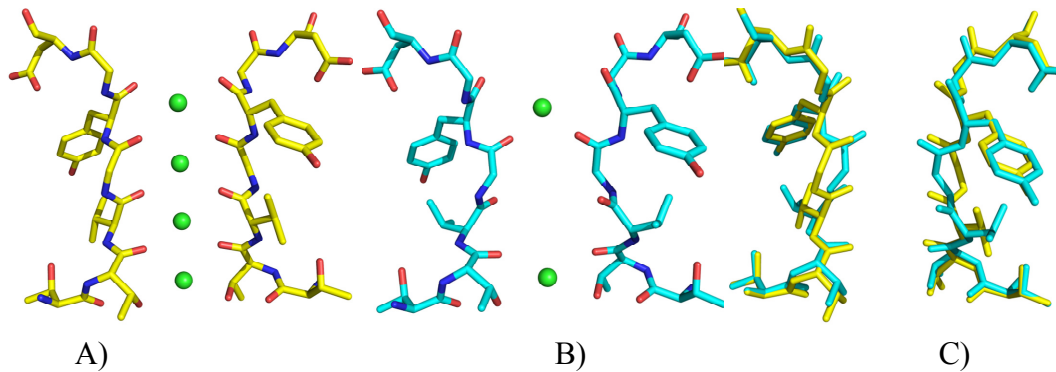


Figure 2-10 – Structure of the KcsA K^+ channel selectivity filter in high (A, PDB ID 1K4C) and low (B, PDB ID 1K4D) K^+ concentration and (C) is a structural alignment of the two. Front and back subunits are removed for clarity. In (A) K^+ ions (green spheres) occupy all four ion binding sites keeping the selectivity filter intact. However, the low- K^+ structure (B) shows considerable structural rearrangement and only two K^+ ions inside the selectivity filter. Red spheres represent water molecules, dashes show distances between interacting atoms.

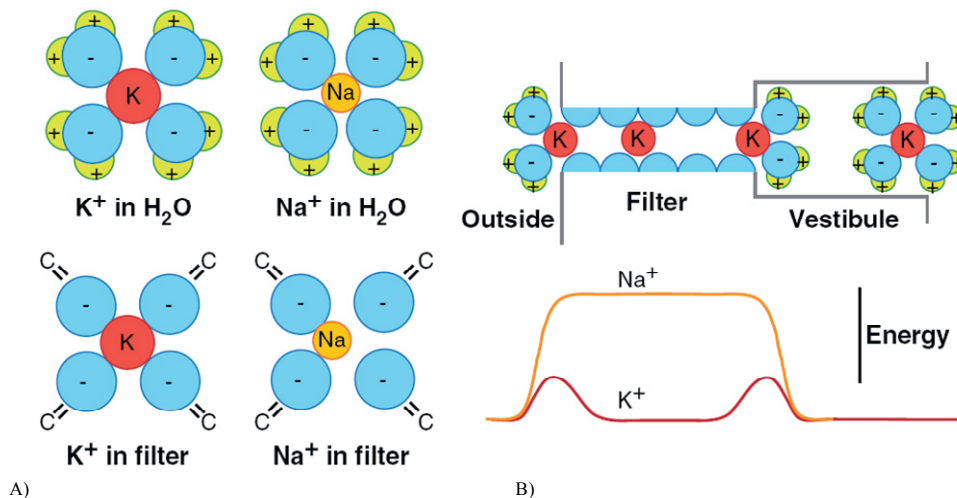


Figure 2-11 – The snug-fit model of selectivity (adapted from Armstrong, 2007). The bigger K^+ ions (orange spheres) fit snugly in the coordination environment made by the carbonyl ligands in the selectivity filter of the potassium channel as it would be hydrated in an aqueous solution (A). Na^+ ions (yellow spheres) on the other hand being small cannot fit snugly in the carbonyl coordination environment as it would in an aqueous environment. Ions must be completely dehydrated to pass through channel losing their stabilizing hydration energies. Compensatory energies during ion conduction through the channel are thus favorable for K^+ but not for Na^+ ions (B), resulting in selectivity.

A major counter argument to the geometrical model invokes the intrinsic dynamics of proteins. Based on molecular dynamics simulations on KcsA Beniot Roux argues that root-mean-square fluctuations of the atoms lining the selectivity filter are in the order of 0.75 to 1Å, in agreement with the B-factors of those atoms in KcsA (Noskov et al., 2004; Noskov and Roux, 2006). This thermal fluctuation is significantly greater than the difference in ionic radii of K⁺ and Na⁺ ions (~0.38Å), arguing that the selectivity filter is flexible enough to accommodate sodium without undergoing drastic rearrangement, thus suggesting that selectivity may not result purely from geometrical constraints. He proposed that selectivity may arise locally, “from the intrinsic physical properties of the ligands coordinating the ions passing through the channel”, more importantly the attractive and repulsive forces between ions and/or coordinating ligands. Asserting the fluid-like nature of the coordinating carbonyl ligands through molecular dynamics calculations, Roux proposes that selectivity arises from properly oriented freely fluctuating dipoles of correct strength (Noskov et al., 2004).

The above ‘fluctuating dipole’ model starts with several assumptions. First, it leaves out any geometrical contributions/constraints from the protein. It is not clear how the coordinating ligands are held in place without such contribution. Second, it emphasizes the unique suitability of carbonyl moieties as ligands for K⁺ complexation. Taking these and other factors into consideration Bostick and

Brooks provided an alternative mechanism emphasizing the coordination chemistry as determining ion selectivity (Bostick and Brooks, 2007). Based on their molecular dynamics simulations, they propose that, provided coordination number constraints, water molecules can provide selective environments as carbonyl groups can. As a result, they argue that selectivity arises because the ions have optimal coordination environments; eight for K^+ , six for Na^+ and four for Li^+ . Though many factors contribute to attain selectivity, this approach does have its merits since the crystal coordination chemistry differs among the ions and it emphasizes structural constraints. This will be further discussed in the next section.

NAK CHANNEL AND NON-SELECTIVITY

In their breakthrough paper (Doyle et al., 1998) the MacKinnon group proposed that the inverted teepee pore architecture of the KcsA potassium channel structure is probably shared with other tetrameric cation channels, including the voltage-gated sodium and calcium channels and the cyclic nucleotide-gated channels. This, however, has not yet been confirmed or disproved, as there has not been success in getting X-ray crystal structure of any of the other members of the tetrameric cation channel family.

In an attempt to model the pore architecture of cyclic nucleotide-gated channels and study their selectivity filter, our lab crystallized and determined the X-ray crystal structure of a Na⁺ and K⁺ conducting channel from *Bacillus cereus*, thought to be a bacterial homologue of CNG channels (Shi et al., 2006). Many interesting features emerged from the structure in comparison to the KcsA structure. Overall topology and the inverted teepee pore architecture remain essentially the same (Figure 2-12A, B) as had been proposed by the MacKinnon group. There also is a central aqueous cavity and the pore helices are oriented with their dipoles toward the cavity, also similar to KcsA and other potassium channels. The most distinct difference arose in the selectivity filter region of the protein. Comparing their amino acid sequences (Figure 2-12C, D) the NaK channel replaces the Tyrosine within the TVGYG sequence of the KcsA

selectivity filter with an Aspartate resulting in a TVGDG sequence. Though ions are still coordinated with main chain carbonyl groups in the resulting structure, just like in KcsA, this single amino acid change resulted in a dramatic conformational change in the selectivity filter. The carbonyl groups of the Aspartate and the first Glycine move away from the ion conduction pathway forming a vestibular structure (Figure 2-12D) leaving only two of the four ion binding sites, equivalent to sites 3 & 4 of KcsA. The carbonyl group of the second Glycine forms a well defined external ion binding site in NaK, which is unique compared to all previous structures. In the vestibule of NaK, ions can diffuse in and out but cannot specifically bind, which presumably is the cause for the non-selective nature of NaK. This non-selective nature of NaK has been shown with a radioactive tracer uptake assay using $^{86}\text{Rb}^+$ as the tracer ion (Shi et al., 2006) and also by several recent high resolution structures of NaK in different ions, especially Na^+ (Alam and Jiang, 2009a, b). The fact that NaK can be crystallized in Na^+ -only crystallization conditions is in sharp contrast to KcsA where the selectivity filter collapses in low K^+ and high Na^+ conditions (Zhou et al., 2001).

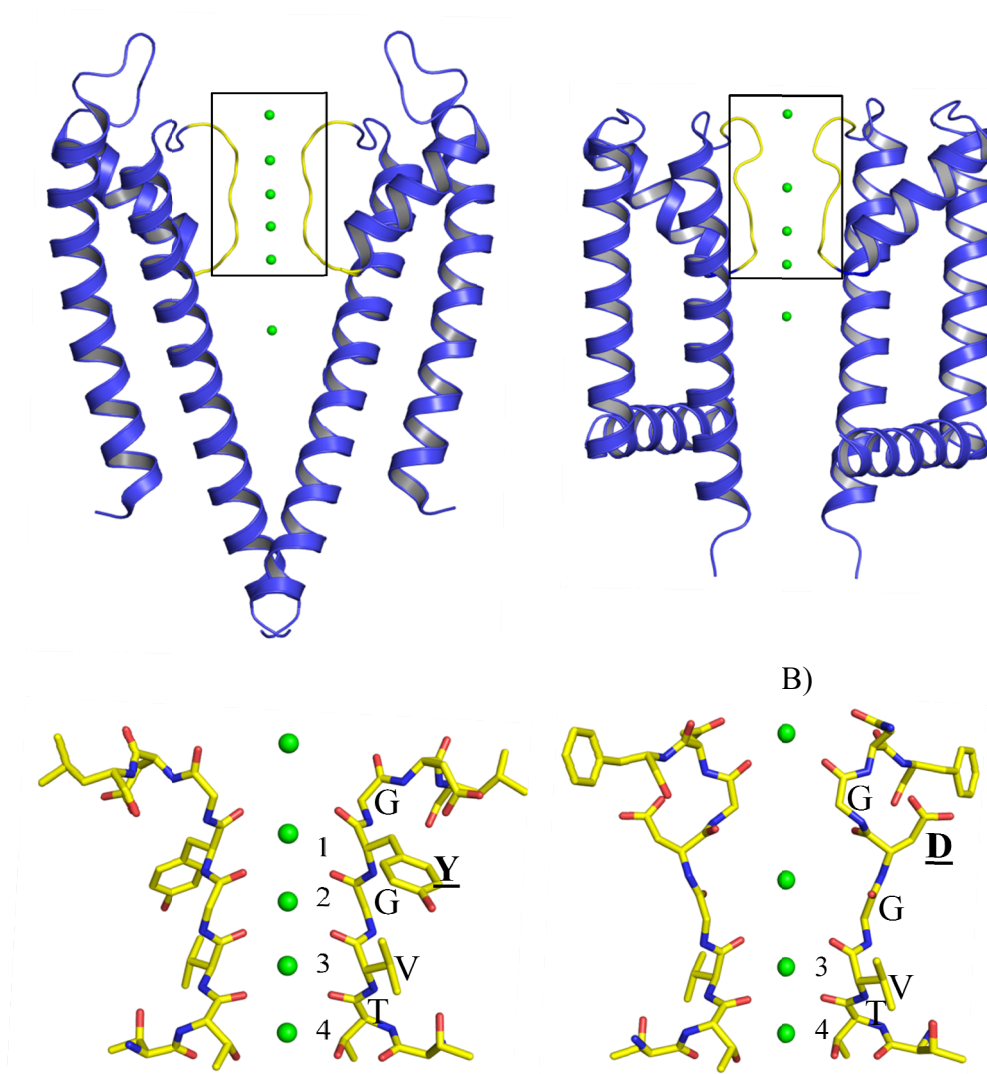


Figure 2-12 – Structure of the NaK channel (B, PDB ID-3E8H) in comparison to that of KcsA (A, PDB ID-1K4C). Both have outer (M1) and inner (M2) helices, but NaK has an additional M0 helix and significant differences are observed in their selectivity filters shown in orange (boxed); green spheres represent K⁺ ions. C) and (D): details of the selectivity filters of KcsA and NaK. Ion binding sites are labeled, 1-4 for KcsA and 3&4 for NaK. Selectivity filter residues are shown, emphasizing differences (underlined residues) that contributed to the different structures of the two channels.

Several peculiar features emerged out of the NaK structures. First is the coordination of Na^+ ions. Unlike in KcsA the NaK selectivity filter didn't collapse in Na^+ , it remains intact and the protein can be crystallized in the absence of K^+ (Alam and Jiang, 2009b). More important for our understanding of selectivity is that while Na^+ is coordinated within the selectivity filter the mode of coordination was very different from that of K^+ (Figure 2-13). K^+ coordination is similar to that observed in K^+ channels – eight coordinating ligands forming a square-antiprism coordination (Figure 2-13 A, B). In contrast, Na^+ ions were shown to coordinate in-plane with the carbonyl ligands, effectively reducing the number of ligands as a result of spatial constraints thus having a coordination number of five together with additional water molecules (Figure 2-13 C, D) (Alam and Jiang, 2009b). This finding argues for a combination of structural and coordination constraints as the determining factors for selectivity.

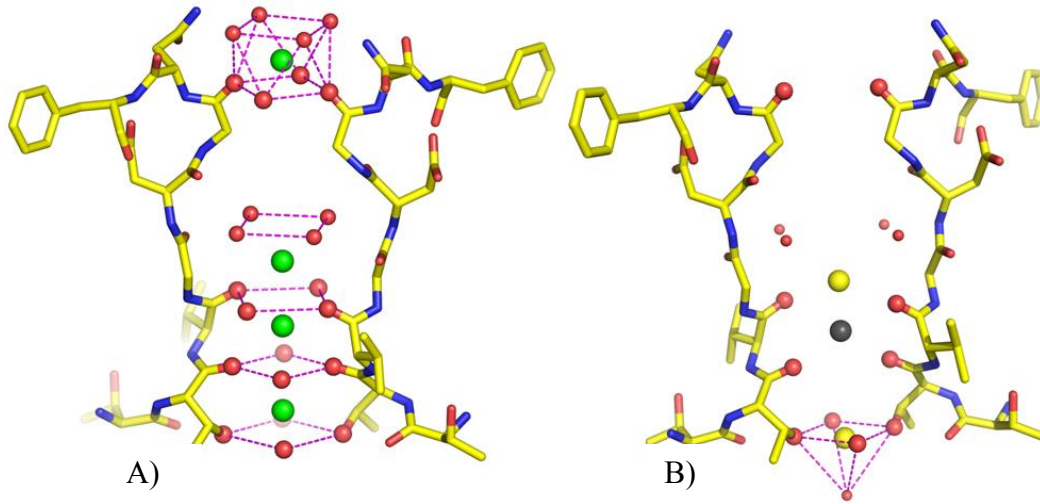


Figure 2-13 – K^+ and Na^+ coordination in the NaK channel. Panels (A) and (B) depict selectivity filter structures of NaK in K^+ (PDB ID-3E8H) and in Na^+ , respectively. Coordinating oxygen ligands from main chain carbonyl groups and water molecules are represented by large and small red spheres, respectively. K^+ ions (green spheres) in the selectivity filter and extracellular entryway are coordinated by carbonyl ligands with or without additional water ligands (A), showing virtually identical square-bipyramidal coordination as in K^+ channels. In contrast, Na^+ (yellow spheres) coordination at the intracellular end of the selectivity filter (B) shows Na^+ coordinated with four hydroxyl oxygens from Thr63 and a water ligand creating a square-pyramidal coordination. Front and back subunits are removed for clarity. Brown sphere represents an ion not clearly identified in the report.

Another important outcome of the structural studies on NaK is the coordination of Ca^{2+} exclusively with the main chain carbonyl groups similar to the coordination of monovalent cations. Earlier thoughts of Ca^{2+} coordination, in CNG and Ca^{2+} channels or other Ca^{2+} binding proteins, generally revolved around the necessity of binding sites formed by carboxylate groups of acidic amino acid residues (Glutamate or Aspartate), emphasizing the need to offset its double positive charge (Ellinor et al., 1995; Pidcock and Moore, 2001). The structure of

NaK, however, clearly showed that Ca^{2+} is chelated purely by main chain carbonyl groups. Ca^{2+} binds in the extracellular entryway and in site 3 of the NaK selectivity filter. Structural analysis of several point mutations revealed that the Aspartate residue at the external mouth, though not directly involved in Ca^{2+} chelation, plays an essential role in Ca^{2+} binding at the external site, probably via a through-space interaction that enhances the dipole strength of the coordinating ligands at that binding site (Alam et al., 2007).

These results led to the suggestion that NaK may be a good structural model of the selectivity filter of cyclic nucleotide channels as both NaK and CNG channels are notably non-selective and both have clear Ca^{2+} permeation and subsequent blockage of monovalent current, features critical for the physiological function of CNG channels. However, several contradicting properties emerged subsequently. A detailed analysis of protein sequence showed sharp deviations in the C-terminal of the selectivity filter. Moreover, analysis of Ca^{2+} blockage revealed that NaK and CNG channels exhibit substantial differences. An Aspartate-to-Glutamate mutation in the NaK filter led to higher Ca^{2+} affinity, whereas the reverse is true for CNG channels. In addition, NaK has a sub-millimolar Ca^{2+} affinity, much weaker than most CNG channels. As a result, wild-type NaK, though it captures some properties of CNG channels, lacks other critical characteristics and as such may not be a good structural model of the selectivity filter of cyclic nucleotide-gated channels.

CYCLIC NUCLEOTIDE-GATED (CNG) CHANNELS

Since ion channels are gated ion pores, they respond to a stimulus to open and close. Voltage-gated K^+ , Na^+ and Ca^{2+} channels are gated by change in membrane potential, cyclic nucleotide channels, as their name implies, are gated directly by binding of cyclic nucleotides to their C-terminal cyclic nucleotide binding domains while mechanosensitive channels are gated by a change in membrane tension.

The first report of a channel directly activated by a cyclic nucleotide came from Fesenko et al in 1985 (Fesenko et al., 1985), where intracellular cGMP was shown to activate cation selective channels of the frog retinal rods in the absence of nucleoside triphosphates. Before this report of direct interaction, cyclic nucleotides were thought to control the activity of proteins via phosphorylation mediated cyclic nucleotide dependent kinases. However, in this study neither ATP nor GTP was able to elicit channel activity even at 1mM concentration. Subsequently, similar channels were discovered in cone photoreceptors (Haynes and Yau, 1985) and olfactory sensory neurons (Nakamura and Gold, 1987). Several subsequent reports helped establish the functional importance of these nucleotide activated channels in rods, cones and olfactory sensory neurons beyond any reasonable doubt. Despite many reports of these channels in other cell

types of vertebrates or lower organisms their molecular function has yet to be fully established (Kaupp and Seifert, 2002).

Mode of operation of CNG channels in light sensing and olfaction is different. In CNG channels of photoreceptors, the rods and cones of the eye, cGMP is bound in the dark keeping the channels open and maintaining a steady inward current. This current, made up primarily of Ca^{2+} and Na^+ , is called the dark current and results in the depolarization of outer segment. These channels are so sensitive that they can respond to a single photon of light. When light strikes the retina the photo-transduction cascade is activated (Figure 2-14A) (Craven and Zagotta, 2006). In rods, photoreceptors responsible for vision in dim light, when light strikes the retina a photon of light is absorbed by the chromophore of rhodopsin (the rod visual pigment), 11 cis-retinal, causing its isomerization and activating the protein. Rhodopsin then activates the G-protein transducin that will activate phosphodiesterase (PDE). PDE hydrolyzes cGMP into 5'-GMP reducing the intracellular cGMP concentration leading to the closure of the CNG channels. This will result in a decrease in the dark current and then hyperpolarization of the photoreceptor's outer segment. Downstream neurons and cells then translate this termination of neurotransmitter signal as the detection of a photon. Cones, photoreceptors responsible for vision in bright light, also have similar transduction mechanism the only differences being the ability of cones to adapt to

a wider spectrum of light because they have three light pigments (blue, green, and red) and their decreased light sensitivity.

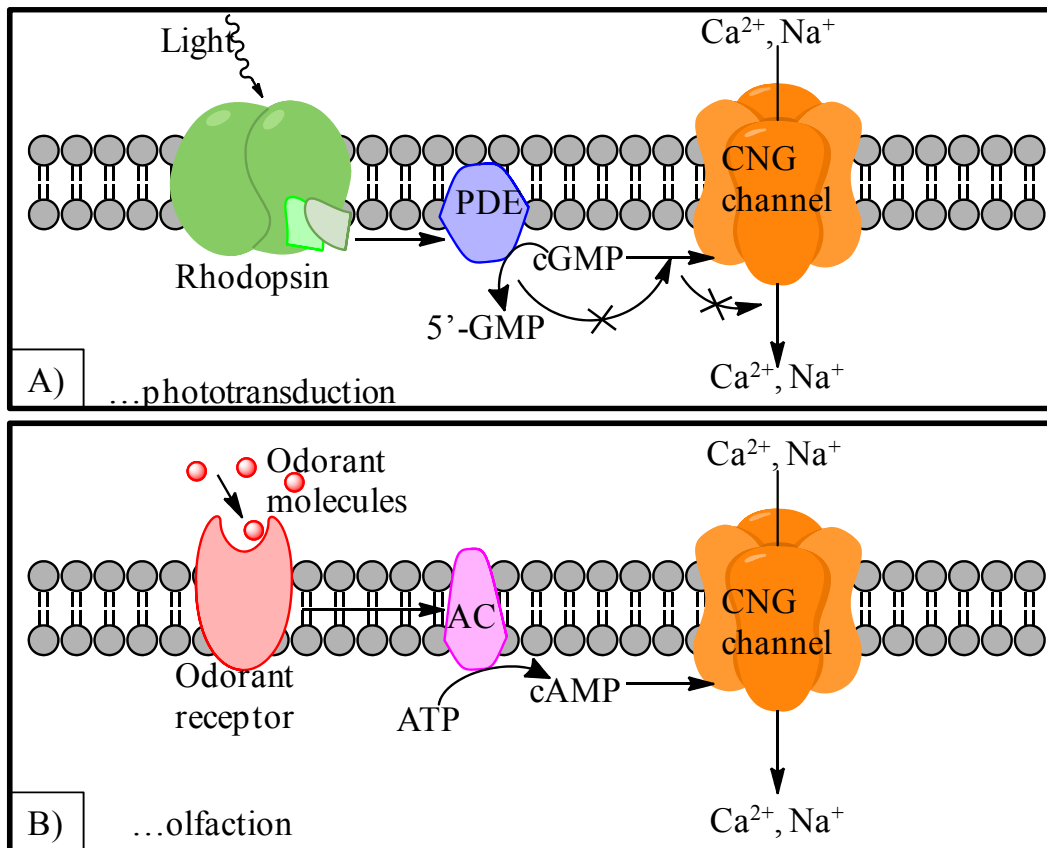


Figure 2-14 – Simplified cartoon comparing mode of action of CNG channels in photo (A) and olfactory (B) transduction. A) shows the transduction cascade in rod photoreceptors, in which rhodopsin is activated after absorption of a photon activating g-protein coupled signal transduction that in the end reduces the concentration of cGMP thereby closing the CNG channel. In contrast, in the olfactory transduction cascade (B) odorant reception results in production of more cAMP resulting in the opening of the CNG channel; PDE- phosphodiesterase, AC- adenylyl cyclase.

While photoreceptors react to removal of cyclic nucleotide ligand, the olfactory system is based on its production with stimulation. As shown in Figure 2-14B, when odorant molecules bind to olfactory receptors, adenylate cyclase is subsequently activated producing more cAMP and increasing the intracellular cAMP concentration. This newly produced cAMP will bind to CNG channels opening them, allowing ion flow and depolarizing the olfactory neuron. Olfactory sensory neurons (OSN) are highly selective due to the presence of many different odorant receptors. For instance, OSNs of humans can discriminate between more than 10,000 different odorous compounds and most other mammals even more (Craven and Zagotta, 2006; Prasad and Reed, 1999). In addition, given the signal amplification of this cascade, olfactory neurons are sensitive to the presence of only a few odorant molecules.

The first CNG channel gene, CNGA1 following new nomenclature (Bradley et al., 2001), was cloned in 1989 by Kaupp and coworkers from bovine retinal rods (Kaupp et al., 1989). Other names referring to CNGA1 in the older literature include CNG1, RCNC1, and $\alpha 1$ (see below for standardized nomenclature). Subsequently, five more vertebrate CNG channel genes were found (Kaupp and Seifert, 2002). These channels were divided into two groups based on sequence similarity, the CNGAs and CNGBs (Kaupp and Seifert, 2002). The first group, the CNGAs (previously called CNG α s), has four members- CNGA1, CNGA2, CNGA3 and CNGA4. The CNGA's are the principal channel

forming subunits, which, except for CNGA4, can form functional homotetrameric channels on their own that recapitulate most properties of native channels in a heterologous expression system. CNGA1 is the rod principal subunit, CNGA2 is the primary ‘A’ channel in cones while both CNGA2 and CNGA4 are expressed in olfactory sensory neurons. The second group contains the modulatory/auxiliary subunits, which has two members, CNGB1 of rods and CNGB3 of cones. These subunits cannot form functional channels by themselves but modify the functions of the ‘A’ subunits when co-expressed. The absence of CNGB2 designated subunit is a nomenclature discrepancy. CNGA4 was initially named olfactory β subunit or CNGB2, but later grouped with the ‘A’ subunits based on overall sequence similarity and functional sequence motifs. The CNGB3 was to maintain its designation than to be named CNGB2 (Bradley et al., 2001).

Table II. Standardized nomenclature of cyclic nucleotide-gated ion channels (Bradley et al., 2001)

Adopted nomenclature	Previous designations
CNGA1	CNG1/CNG α 1/RCNC1
CNGA2	CNG2/CNG α 3/OCNC1
CNGA3	CNG3/CNG α 2/CCNC1
CNGA4	CNG5/CNG α 4/OCNC2/CNGB2
CNGB1	CNG4/CNG β 1/RCNC2
CNGB3	CNG6/CNG β 2/CCNC2

Further variations result from alternative splicing, especially for CNGA3 and CNGB1 subunits (Kaupp and Seifert, 2002). The splice variants of CNGA3 vary in their NH₂-terminus and they physiologically occur in different cell types or organisms but their comparative difference is not well understood. The CNGB1 subunit also have several splice variants among which the two most important are B1a and B1b, expressed in rods and OSNs, respectively.

As a member of the tetrameric cation channel family, CNG channels function as tetramers. Initially, they were thought to function as homotetramers of the A(α) subunit (Kaupp et al., 1989). However, subsequent identification of the B(β) subunits as auxiliary subunits that fine-tune functions of the A(α) subunits indicated that these channels may function as heterotetramers. Heterologously expressed, the A(α) subunits form functional channels, perceived as homotetramers, with only slight variation in their properties from native heteromeric channels. Though the heterotetrameric nature has subsequently been generally accepted, the stoichiometry of the A and B subunits has not been well established. The rod CNG channel has been proposed to have 2A:2B stoichiometry (Shammat and Gordon, 1999). Using cross linking, non-denaturing gel electrophoresis and analytical ultracentrifugation Zhong *et al* identified a carboxy terminal leucine zipper domain in the 'A' subunits of rod and cone CNG channels that mediates a trimeric interaction, suggesting a 3A:1B stoichiometry (Figure 2-15) (Zhong et al., 2002). The olfactory CNG channel has also been

found to assume the 3A:1B stoichiometry but since it has two types of ‘A’ subunits (A2 & A4) the specific stoichiometry follows 2A2:1A4:1B1b (Figure 2-15) (Zheng and Zagotta, 2004).

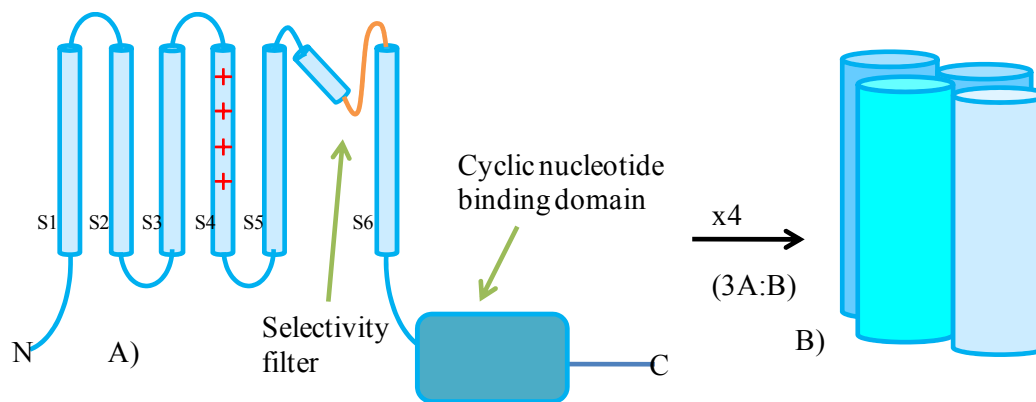


Figure 2-15 – Topology of CNG channels. Monomer (A) has six transmembrane segments and a C-terminal cyclic nucleotide binding site. Selectivity filter is shown in orange. Tetramer (B) is the biologically relevant molecule.

Sequence similarities with voltage-gated K^+ , Na^+ and Ca^{2+} channels suggested that CNG channels monomers consist of six-transmembrane spanning segments, designated S1-S6, harboring the ion conduction pore between the 5th and 6th transmembrane segments, followed by a cyclic nucleotide binding domain in the C-terminus (Figure 2-15). The S4 segment in these channels has similar, albeit fewer, positively charged residues as those thought to be responsible for voltage sensing in voltage-gated K^+ , Na^+ and Ca^{2+} channels. However, CNG

channels are not gated by voltage and the function of the voltage sensor domain is not well understood, except that channel function can be modulated by voltage.

As a member of the pore-loop family of ion channels CNG channel pores share the basic pore loop architecture with other members (Ashcroft, 2006). Sequence comparison with K^+ channels reveals a striking resemblance in the pore region, especially in the selectivity filter, though these two channels have markedly different function and ion permeation properties - CNG channels are largely non-selective to most group I and II cations while K^+ channels are highly selective. Both CNG and K^+ channels share a highly conserved T(V/I)G sequence in the N-terminus of their selectivity filters. This conservation and the presence of the S4 segment in CNG channels, albeit of no known function, may suggest a common ancestor for CNG and K^+ channels. Moreover, this similarity in their p-regions suggests that they have same or closely related pore structure. In support of this, a very clever work by Heginbotham et al deleted two residues from the *Shaker* K^+ channel selectivity filter signature sequence (YG of the TVGYG) based on a sequence alignment with CNG channels (Heginbotham and MacKinnon, 1993). The deletion mutant displayed many of CNG channel permeation properties- it became non-selective and showed blockage of monovalent current by divalent cations, especially Ca^{2+} . Therefore, though these two groups of channels have the same pore architecture and have the same protein sequence in the N-terminal portion of their selectivity filters, the difference in

their permeation properties may have resulted from difference in the protein sequence of their C-terminal half of the selectivity filters and/or structural differences in their selectivity filters.

CNG channels are known to discriminate poorly among monovalent cations and are permeable to divalent cations, especially Ca^{2+} , which has direct relevance to their cellular function because Ca^{2+} permeability is associated with blockage of monovalent current. Relative permeability values of CNG channels for monovalent cations shows that different CNG channels have very little variation in their ion selectivity sequence (Table III). Heterologously expressed homotetramers (A subunits) or heterotetramers (3A + B) generally have similar permeability ratios as the corresponding native channels.

Table III. Ion permeability ratio of different CNG channels

Source of CNG channel	PX^+/PNa^+ , X- other ion					Reference
	Li^+	Na^+	K^+	Rb^+	Cs^+	
Salamander rods	1.14	1.00	0.98	0.84	0.58	(Menini, 1990)
Cones	0.99	1.00	1.11	0.96	0.80	(Picones and Korenbrot, 1992)
OSNs	0.74	1.00	0.81	0.60	0.52	(Frings et al., 1992)

Calcium permeation and block in CNG channels

Ca^{2+} permeation and subsequent blockage of monovalent cation current is crucial for the cellular function of CNG channels. Under physiological conditions CNG channels are in fact more permeable to Ca^{2+} than Na^+ . In CNG channels of photoreceptors and olfactory sensory neurons Ca^{2+} entry provides a signal important for both excitation and adaptation. In photoreceptors, it is part of a negative feedback mechanism that regulates recovery of the light response and light adaptation. Ca^{2+} permeation lowers channel conductance by effectively blocking monovalent cation currents. In rods, photoreceptors responsible for vision in dim light, this reduces membrane potential noise and allows the photoreceptor cells to detect photons with high sensitivity making them capable of detecting even a single photon of light (Yau and Baylor, 1989).

Several studies suggested that a highly conserved acidic residue (a Glutamate) in the pore loop of the A subunits is responsible for the Ca^{2+} blockage properties exhibited by these channels (Eismann et al., 1994; Gavazzo et al., 2000; Root and MacKinnon, 1993). For Ca^{2+} to both permeate the channel and block monovalent current it must bind at a site inside the pore. Different experimental maneuvers aimed at changing the negative charge of the acidic residue resulted in changes in Ca^{2+} binding/blockage property, especially from the extracellular side. Eismann, et al (Eismann et al., 1994) mutated the Glu363 of A1

channel to Glutamine resulting in a severe reduction of extracellular Ca^{2+} blockage. Gavazzo et al studied the effect of mutating the Glu340 residue of the bovine olfactory A2 channel (Gavazzo et al., 2000) into different amino acids on divalent cation permeation and blockage and found that mutations that eliminate the negative charge severely reduced extracellular divalent cation blockage. Similarly, Root et al, found that mutating the Glu363 of the A1 channel to residues that do not carry a negative charge abolished extracellular divalent cation blockage, arguing that the acidic residue is necessary and sufficient for this property (Root and MacKinnon, 1993). In a related note, the latter group also reported that among divalent cations Ca^{2+} exhibits a much higher affinity and permeates more than Mg^{2+} , Sr^{2+} or Ba^{2+} (Park and MacKinnon, 1995). All groups also tested the effect of the chemically conservative Glutamate to Aspartate (E→D) mutation, which maintains the negative charge and found that generally Ca^{2+} blockage is enhanced. It is important to note that different native channels do exhibit substantial differences in their Ca^{2+} permeation and blockage properties (Frings et al., 1995). In addition, lowering the pH presumably protonated those acidic residues and correspondingly reduced Ca^{2+} blockage (Root and MacKinnon, 1994). It was reasoned that the Glutamate residues forming two independent proton binding sites with a carboxyl-carboxylate pair (Morrill and MacKinnon, 1999).

Ca^{2+} can block monovalent current both from the intracellular or extracellular side in a strongly voltage dependent manner, inward currents being suppressed stronger than outward currents (Eismann et al., 1994). This property is characteristic of a binding/ permeating positively charged molecule indicating the presence of a Ca^{2+} binding site inside the channel pore (Colamartino et al., 1991; Karpen et al., 1993). In Kaupp et al study of the rod photoreceptor Ca^{2+} blockage properties, a plot of fraction of unblocked current against holding potential shows that blockage by internal Ca^{2+} decreased upon depolarization (Eismann et al., 1994), indicating the blocking ion (Ca^{2+}) binding inside the pore, exit facilitated by increasingly positive voltages. Blockage by external Ca^{2+} shows the decrease of unblocked current upon hyperpolarization up to a certain value ($\sim -30\text{mV}$), but further hyperpolarization enhanced the unblocked current or reduced blockage. This relief of blockage at more negative voltages has been explained as permeation by Ca^{2+} . This also supports the necessity of the blocker ion binding inside the pore. Kaupp et al estimated that divalent cations entering the pore from extracellular side should travel $\sim 35\%$ of the transmembrane field to reach the binding site. Kaupp et al also suggested that at positive voltages blockage by external divalent cations can be described as one blocker ion occluding the pathway. And, at negative voltages, because blockage shows strong dependence both on voltage and concentration they suggested the necessity of two or more blocker ions in the pore to occlude channel. Moreover, these binding sites may be

formed by the carboxylate groups of the glutamate side chain, which has yet to be proved.

CNG channelopathies

Naturally occurring mutations in CNG channel genes of humans have been reported to cause several forms of impairment of vision. Mutations on the human rod CNGA1 and CNGB1 channels have been shown to result in retinitis pigmentosa, a progressive degeneration of the retina that affect night and peripheral vision ultimately leading to total blindness (Dryja et al., 1995). Another human vision disorder called achromatopsia (also referred to as total color-blindness or rod monochromacy (RM)) is caused by mutations on the cone photoreceptor's CNGA3 and CNGB3 channel genes (Kohl et al., 2000; Kohl et al., 1998). This is a rare, autosomal recessive inherited and congenital disorder characterized by total loss of color discrimination, reduced visual acuity and photophobia. Targeted gene disruptions have been used to get phenotypic insight on these and other CNG channels (Biel and Michalakis, 2007; Kaupp and Seifert, 2002; Pifferi et al., 2006).

CHAPTER THREE

Methodology

The ultimate objective of this study is to get a detailed molecular picture from the perspective of structure about the ion selectivity mechanism and permeation properties of CNG channels using the bacterial NaK channel as a model system. As described earlier, CNG channels are non-selective cation channels that are important in visual and olfactory systems. Though these channels have high homology with tetrameric cation channels such as the voltage-gated K^+ , Na^+ and Ca^{2+} channels and are considered to be members of this family, they are noted for their non-selectivity while the other members exhibit a high degree of ion selectivity. The CNG channels conduct all alkali and some alkaline earth metal ions, most notably Ca^{2+} . How the CNG channel pore can adapt to all these cations, which have substantially different ionic radii and formal charges, is not well understood.

CNG channel function is very well established from a wealth of functional information. Mechanistic insights, especially as it relates to their ion selectivity and permeation properties, has however been lacking due to absence of detailed structural information. Recent structural work on the prokaryotic non-selective cation channel NaK has shed light on the molecular mechanisms underlying mono and divalent cation binding (Alam and Jiang, 2009b; Shi et al., 2006). NaK bears

some sequence and functional similarities with CNG channels. These two channels share a highly conserved N-terminal T(V/D)G sequence in their selectivity filters. In addition, NaK carries an Aspartate residue after this sequence, which is at an equivalent position as the key acidic residue (usually Glutamate) of CNGA channels (Figure 3-1). NaK is also non-selective and exhibits divalent cation blockage of monovalent current, both of which are characteristic properties of CNG channels. The NaK selectivity filter structure markedly differs from that of K^+ channels and is thought to underlie its non selective nature and divalent cation binding properties (Figure 2-12). Most importantly, work on the NaK channel demonstrates that selective Ca^{2+} chelation can be accomplished utilizing backbone carbonyl groups from the selectivity filter alone with nearby acidic residues imparting Ca^{2+} specificity via a through space interaction with the Ca^{2+} chelating groups (Alam and Jiang, 2009b; Alam et al., 2007). These similarities pointed to the possibility of NaK being a homologue of CNG channels and its structure insightful of CNG pores. However, even though general principles learned from NaK likely hold true for CNG and other Ca^{2+} permeable channels, the approach is limited in its ability to model certain aspects of CNG channel biology. Close examination of the protein sequences of these channels shows that considerable differences exist at the C-terminal end of their selectivity filters both in amino acid composition and sequence length (Figure 3-1). Moreover, the sub-milimolar affinity of external Ca^{2+} binding observed in

NaK is much weaker than that of most CNG channels and an Asp-to-Glu mutation in the NaK filter leads to a higher Ca^{2+} binding affinity whereas the opposite holds true for CNG channels. These key discrepancies suggest that the structure of NaK may not represent well the structure of CNG channel selectivity filters. Therefore, to accurately recapitulate the ion selectivity and Ca^{2+} blockage properties in CNG channels, several mutant NaK channels were generated by altering its selectivity filter sequence to match those of CNG channels and their structures determined in complex with various cations at high resolution. Furthermore, quantitative electrophysiological and complimentary radioactive uptake assays which show that the mutants share the same ion selectivity properties as CNG channels were established. Data strongly suggest that the mutant structures represent quite well the structures of CNG channel pores and provide novel insights into understanding the ion selectivity in CNG channels.

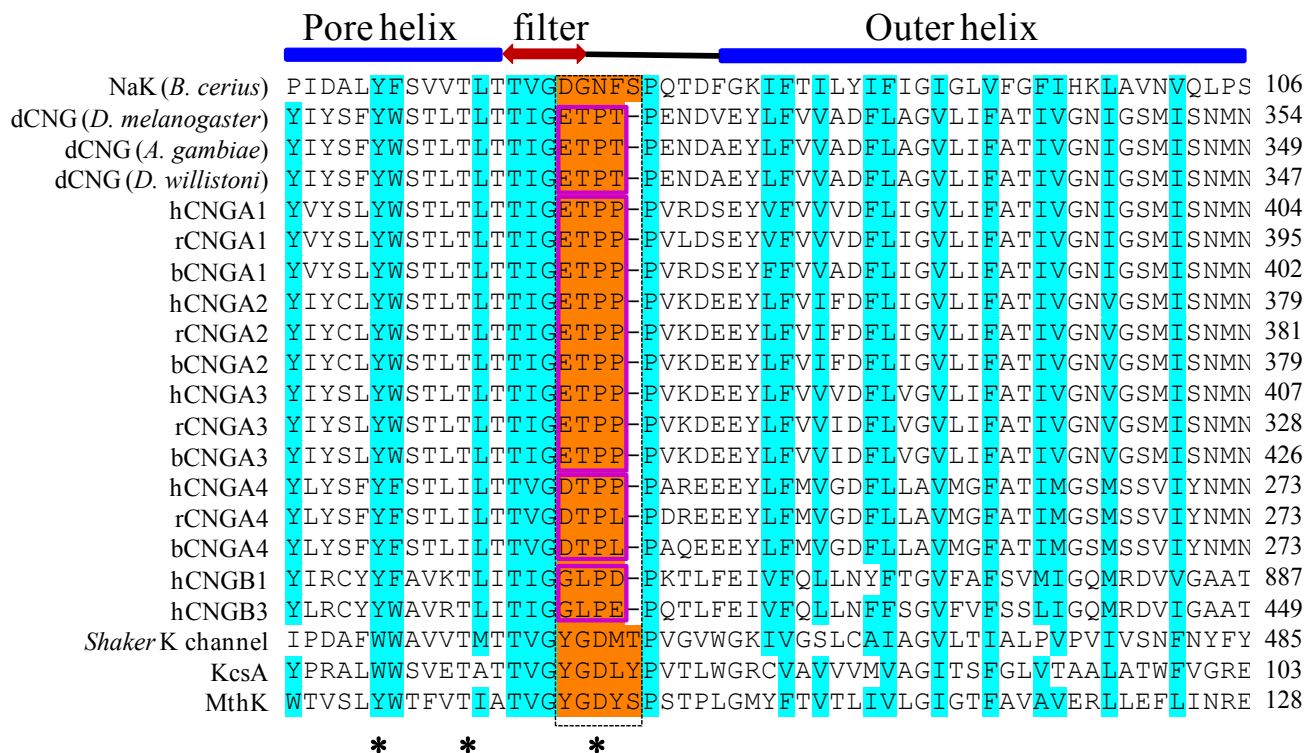


Figure 3-1 – Partial sequence alignment between NaK, K⁺ channels KcsA, MthK and Shaker K channel and CNG channels from drosophila (designated by dCNG), human (hCNG), rat (rCNG) and bovine (bCNG). Shaded in orange are the residues in NaK that were being replaced by corresponding residues in CNG channels; boxes in magenta show the difference at the c-terminal selectivity filter sequences in different CNG channels/subunits. Secondary structure assignment is based on NaK Δ 19 structures (PDB code 3E86) and only regions corresponding to the start of the pore helix to the end of the inner helix in NaK are shown. Asterisks mark the positions where mutagenesis were performed on bovine CNGA1 based on NaK-ETPP mutant structure and arrows indicate the residues for swap mutation.

Generation of NaK mutants that mimic CNG channel pores

Several mutants of NaK that carry selectivity filter sequences of CNG channels were generated based on a sequence alignment (Figure 3-1) between NaK, K⁺ channels, and various CNG channels. Significant differences were observed in the selectivity filter region C-terminal to the conserved T(V/I)G residues shared by all three groups. In CNG channels four patterns are observed. Most vertebrate CNG channels contain a sequence of ETPP right at the C-terminal end of their selectivity filters in which the conserved glutamate plays an important role in Ca²⁺ binding. Replacing this Glutamate with Aspartate was shown to enhance Ca²⁺ binding while replacing it with neutral residues (Asparagine or Glutamine) significantly diminishes the Ca²⁺ affinity. The auxiliary CNGA4 channels have a DTPP/L sequence, CNGB channels have GLPE/D sequence while those mainly occurring in insects have a sequence of ETPT. On the other hand, the NaK channel has an amino acid sequence of DGNFS at the equivalent region which only shares the conserved acidic residue (Asp66) with CNGA subunits. Furthermore, the length of the sequence at this region seems to be one residue longer in NaK than in CNG channels. Accordingly, the five residues of NaK were replaced with four residues of CNG channels. Specifically, the NaK filter sequence of TVGDGNFSP was replaced with TVGETPPP to mimic the filter of most common CNG channels, with

TVGDTPPP to mimic the charge conservative Glu-to-Asp mutant of CNG (A1-A3) channels and the auxiliary A subunit CNGA4, with TVGNTPPP and TVGQTPPP to mimic the uncharged Glu-to-Asn, and Glu-to-Gln mutants of CNGA channels, respectively, with TVGETPTP to represent insect CNG channels and TVGGLPEP to represent the auxiliary B channels. In order to minimize perturbation, two other modest mutations- TVGDTPSP and TVGNTPSP- were also made with three of the four residues mutated to two. These mutants will be referred to as- NaK-ETPP, NaK-DTPP, NaK-NTPP, NaK-QTPP, NaK-ETPT, NaK-GLPE, NaK-DTPS and NaK-NTPS.

All of the above CNG-mimicking NaK mutants were generated on the background of NaKN Δ 19 channel, a truncated form of the NaK channel from *Bacillus cereus* lacking the N-terminal 19 residues. The gene encoding NaK-Nd19 was cloned into pQE60 expression vector between NcoI and BglII restriction sites with a c-terminal thrombin cleavage site preceded by a hexahistidine sequence. For functional studies, an extra Phe-to-Ala mutation was generated at position equivalent to Phe92 of NaK using the QuickChange II mutagenesis kit.

The NaK mutants exhibit similar biochemical behavior to wild type NaK with only minor differences: they all express, can be purified as stable tetramers and can be crystallized in similar conditions as NaK, with the exception of NaK-GLPE. In order to recapitulate properties of the most widely occurring CNG

channels the current study focused mainly on mutants similar to most vertebrate channel forming subunits (CNG A1, A2 and A3), its corresponding Glu-to-Asp and Glu-to-Asn mutants to study the important Ca^{2+} binding property. Accordingly, most of the work and discussion is dedicated to NaK-ETPP, NaK-DTPP and NaK-NTPP, with some supporting data from NaK-DTPS and NaK-NTPS. NaK-ETPT and NaK-QTPP exhibit peculiar structural features. They will be the focus of future studies.

Protein expression and purification

Protein expression and purification were performed as reported for NaKN Δ 19 (Alam and Jiang, 2009b). Proteins were expressed either in XL1B or SG13009 *Escherichia coli* cells by induction with 0.4mM isopropyl- β -D-thiogalactopyranoside (IPTG) at OD₆₀₀ of 0.8-0.9 overnight at 25⁰C for about 16hrs. For NaK-ETPP, 5mM BaCl₂ was added to the culture media to achieve optimal expression. After harvesting, cells were resuspended in a solution containing 50mM Tris-HCl pH 8, 100mM NaCl or KCl and protease inhibitors pepstatin, leupeptin, aprotinin and PMSF. Cells were lysed by sonication and expressed proteins extracted by incubating for 3hrs at room temperature with n-decyl- β -D-maltopyranoside (DM) added to a final concentration of 40mM. This was followed by Co²⁺ affinity purification (Clontech) in 4mM DM with 50mM

Tris-HCl pH 8 and 100mM NaCl or KCl and protein was eluted by 300mM imidazole after an initial wash step with 15mM imidazole. The imidazole elute was incubated overnight with thrombin at room temperature to remove the hexahistidine tag. Final purification was performed by size exclusion chromatography using Superdex-200 (10/300) column in 4mM DM buffer containing 20mM Tris-HCl pH 8 and 100mM NaCl or KCl.

Crystallization and soaking experiments

Purified proteins were concentrated to about 20 mg/ml using an Amicon Ultra centrifugal filtration device (50kD MW cutoff) and crystallized at 20°C using the sitting drop vapor diffusion method by mixing equal volumes of concentrated protein and well solution containing 62.5-70% (\pm)-2-Methyl-2,4-pentanediol (MPD) and 100mM buffer of various pH (MES for pH 6.5, HEPES for pH 7.0-7.5 and Tris-HCl for pH 8.0 – 8.5). All crystals were frozen in liquid propane with the crystallization solution serving as the cryo-protectant. Crystals were of space group I4 with unit cell dimensions around $a=b=68$ Å, $c=89$ Å, $\alpha=\beta=\gamma=90^\circ$ and contained 2 molecules per asymmetric unit. The four-fold axis of the channel tetramer coincided with the crystallographic tetrad.

To obtain the structures of NaK mutants in complex with various other cations, K⁺ complex crystals were soaked in different stabilization solutions. In

general, the crystals were soaked overnight at 20°C in stabilization solutions containing 70% MPD, 10mM DM, 100mM HEPES, pH 7.5, and the chloride salt of respective cations which are 100mM NaCl for Na⁺ complexes, 100mM NaCl and 25mM CaCl₂ for Ca²⁺ complexes, or 100mM KCl and 10mM BaCl₂ for Ba²⁺ complexes. All soaked crystals were also directly frozen in liquid propane.

Data collection and Structure determination

X-ray data were collected at the Advanced Photon Source (APS) Beamlines 19-ID/BM and 23-ID, and at the Advanced Light Source (ALS) of the Lawrence Berkeley Laboratory (LBL) beamlines 8.2.1/8.2.2. Data processing and scaling was performed using the HKL2000 software (Otwinowski and Minor, 1997). The structures were determined by molecular replacement using the NaKNΔ19 structure with selectivity filter region omitted as an initial search model followed by repeated cycles of model building in O (Jones et al., 1991) and refinement in CNS (Brunger et al., 1998). 95.1 % of the residues were in most favored regions and 4.9 % in additionally allowed regions on a Ramachandran plot. Some discontinuous electron density peaks can be attributed to bound lipid, detergent, or other solvent molecules and were assigned as water molecules for simplicity. Detailed data collection and refinement statistics are listed in Table IV.

Data of soaked and reference crystals were all scaled in the CCP4 suite (Bailey, 1994) and their difference maps calculated using Fourier coefficients ($F_{\text{soak}}-F_{\text{reference}}$) with phases from a model that was refined against the reference dataset. All ion-omit difference maps using Fourier coefficients (F_o-F_c) were calculated with phases from refined models that contained no ions in the selectivity filters. All structure figures were generated in Pymol (deLano, 2002).

Functional studies

Functional characterization of ion channels has largely been based on electrophysiological recordings, usually in heterologous expression system coupled with protein sequence manipulations. This has yielded enormous amount of information for eukaryotic ion channels as they can be readily expressed in mammalian cells or in the frog oocyte. In contrast, ion channels from prokaryotes, though more suitable for structural studies, have been difficult to study using electrophysiological techniques primarily because they do not express readily in a heterologous expression system and their gating mechanism is not always clear. Past approaches used to get functional information from prokaryotic ion channels involved reconstituting protein into lipid vesicles of chosen composition, which relies on chance survival of the channel during detergent extraction and lipid reconstitution. The proteoliposome thus prepared is studied by radioactive tracer

uptake (Enkvetchakul et al., 2004; Garty et al., 1983; Heginbotham et al., 1998), planar lipid bilayer setup for single-channel activity (Cuello et al., 1998) or direct giant proteoliposome patching for macro- or microscopic current analysis (Cheng et al., 2009). Another approach is to express desired bacterial protein in *E. coli* and enlarge the cells into giant spheroplasts by chemically inhibiting cell division, which are large enough for direct patch-clamping (Kuo et al., 2007). Of these, the radioactive tracer uptake assay and the giant liposome methods are employed in this study and will be described.

Liposome preparation

Lipid vesicles are prepared by hydrating thin lipid films or lipid cakes. To obtain the lipid films, solvent is removed by evaporation either by dry stream of nitrogen or argon (for small volumes) or a rotary evaporator (for large volumes). If the lipid stocks were in powder form it is imperative to dissolve in an organic solvent, chloroform or chloroform:methanol mixture, to get a homogenous lipid mixture. Complete removal of solvent is key to the quality of the liposomes and is achieved by rotating lipid mixture while drying to avoid solvent occlusion in clumps of lipid and/or dissolving lipid film in one volume of pentane and re-drying. The lipid film is finally dried under vacuum for about an hour at the lowest setting and tightly sealed and stored until ready to rehydrate.

The dry lipid film is hydrated by adding buffer of interest and mixing vigorously. Though hydration time may differ based on lipid composition or type, one hour of vigorous mixing is usually recommended (AvantiPolarLipids). This process produces large, multi-lamellar vesicle (LMV), with each lipid bilayer separated by a water layer. To reduce the size of the LMV's either sonication or extrusion can be used. Sonication typically produces small, uni-lamellar vesicles (SUV) with diameters ranging from 15-50nm. Bath sonication is the most widely used method to produce SUV's. Probe-tip sonicators, though can be used, suffer from the risk of overheating the lipid suspension causing degradation mainly because they deliver high energy in a localized area. Several factors, such as composition, concentration and temperature affect mean size and distribution of SUVs produced by sonication. And because it is impossible to reproduce the conditions of sonication, different sizes of SUV's are produced on different batches of sonication. In addition, due to the high degree of membrane curvature, SUV's are inherently unstable and will spontaneously fuse to form larger vesicles. Extrusion on the other hand produces SUV's of more controlled and reproducible size. The method involves forcing the lipid suspension through a polycarbonate filter with a defined pore size to yield particles having a diameter near the pore size of the filter.

Protein reconstitution

In our experiments the dried lipid is usually hydrated with the reconstitution buffer to a final concentration of 10mg lipid per milliliter buffer. The reconstitution buffer contains the chloride salt of ion of interest at a concentration of 450mM for radioactive uptake assays and 100mM for electrophysiological studies, 10mM HEPES, with or without 4mM NMG, pH adjusted to 7.4 with the hydroxide base of the corresponding salt. Complete re-suspension of lipid is achieved by pipetting up and down or a brief sonication. This lipid mix is then vigorously shaken on a vortexer at room temperature for about an hour and then sonicated until clear to generate SUVs as described above. Since our channel protein is purified in a detergent buffer, decyl maltopyranoside (DM), detergent is added to the hydrated lipid mix to a final concentration of 10mM and incubated gently, with mixing, over a vortexer for at least two hours. After this, the protein is added to the desired protein:lipid (mass) ratio. For radioactive uptake assays 1:100 ratio is customarily used while 1:10000 or 1:5000 ratio is preferred for electrophysiological measurements to reduce channel density, which improves the chance of obtaining single channel recordings in vesicle patches. A control lipid mix, one without any added protein, is usually necessary to establish a baseline. To enhance incorporation of the protein into the lipid vesicles, the detergent has to be removed from the mixture. Two methods are used for this step, gel filtration (Heginbotham et al., 1998) and dialysis

(Nimigean, 2006). The former has the advantage of being fast, while the later is more reliable to remove detergent efficiently. Gel filtration may be better for less stable proteins since dialysis could take several days. In our experiments the dialysis method was used, in which the protein-lipid-detergent mix is dialyzed for two or three days against reconstitution buffer in a dialysis membrane with constant but gentle stirring and frequently changing the buffer. The reconstituted vesicles are aliquoted into suitable volumes and stored at -80°C until needed.

In this study, proteins were reconstituted into lipid vesicles composed of either asolectin (Fluka) alone (for current recordings) or 3:1 ratio of POPE (1-palmitoyl-2-oleoyl-phosphatidylethanolamine) and POPG (1-palmitoyl-2-oleoyl-phosphatidylglycerol (Avanti Polar Lipids). Liposomes of different protein-to-lipid ratio were prepared for different purposes. Liposomes with protein-to-lipid ratio of $0.1\mu\text{g}/\text{mg}$ (1:10000) were used for single channel electrophysiological studies, $2\mu\text{g}/\text{mg}$ (1:500) for macroscopic current recordings and $10\mu\text{g}/\text{mg}$ (1:100) for radioactive uptake experiments. To remove DM detergent, the protein-lipid-detergent mixtures were dialyzed against a reconstitution buffer for three days changing buffer at least once every 24hrs. Reconstitution buffer contains 10mM HEPES, chloride salt of cation of interest (KCl, NaCl or LiCl - 100mM for electrophysiological studies or 450mM for radioactive assays), with or without 4mM NMG, pH adjusted to 7.4 with the corresponding hydroxide base and . Proteoliposomes were aliquoted in $100\mu\text{L}$ portions and stored at -80°C until

needed. In all preparations control liposomes that do not have protein were made to establish baseline.

Radioactive tracer uptake assay

The principle of this assay is previously described by Garty (Garty et al., 1983) and Nimigean (Nimigean, 2006). It involves measuring the time course of radioactive tracer accumulation inside lipid vesicles with reconstituted protein. For this to be useful, the ion channel should be permeable to the radioactive tracer ion; $^{86}\text{Rb}^+$ in this particular case. After removing extraliposomal solution, usually by gel filtration, when the proteoliposome is placed in a low salt concentration medium of the salt loaded-with in the previous step together with a spike of radioactive tracer, a huge electrochemical gradient is established (inside negative) across the proteoliposomal membrane if the channel is permeable to the ion (Figure 3-2A). This results in equilibration of the radioactive tracer ion around the proteoliposome and subsequent accumulation inside. Rate and magnitude of tracer accumulation depends on the permeability of the channel to test and tracer ions, amount of functional protein and other factors. To determine the maximal intraliposomal volume, small organic channels that render the vesicle permeable to the test ion, for instance valinomycin for K^+ , were employed at end of experiment.

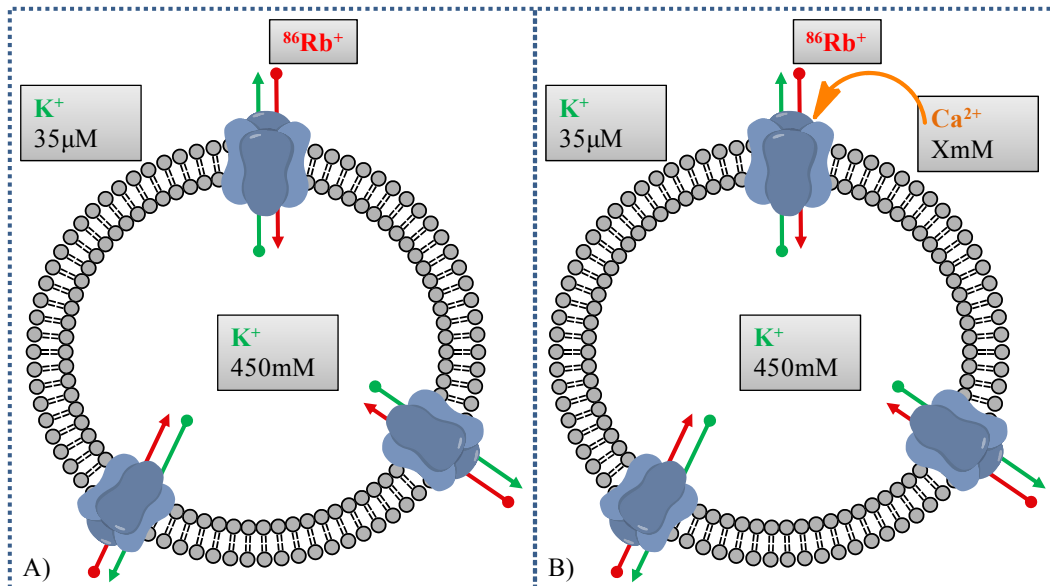


Figure 3-2 – Depiction of the radioactive uptake assay (A) and its slightly modified competition assay (B). Protein (light blue) is reconstituted in lipid vesicles with high salt inside, KCl in this case (K^+ in green). In the assay (A) the proteoliposome is placed in low salt spiked with the radioactive tracer ion, $^{86}Rb^+$ in this case (red), and if protein is permeable to ion of interest an electrochemical gradient (inside negative) will be established, which $^{86}Rb^+$ follows, hence $^{86}Rb^+$ accumulated inside. In (B), the competition assay, different concentrations of ‘competitor’ ion is added to the external buffer. Any permeation by competitor ion will reduce $^{86}Rb^+$ on a concentration dependent manner.

Specific protocol is as follows: Frozen proteoliposomes (protein/lipid ratio of 1/100, in 3PE:PG) were thawed and sonicated in a bath sonicator. This was then passed through a pre-spun Sephadex G-50 fine gel-filtration column (1.5 bed volume in a 5mL disposable spin column) swollen in sorbitol buffer (400mM Sorbitol, 10mM HEPES, 4mM NMG, pH 7.4) to remove extraliposomal salt. 160 μ L of the flow through was mixed with 320 μ L of $^{86}Rb^+$ flux buffer (35 μ M NaCl, KCl or LiCl in sorbitol buffer and 5 μ M $^{86}RbCl$). At desired time points

75 μ L of this mixture was spun with another column as above. Each elute was then mixed with 10mL scintillation cocktail and radioactivity quantified using a liquid scintillation counter.

A modified form of the assay, called the competition assay is used to assess the relative conductance of ions in an ion channel (Figure 3-2B) (Heginbotham 1998). This modified assay was especially useful to assess the Ca^{2+} blockage properties of these CNG-mimicking NaK mutants. In this assay the flux buffer, in addition to loaded ion and $^{86}\text{Rb}^+$, contains cation of interest at different concentrations. If channel is permeant to the test cation there will be competition with the tracer ion reducing the tracer ion's flux into the liposomes. A concentration dependent $^{86}\text{Rb}^+$ accumulation would indicate this property. If on the other hand test cation cannot permeate the channel, $^{86}\text{Rb}^+$ uptake will be independent to the test cation's concentration or its presence at all.

This radioactive tracer uptake assay, although useful to proteins not amenable for electrophysiological studies, as is the case for most bacterial channels, suffers from serious drawbacks. First, uniformity in liposome quality between different preparations is impossible to attain. This introduces variations in relative channel density, liposome integrity, and other factors. As a result, widely different readings are not uncommon for different preparations of the same protein and test ion. Second, the information obtained is mainly qualitative. Using this method it is not possible to extract information such as rate of ion transport,

dose-response or other quantitative parameters. So, in this study this method is used to crudely assess the permeability of the CNG-mimicking NaK mutant channels to several ions.

Electrophysiological analyses

Electrophysiological methods have been indispensable to ion channel research. Early on Hodgkin and Huxley used the two electrode voltage clamp method to study the squid giant axon and accurately characterize the action potential, for which they were awarded the 1963 Nobel Prize in Physiology or Medicine. This method was usually useful to study large cell types such as the squid axon or giant snail neurons. In the past two decades the patch-clamp technique developed by Sakmann and Neher (Hamill et al., 1981; Neher and Sakmann, 1976; Neher et al., 1978), for which they were awarded the 1991 Nobel Prize in Physiology or Medicine, have been crucial in ion channel research. It allowed the study of smaller cells in many different configurations and measure or manipulate currents from single channels generating a lot of useful information that helped better understand these proteins.

This method, though very important for eukaryotic ion channels, have not been easily adaptable to prokaryotic ion channels, probably because the gating mechanism of these later proteins is not clearly understood. On the contrary, prokaryotic ion channels can be relatively easier to manipulate and overexpress.

As a result, functional information from bacterial channels has been generated using other methods (discussed elsewhere in this chapter). One of these methods most often used is the radioactive tracer uptake assay described above, but it suffers from serious drawbacks. So, to get deeper insight into the functional properties of our mutants, direct patching of reconstituted liposomes was employed in this study in addition to radioactive tracer uptake assay.

Among the many possible patch configurations (Hamill et al., 1981; Neher and Sakmann, 1976; Neher et al., 1978) one similar to the inside-out setup was employed in most measurements (Figure 3-3B) (all liposome patch-clamp experiments performed by WeiZhong Zeng). First, giant liposome was obtained by air drying 2-3 μ l of proteoliposome sample on a clean cover slip overnight at 4°C followed by rehydration in reconstitution solution at room temperature. Patch pipettes were pulled from Borosilicate glass (Harvard Apparatus) to a resistance of 8-12 M Ω . The pipette solution contains 150mM KCl or NaCl, 10mM HEPES, 1mM EGTA, pH 7.4 buffered with KOH or NaOH. The standard bath solution contains 150mM KCl, 10mM HEPES, 1mM EGTA, pH 7.4 buffered with KOH. A giga seal (> 10 G Ω) was obtained by gentle suction when the patch pipette attached to the giant liposome. To get a single layer of membrane in the patch, pipette was pulled away from the giant liposome and the tip was exposed to air for 1-2 seconds. Membrane voltage was controlled and current recorded using an Axopatch 200B amplifier with a Digidata 1322A analogue-to-digital converter

(Axon Instruments). Currents were low-pass filtered at 1 kHz and sampled at 20 kHz.

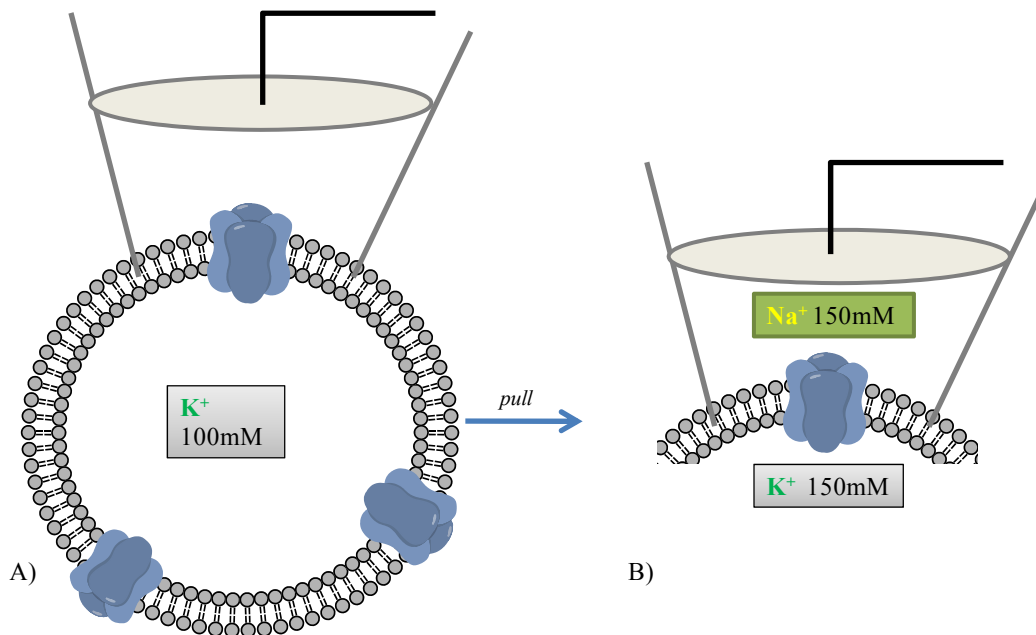


Figure 3-3 – Liposome preparation and generation of the giant liposome single channel patch clamping. Shown in (A) is proteoliposome prepared in 100mM KCl. Depicted in (B) is the representation of the patch generated from (A) and placed under bi-ionic conditions, equal concentrations of Na⁺ and K⁺ in the pipette and bath solutions, respectively. Configuration is similar to the inside-out patch setup of Sakmann and Neher (Hamill et al., 1981; Neher et al., 1978) in which a pipette with highly polished tip fuses with the vesicle membrane (A) and suction applied to create a giga seal. Pulling the pipette breaks the vesicle resulting in the inside-out patch setup (B). All liposome patching experiments done by WeiZhong Zeng.

In the study of extracellular Ca²⁺ blocking, various concentrations of Ca²⁺ were added to the bath solution. The free Ca²⁺ concentration in the range of 0-100 μM was controlled by mixing 5mM EGTA with an appropriate amount of CaCl₂

calculated using software MAXCHELATOR (MAXCHELATOR). No EGTA was added in the bath solution for $[Ca^{2+}]$ above 100 μ M. Owing to the two possible orientations of reconstituted NaK mutants in the liposomes, 30 μ M tetrapentyl ammonium (TPeA), an intracellular open pore blocker for NaK channel, was also added in the bath solution to ensure that the channel in the recording has its extracellular side facing the bath solution.

For cross validating structural findings a comparative electrophysiological study of eukaryotic bovine CNGA1 channel was undertaken (experiments performed by Yang Li). For this purpose, the gene encoding bovine retinal cyclic GMP-gated channel (CNGA1) was cloned into pcDNA3.1(+) plasmid between *EcoRI* and *XhoI* restriction endonuclease sites. The channel was expressed in HEK 293 cells by transfecting 2mL of culture with 1 μ g of plasmid. To assist in the selection of cells for patch, the cells were co-transfected with 0.02 μ g of GFP containing plasmid. The channel currents were recorded 2-4 days after transfection using outside-out patch configuration. Patch pipettes were pulled from borosilicate glass capillaries (World Precision Instruments) using a micropipette puller P-97 (Sutter Instruments Co.) and were polished (MF-83, Narishige) to a resistance of 2–3 M Ω . The pipette solution contains 170mM NaCl, 1mM cGMP, 10mM HEPES, 1mM EGTA and 3mM EDTA. The bath solution contains 170mM NaCl, 10mM HEPES and 3mM EDTA. Both solutions were adjusted to pH 7.6 with NaOH. For Ca^{2+} blockage assay, the free calcium

concentrations in the bath solution were controlled by mixing 3mM EDTA with appropriate amounts of CaCl_2 calculated by MAXCHELATOR (MAXCHELATOR). Membrane voltage was controlled and current recorded using an Axopatch 200B amplifier with a Digidata 1322A analogue-to-digital converter (Axon Instruments). Currents were low-pass filtered at 1 kHz and sampled at 10 kHz.

CHAPTER FOUR

Results

ION SELECTIVITY STUDIES OF CNG-MIMICKING NaK MUTANTS

All group IA and some group IIA cations can permeate through CNG channels (see literature review) with largely similar selectivity sequence among different CNG channels (Table III). These cations, despite having widely differing ionic radii, formal charges and other physico-chemical properties, permeate through CNG channels to a similar extent. As a member of pore loop family of ion channels, ion selectivity and permeation properties of CNG channels is determined by the organization of the selectivity filter. However, despite considerable functional characterization, detailed molecular understanding of CNG channel ion selectivity and permeation remains absent mainly due to lack of structural information of their selectivity filters. This study aims to get structural insight into the selectivity filter of CNG channels using NaK as a model system.

NaK is a prokaryotic non-selective cation channel permeable to several group IA and IIA cations (see literature review). It exhibits sequence and functional similarities with CNG channels. First, its selectivity filter sequence of TVGDG shares the T(V/I)G sequence of CNG channel selectivity filters. The Aspartate residue of NaK's selectivity filter is also at equivalent position as the

highly conserved, critical Glutamate residue of most CNG channel pores. Based on these similarities NaK was thought to be a bacterial homologue of CNG channel pores and its structure invoked to understand ion selectivity and permeation in the later. Indeed, the selectivity filter architecture of NaK shows marked variations from that of K^+ channels with only two ion binding sites, thought to underlie its non selective nature and divalent cation binding properties. Most importantly, work on the NaK channel demonstrates that selective Ca^{2+} chelation can be accomplished utilizing backbone carbonyl groups from the selectivity filter alone with nearby acidic residues imparting Ca^{2+} specificity via a through space interaction with the Ca^{2+} chelating groups. These principles learned from NaK likely hold true for CNG and other Ca^{2+} permeable channels. However, considerable discrepancies between NaK and CNG channels emerged upon close examination. First, other than the acidic residue, the protein sequence at the C-terminal end of their selectivity filters shows considerable variation both in amino acid composition and sequence length (Figure 3-1). In addition, the sub-milimolar affinity of external Ca^{2+} binding observed in NaK is much weaker than that of most CNG channels and an Asp-to-Glu mutation in the NaK filter leads to a higher Ca^{2+} binding affinity whereas the opposite holds true for CNG channels. These differences suggest that CNG channel selectivity filters may not adopt the same structure as NaK. Thus, to more accurately recapitulate the ion selectivity and Ca^{2+} blockage properties in CNG channels, several mutant NaK channels

were generated by altering its selectivity filter sequence to match those of CNG channels and determined their structures in complex with various cations at high resolution. Furthermore, a quantitative electrophysiological assay and a complimentary radioactive tracer assay which shows that the mutants share the same ion selectivity properties as CNG channels were established. All data strongly suggest that the mutant structures represent quite well the structures of CNG channel pores and provide novel insights into understanding the ion selectivity in CNG channels.

A sequence alignment between NaK, several K⁺ channels, and various CNG channels (Figure 3-1) shows that all three contain the conserved T(V/D)G sequence at the N-terminus of the selectivity filter. However, significant variations are observed in the C-terminal end of the selectivity filter. Majority of CNG channels contain a sequence of ETPP right at the C-terminal end of selectivity filter in which the conserved Glutamate plays an important role in Ca²⁺ binding. Several studies have shown that replacing the Glutamate with Aspartate enhances Ca²⁺ binding while replacing it with neutral residues (Asparagine or Glutamine) significantly diminishes the Ca²⁺ affinity (see literature review). CNG channels from insects contain an ETPT sequence while auxiliary subunits have either DTPP/L (A4 subunits) or GLPE/D (B subunits) sequence. The NaK channel has an amino acid sequence of DGNFS at the equivalent region which only shares the conserved acidic residue (Asp66) with most CNG channels.

Furthermore, the length of the sequence at this region seems to be one residue longer in NaK than in CNG channels. Accordingly, several mutant NaK channels with selectivity filters matching those of CNG channels were generated (see methodology). Specifically, the NaK filter sequence of TVGDGNFSP was replaced with TVGETPPP to mimic the filter of commonly seen CNG channels (A1, A2 & A3). Two other mutations were made specifically to study Ca²⁺ binding properties of the CNG-mimics: TVGDTPPP to mimic the Glu-to-Asp mutant of most common CNG channels or the less common auxiliary A4 CNG channel subunit and TVGNTPPP to mimic the Glu-to-Asn mutant. Two other modest mutations- TVGDTPSP and TVGNTSPS were also made with three of the four residues mutated to two (see methodology).

Functional Analyses- CNG-mimicking NaK mutants are non-selective

Biochemical characterization of mutant NaK channels indicate that despite a significant alteration of protein sequence in the filter region, they all exhibit similar biochemical properties as the wild-type NaK and can be purified as stable tetramers. The first issue to address was then their functional competence and for that the mutant proteins were reconstituted into lipid vesicles (see methodology). Two methods were employed to probe their ion selectivity properties – giant liposome patching for electrophysiological recordings and radioactive ⁸⁶Rb⁺ uptake assay. Results from the two methods complement each other. Based on

recent studies (Alam and Jiang, 2009b), the mutant constructs used for functional studies carried an additional Phe92Ala mutation and a deleted N-terminal M0 helix (N-terminal 19 residues), both modifications shown to increase ion flux through the channel pore and allow for robust single channel recordings or flux readings.

Single channel electrophysiological studies were performed as described in methodology section between ± 100 mV. To study channel conductance both the pipette solution and the bath solution contained 150mM KCl. For ion selectivity studies bi-ionic conditions were employed in which the pipette solution contained 150mM NaCl and the bath solution contained 150mM KCl (Figure 3-3B). Figure 4-1 presents single channel current traces at ± 80 mV and their corresponding I-V curves between ± 100 mV for NaK-ETPP (Figure 4-1A), NaK-DTPP (Figure 4-1B) and NaK-NTPP (Figure 4-19) recorded with 150mM KCl and 150mM NaCl in the bath and pipette solutions, respectively. The mutant channels exhibit a high single channel conductance in both directions with a reversal potential of 0 mV, which using a modified Goldman-Hodgkin-Katz equation (see below) gives a permeability ratio P_{Na^+}/P_{K^+} of 1, indicating that the channels are indeed non-selective and have virtually the same permeability for Na^+ and K^+ . All mutant channels also exhibit very high open probability (>0.9). Even though the channel's gating mechanism is not yet known, this high open probability greatly aided with the functional analysis in this study.

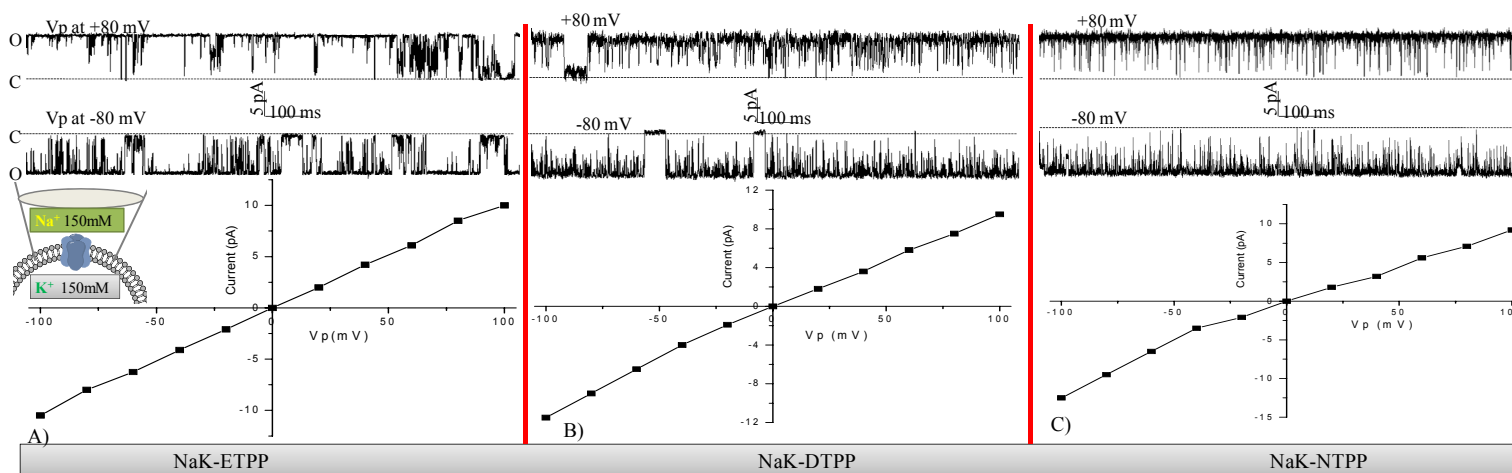


Figure 4-1 – Single channel traces of NaK-ETPP (A), NaK-DTPP (B) and NaK-NTPP (C) at ± 80 mV and their corresponding I-V curves between ± 100 mV. Currents were recorded using giant liposome patch with 150 mM NaCl and 150 mM KCl in the pipette and bath solutions, respectively, as shown on (A) and also Figure 3-3. Experiment performed by WeiZhong Zeng.

The Goldman-Hodgkin-Katz (GHK) voltage equation provides an expression for the membrane potential at which no net current flows (Hille, 2001). For a simple case of singly charged Na^+ , K^+ and Cl^- as the permeant ions, the GHK equation is given as follows:

$$E(\text{rev}) = \frac{RT}{F} \ln \frac{P_{\text{K}}[\text{K}]_{\text{o}} + P_{\text{Na}}[\text{Na}]_{\text{o}} + P_{\text{Cl}}[\text{Cl}]_{\text{i}}}{P_{\text{K}}[\text{K}]_{\text{i}} + P_{\text{Na}}[\text{Na}]_{\text{i}} + P_{\text{Cl}}[\text{Cl}]_{\text{o}}} \quad (\text{i})$$

$E(\text{rev})$ = reversal or zero current potential; potential at which no net current flows

R = universal gas constant, 8.314J/mole-K

T = temperature ($^{\circ}\text{K}$)

P_{X} = permeability of ion X (K^+ , Na^+ or Cl^-)

$[\text{X}]$ = concentration of the ions

$_{\text{o}}$, $_{\text{i}}$ = outside and inside, to refer to the two sides of the setup

Under the special case of bi-ionic conditions where equal concentrations of two ions are maintained in opposite ends of the setup (Figure 3-3), reversal potential measurements provide relative permeability of ions. So, for equal concentrations of NaCl and KCl on opposite sides, the above GHK equation reduces to equation (ii). In the giant liposome setup used for this study the two sides are the bath and pipette solutions, containing 150mM KCl and 150mM NaCl, respectively. Taking

this into consideration and rearranging gives a more simplified equation (iii), which upon more rearranging considering that K^+ and Na^+ are of equal concentration reduces to a simple equation (iv) to calculate permeability ratio of K^+ versus Na^+ by measuring the reversal potential. In our measurements the reversal potentials of the CNG-mimicking NaK mutants is zero, which using equation (iv) results a permeability ratio P_{Na^+}/P_{K^+} of 1.

$$E(\text{rev}) = \frac{RT}{F} \ln \frac{PK[K]_o + PNa[Na]_o}{PK[K]_i + PNa[Na]_i} \quad (\text{ii})$$

$$E(\text{rev}) = \frac{RT}{F} \ln \frac{PK[K]_{\text{bath}}}{PNa[Na]_{\text{pipette}}} \quad (\text{iii})$$

$$e^{\frac{FE(\text{rev})}{RT}} = \frac{PK}{PNa} \quad (\text{iv})$$

Giant liposome patching has unequivocally proved the non-selective nature of the mutants for Na^+ and K^+ . However, NaK was not amenable for electrophysiological studies until this method was developed very recently and early functional characterization of the mutants was done using the $^{86}\text{Rb}^+$ uptake assays. Results from these two functional analyses augment each other. More importantly, the $^{86}\text{Rb}^+$ uptake assay provides functional information on the mutant channels with respect to Li^+ and Rb^+ , in addition to K^+ and Na^+ and will be presented.

$^{86}\text{Rb}^+$ uptake assays were done for NaK-DTPS and NaK-ETPP liposomes loaded with 450mM LiCl, NaCl or KCl (see methodology) to assess permeability of the mutants for Li^+ , Na^+ and K^+ . Liposome preparation, protein reconstitution and uptake assays are as described in methodology. Since the proteoliposomes were prepared with very high salt (450mM) inside, upon placement in a very low concentration buffer (35 μM) (Figure 3-2A) an outwardly directed concentration gradient will be established. This gradient drives ions outside and if the channel conducts the cation, a resulting outflow would leave the negatively charged anions inside that drives partitioning of the external Rb^+ ions across the liposomal membrane and subsequent inflow of radioactive Rb^+ ions, provided the channel conducts Rb^+ . The extent and rate of radioactive Rb^+ accumulation depends on the amount of functional protein in the preparation and the number of ions that passed through these channels. This is monitored by scintillation counting and would indicate whether the channel conducts the cation or not. Shown in Figure 4-2A is time dependent $^{86}\text{Rb}^+$ accumulation into NaK-DTPS liposomes loaded with high Li^+ , Na^+ or K^+ . It can be observed that in all the three cases $^{86}\text{Rb}^+$ accumulates inside the liposomes saturating in a time dependent manner. Uptake assays performed with control liposomes, those without any reconstituted protein, did not show any appreciable accumulation. The extent of flux varies among the cations tested but does not necessarily imply preference of one ion over another because the difference presumably arose due to the limitations of the method, discussed

earlier. Nevertheless, the data reveals that NaK-DTPS conducts all of these monovalent cations- Li^+ , Na^+ , K^+ - and the tracer ion Rb^+ . Similarly, NaK-ETPP was shown to conduct Na^+ in addition to the tracer ion Rb^+ (Figure 4-2B) and also K^+ (not shown). The important outcome here is that these two CNG-mimicking mutants conduct most group I cations and the results agree well with the single-channel electrophysiological data.

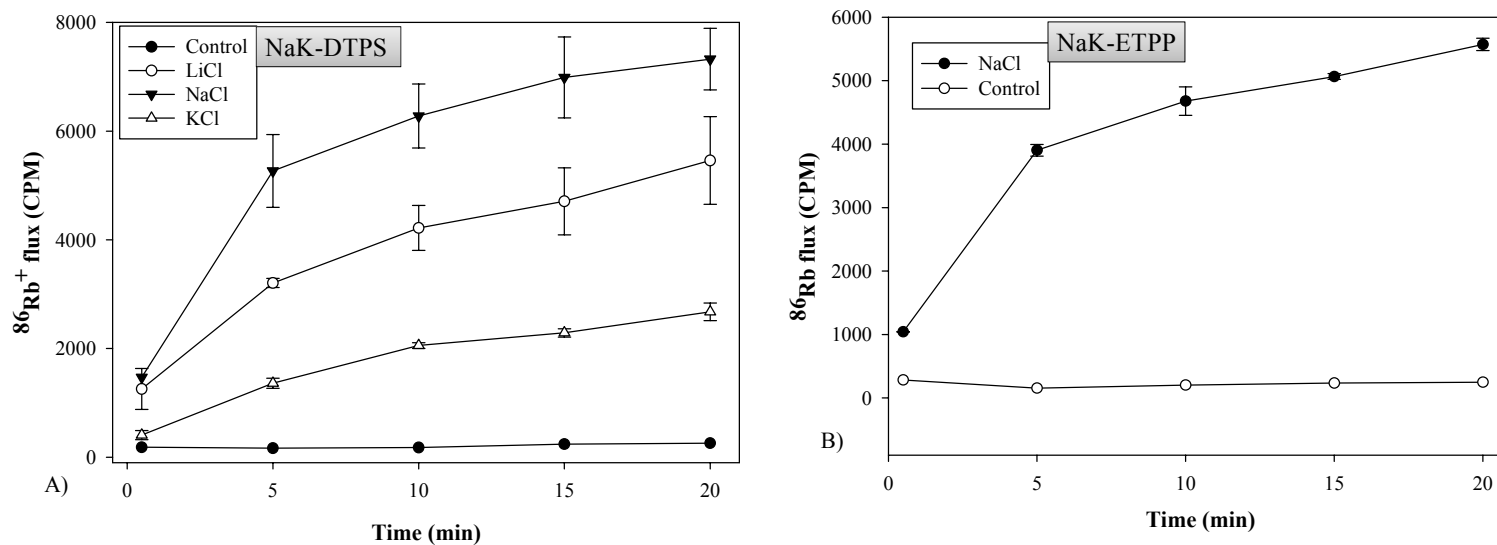


Figure 4-2 – $^{86}\text{Rb}^+$ flux into NaK-DTPS proteoliposomes loaded with 450mM KCl, NaCl or LiCl (A) and into NaK-ETPP proteoliposomes loaded with 450mM NaCl (B) in 3PE:PG at a protein to lipid ratio of 10 μg protein/mg lipid. Each data is an average of at least three trials and the error is as shown. The very bottom traces in both graphs are for control liposomes prepared in exactly the same as the proteoliposomes but without any added protein. $^{86}\text{Rb}^+$ flux readings are in counts per minute (CPM) of light flashes as read by the liquid scintillation counter.

Structural studies of CNG-mimicking NaK mutants

X-ray crystal structures are uniquely suitable to get information at atomic detail. Many recent detail understandings of key biological processes arose from such structural data. For instance, recent high resolution structures of several potassium channels have helped advance mechanistic understandings of underlying potassium channel biology to unprecedented level. As described in previous sections, that however is not the case for CNG channels as there has not been any reported high resolution structures hampering deeper insight into their biology.

To gain structural insights into CNG channel biology, especially their ion selectivity and permeation properties, the non-selective bacterial channel NaK was manipulated in this study to make its selectivity filter mimic those of CNG channels. The CNG-mimicking NaK mutants were crystallized and their structures determined to high resolution. CNG-mimicking NaK mutants were crystallized in similar conditions as the wild type NaK and their structures determined to resolutions ranging from 1.55 to 1.95 Å (Table IV and methodology). The mutants assumed the same overall structure as the recently determined open pore NaK Δ 19 (Figure 4-3) (Alam and Jiang, 2009a). However, significant structural differences were observed in the selectivity filter region between the wild type and mutant channels. Since all mutants share a similar overall architecture in their filters, NaK-DTPP mutant structure in

complex with K^+ will be used to illustrate their structural differences in the selectivity filter compared to NaK as well as the KcsA K^+ channels (Figure 4-3). The NaK-DTPP filter (Figure 4-3C) looks like intermediate between NaK (Figure 4-3D) and KcsA (Figure 4-3E) filters, containing three contiguous ion binding sites inside the filter labeled 2, 3 and 4 in comparison to KcsA's ion binding sites (Figure 4-3F-H). This conversion from wild type to mutant filter structures involves a dramatic main chain conformational change at the acidic residue (Asp66) and the preceding glycine (Gly65) (Figures 4-3, 4-4). In wild type NaK the backbone carbonyl groups of Gly65 and Asp66 moved away from the ion conduction pathway creating a vestibular structure (Shi et al., 2006). However, in NaK-DTPP Gly65 adopts the same main chain conformation as the equivalent glycine (Gly67) in KcsA with its backbone carbonyl pointing towards the central axis of the filter. This results in a replacement of the water-filled vestibule in NaK with an ion binding cage in the mutant utilizing the eight backbone carbonyl oxygen atoms from Val64 and Gly65 as ligands. The position of this site is equivalent to site 2 in the selectivity filter of KcsA and is therefore numbered so for comparison.

Table IV - Data collection and refinement statistics for NaK-DTPP, NaK-NTPP and NaK-ETPP in K^+ and K^+/Na^+ . Values in parenthesis are for highest resolution shell.

NaK mutant		NaK-DTPP		NaK-NTPP		NaK-ETPP		
In complex with ion- (100mM)		K^+	K^+/Na^+	K^+	K^+/Na^+	K^+	K^+/Na^+	
Data collection	Space group	I_4	I_4	I_4	I_4	I_4	I_4	
	Cell dimensions a=b, c (Å)	67.747, 89.444	67.840, 89.380	67.740, 89.789	67.780, 89.511	67.578, 89.996	67.570, 89.539	
	Resolution	50-1.62	50-1.58	50-1.58	50-1.62	50-1.95	50-1.95	
	R_{sym} (%)	4.8 (82.3)	4.9 (68.6)	5.6 (91.7)	4.0 (69.9)	6.4 (90.2)	7.1 (84.6)	
	$I/\sigma I$	39.2 (1.85)	42.9 (1.84)	38.3 (1.83)	44 (1.9)	34 (1.4)	28.4 (1.3)	
	Completeness	99.9 (100)	99.7 (100)	99.9 (100)	99.9 (100)	99.8 (99.1)	99.6 (97.4)	
	Redundancy	7.3 (7.2)	7.5 (7.4)	7.2 (7.0)	7.4 (7.3)	7.2 (4.9)	7.1 (5.1)	
Refinement	Resolution(Å)	1.62	1.58	1.58	1.62	1.95	1.95	
	No. reflections- total (unique)	187040 (25607)	206606 (27690)	124404 (17238)	188537 (25612)	106485 (14778)	104885 (14710)	
	R_{work}/R_{free}	20.7/22.2	21.8/23.5	20.9/21.4	21.2/22.7	20.2/23.9	20.4/22.8	
	No. of atoms	Protein	1446	1446	1446	1446	1448	1448
		MPD/ion	5/9	6/8	7/9	6/10	4/9	5/7
		Water	132	147	121	135	64	67
	R.m .s.d	Bond angles (Å)	1.074	1.074	1.089	1.107	1.086	1.097
Bond lengths (Å)		0.0051	0.0052	0.0051	0.0052	0.0054	0.0057	

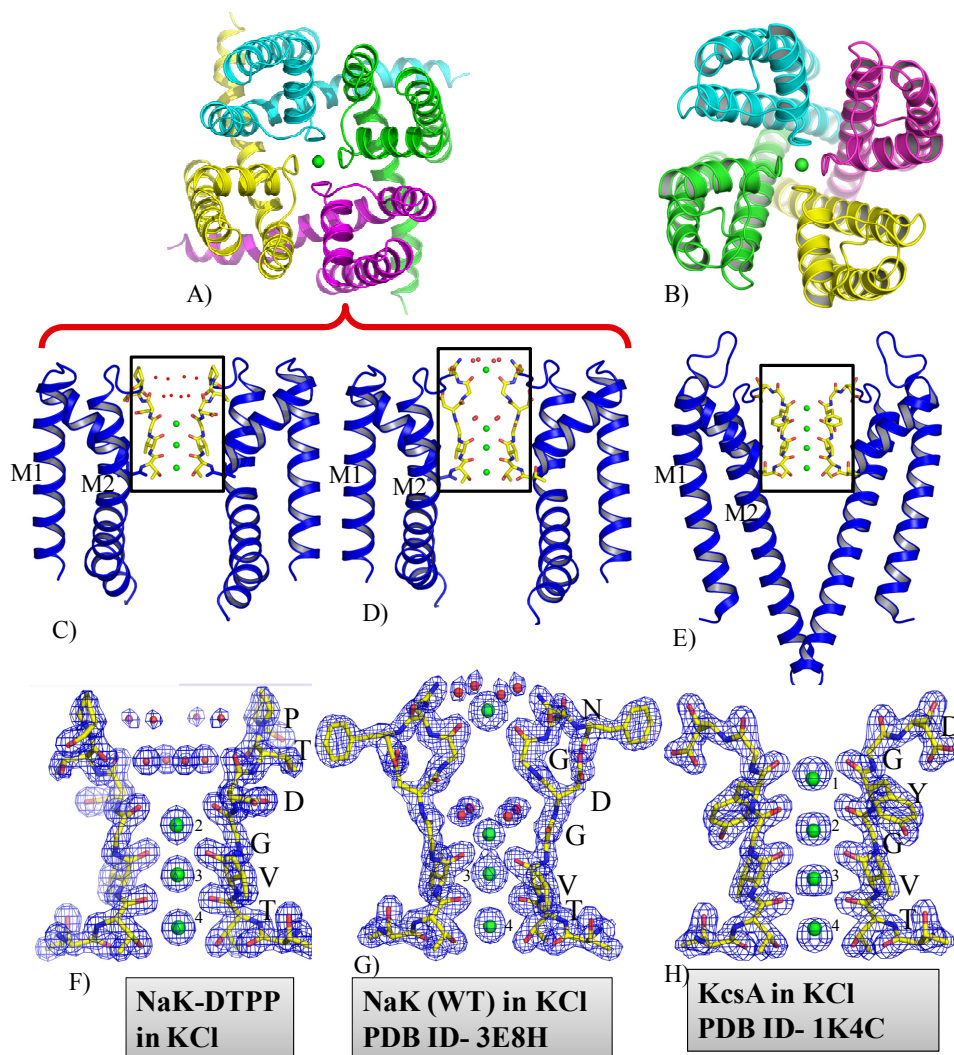


Figure 4-3 – Comparison of structures of NaK mutants using NaK-DTPP as an example with those of wild type NaKN Δ 19 and the KcsA. Top panel presents overall structures (top view) of NaK-DTPP or NaKN Δ 19 (A) and KcsA (B) showing the open conformation in the former and closed in KcsA. Middle panel presents ribbon representation of two subunits of NaK-DTPP (C), NaKN Δ 19 (D) and KcsA (E), front and back subunits removed for clarity. The selectivity filters are boxed and in ball-and-stick representation. M1 and M2 indicate outer and inner helices, respectively; red and green spheres represent water and K⁺ ions, respectively. Bottom panel presents close-up view of selectivity filter structures and 2Fo-Fc electron density maps (blue mesh) of K⁺ complexes of NaK-DTPP (F) (1.62Å) contoured at 2 σ , NaKN Δ 19 (G) (1.8Å) contoured at 1.5 σ and KcsA (H) (2.0Å) contoured at 2.0 σ . Numbers represent the ion binding sites in KcsA and their correspondents in NaK-DTPP and NaKN Δ 19.

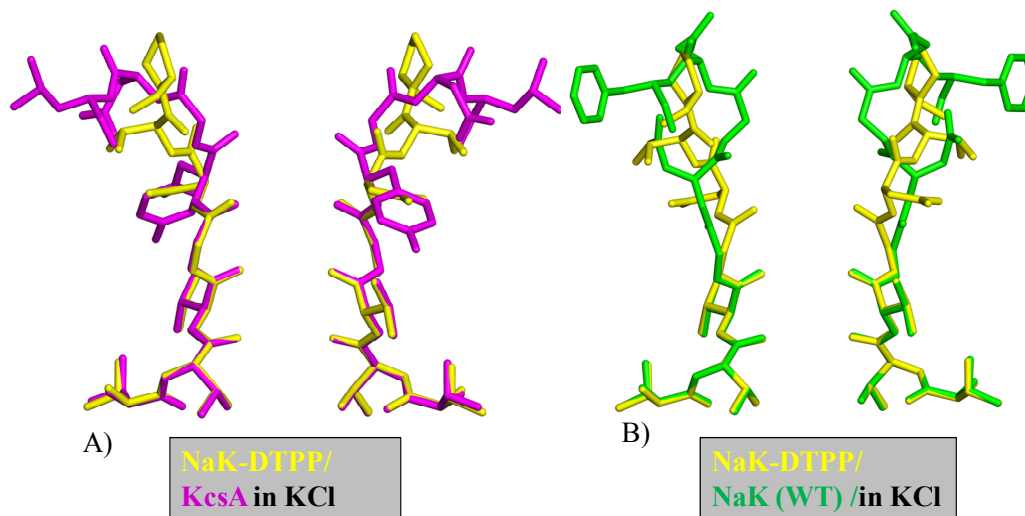


Figure 4-4 – Superimposition of the selectivity filter of NaK-DTPP (yellow) with that of KcsA (magenta) (A) and that of wild type NaK (green) (B).

The mutant structures also exhibit a concave funnel shaped external entryway with the pyrrolidine ring from the first Proline (Pro68) in the filter region, absolutely conserved in CNG channels, forming the wall of the funnel. Two layers of well ordered water molecules, four in each layer, are observed within the funnel (Figure 4-5). These water molecules form a hydration shell that participates in stabilizing various cations in the funnel before entering or exiting the filter. In particular, the four inner layer water molecules right above site 2, along with the 4 backbone carbonyl oxygen atoms from Gly65, form an ion binding cage at a position equivalent to site 1 of a K^+ channel. This site provides an ideal environment for a partially hydrated ion to transiently bind and enter the filter readily (Figure 4-5).

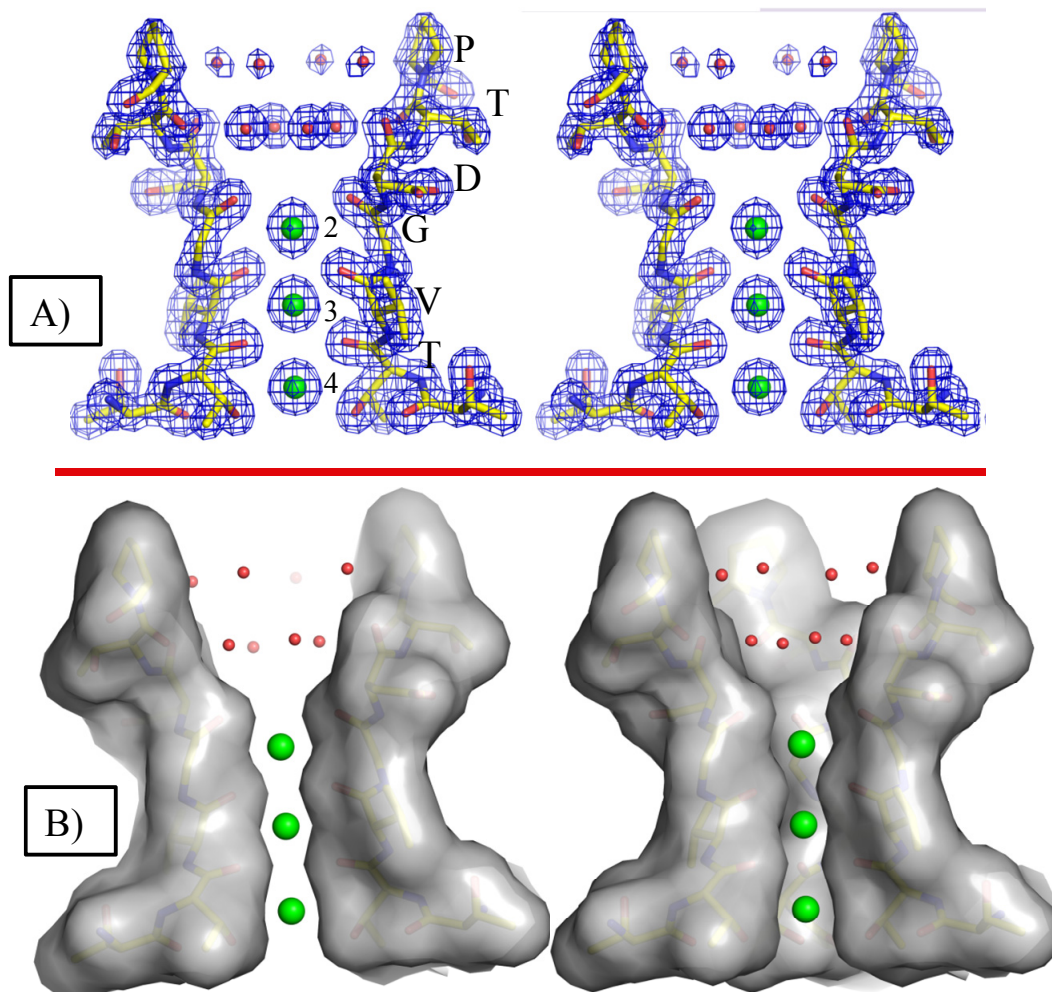


Figure 4-5 – Ordered water molecules and funnel shaped external entryway in selectivity filter of NaK-DTPP. Selectivity filter of NaK-DTPP in K^+ showing the funnel shaped external entryway and the two layers of ordered waters in the region and also the three K^+ ions occupying sites 2 to 4 in the filter. Shown in (A) is a stereo view of the NaK-DTPP selectivity filter (front and back subunits removed) and the $2F_o-F_c$ electron density map (1.62 \AA) contoured at 2.0σ (blue mesh). Bottom figures are surface representation of the selectivity filter with two (left) and one (right) subunits removed, for clarity purposes. Red and green spheres represent water and K^+ ions, respectively.

An important distinction exists among the CNG-mimicking mutants in their protein packing around the selectivity filter, owing to the different amino acid composition of residue 66. These differences likely account for different ion binding profiles and slightly different properties among the mutants. The side chain of residue 66 (Glu, Asp, or Asn) in all three mutants points tangential to the ion conduction pathway and is buried underneath the external surface of the protein (Figures 4-6, 4-7E). Nonetheless, it forms hydrogen bonding interactions with its neighboring residues in different ways. In NaK-DTPP, one of the carboxylate oxygen atoms from Asp66 forms a short range hydrogen bond with the hydroxyl group of Tyr55 (Figures 4-6A, 4-7B). Two buried water molecules reside nearby and mediate an extensive hydrogen bonding network involving the side chains of Asp66 from the neighboring subunit, the hydroxyl groups of Thr60 and Thr67, and the backbone amides of Asp66 and Thr67 (Figure 4-6A). No such water molecules are observed around the NaK-ETPP selectivity filter (Figure 4-6B). Unlike Asp66 in NaK-DTPP, the side chain carboxylate of Glu66 in NaK-ETPP does not interact with Tyr55 (Figures 4-6B, 4-7B). Instead, it forms a hydrogen bond directly with the hydroxyl oxygen of Thr60 from the neighboring subunit. Interestingly, the backbone carbonyl group of Glu66 in NaK-ETPP tilts away from the ion conduction pathway with its oxygen atom forming a hydrogen bond with the hydroxyl group of Tyr55, while the equivalent carbonyl group in

NaK-DTPP points upward and parallel to the ion conduction pathway (Figures 4-6A, B 4-7A, B).

Protein packing interactions in the filter region of NaK-NTPP are less extensive than those in NaK-DTPP (Figure 4-6C). The side chain of Asn66 in NaK-NTPP swings slightly left-ward compared to that of Asp66 in NaK-DTPP, leading to a slightly different hydrogen bonding pattern (Figures 4-6C, 4-7C, D). The γ -amide group of Asn66 interacts directly with hydroxyl group of Tyr55, similar to the carboxylate group of Asp66 in NaK-DTPP. However, only one buried water molecule is observed in NaK-NTPP that mediates the hydrogen bonding interactions between the hydroxyl groups of Thr60, Thr67 and the γ -amide nitrogen of Asn66 from a neighboring subunit. Finally, the Asn66 main chain carbonyl group is tilted slightly away from the central axis albeit not as significantly as the carbonyl group of Glu66 in NaK-ETPP (Figure 4-6C, 4-7C, D).

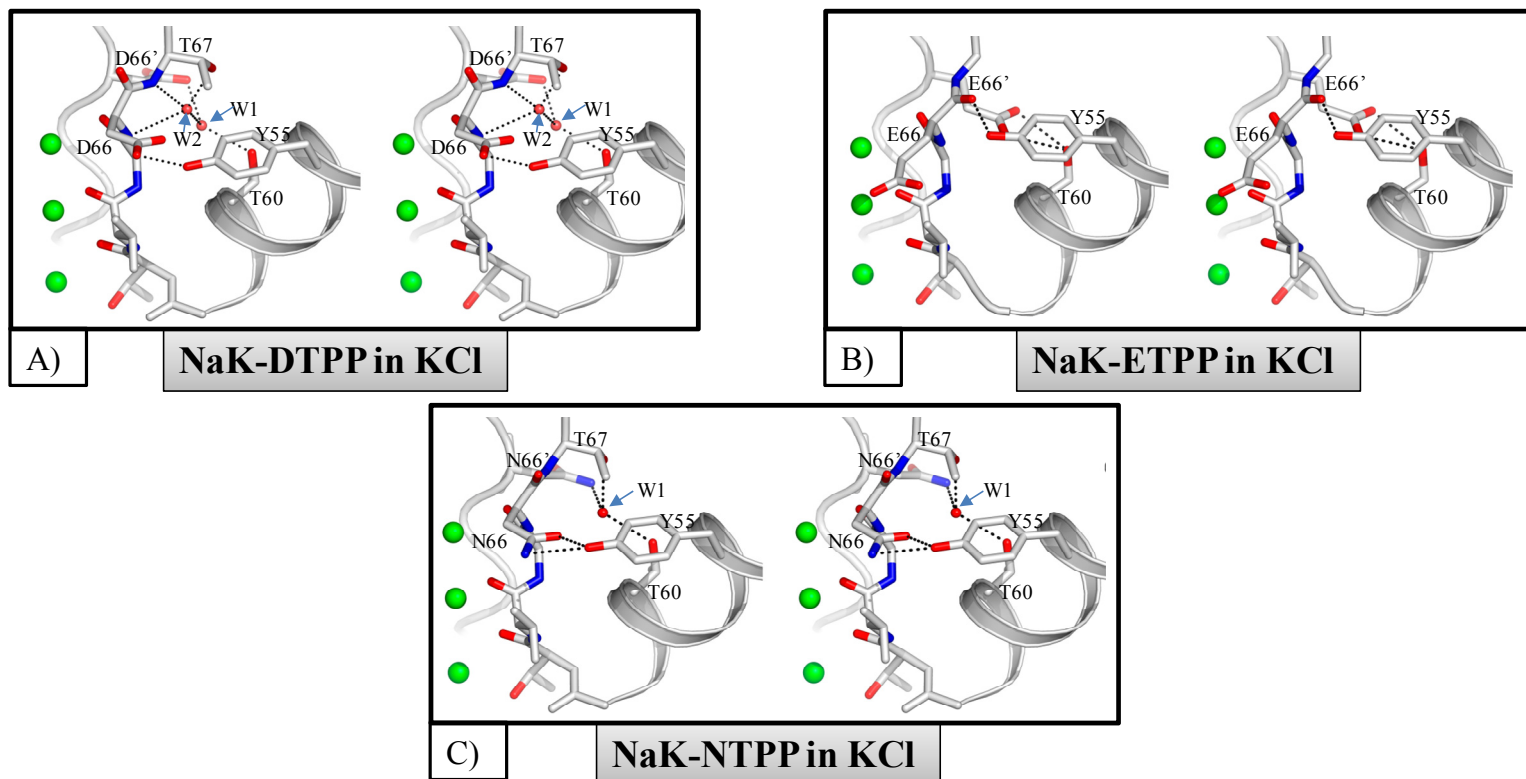


Figure 4-6 – Protein packing around the selectivity filters of CNG-mimicking mutants. Stereo view of the protein packing in NaK-DTPP (A), NaK-ETPP (B) and NaK-NTPP (C). Red spheres represent water molecules that mediate the hydrogen bonding network in NaK-DTPP and NaK-NTPP; residues from neighboring subunits are labeled with an apostrophe and three K^+ ions in the filter are drawn as green spheres.

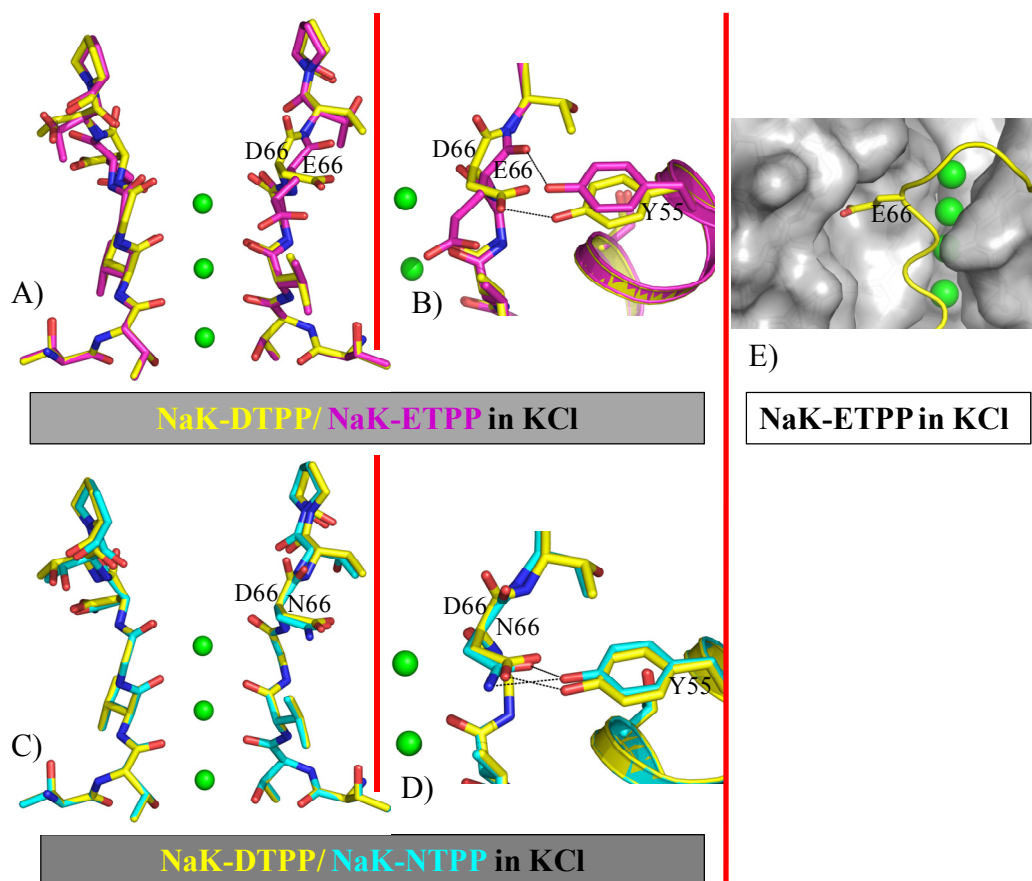


Figure 4-7 – Protein packing around residue 66 in the selectivity filters of CNG-mimicking mutants. (A) and (C) show superimposition of NaK-DTPP (carbon atoms in yellow) structure with NaK-ETPP (carbon atoms in magenta) and NaK-NTTP (carbon atoms in cyan), respectively, at region around residue 66. (B) and (D) show a close-up view of the region with the H-bonding interactions with the pore α -helix Y55. (E) is a surface representation of NaK-ETPP around the residue 66, three subunits shown as surface while the fourth (front) subunit is shown in a cartoon/stick representation.

Monovalent cation binding in the selectivity filter

Crystals of the K^+ complexes of all three CNG-mimicking mutants were obtained in the presence of 100mM KCl and their F_o-F_c ion omit maps reveal the respective K^+ binding profiles. In NaK-DTPP, three electron density peaks with equivalent intensity are observed in the filter, indicating K^+ binding with similar occupancy at each site (Figure 4-8A). A weaker electron density peak, likely from a K^+ ion with lower occupancy, is observed at the center of external funnel sandwiched between the two layers of water molecules. The K^+ binding profile of NaK-NTPP is similar to that of DTPP with three major K^+ binding sites in the filter except that a weakly bound K^+ ion is also observed at the external entrance (Figure 4-8B).

In NaK-ETPP, in addition to the three K^+ binding sites inside the filter, a strong electron density peak from a K^+ ion is observed at the external entrance, partially hydrated by the four inner layer water molecules (Figure 4-8C). In contrast to NaK-DTPP and NaK-NTPP, K^+ binding at the external entrance is much stronger whereas that at site 2 is weakened in NaK-ETPP. A structural comparison at site 2 between NaK-DTPP and NaK-ETPP provides a plausible explanation for this discrepancy (Figures 4-7A, 4-9A). In NaK-ETPP, the backbone carbonyl groups from Gly65s drift away from the central axis and are tilted more upward. This is a consequence of hydrogen bonding interaction between the main chain carbonyl of Glu66 and hydroxyl group of Tyr55, making

the carbonyl oxygen atoms of Gly65 less favorable ligands for K^+ at site 2 but more favorable for external K^+ binding.

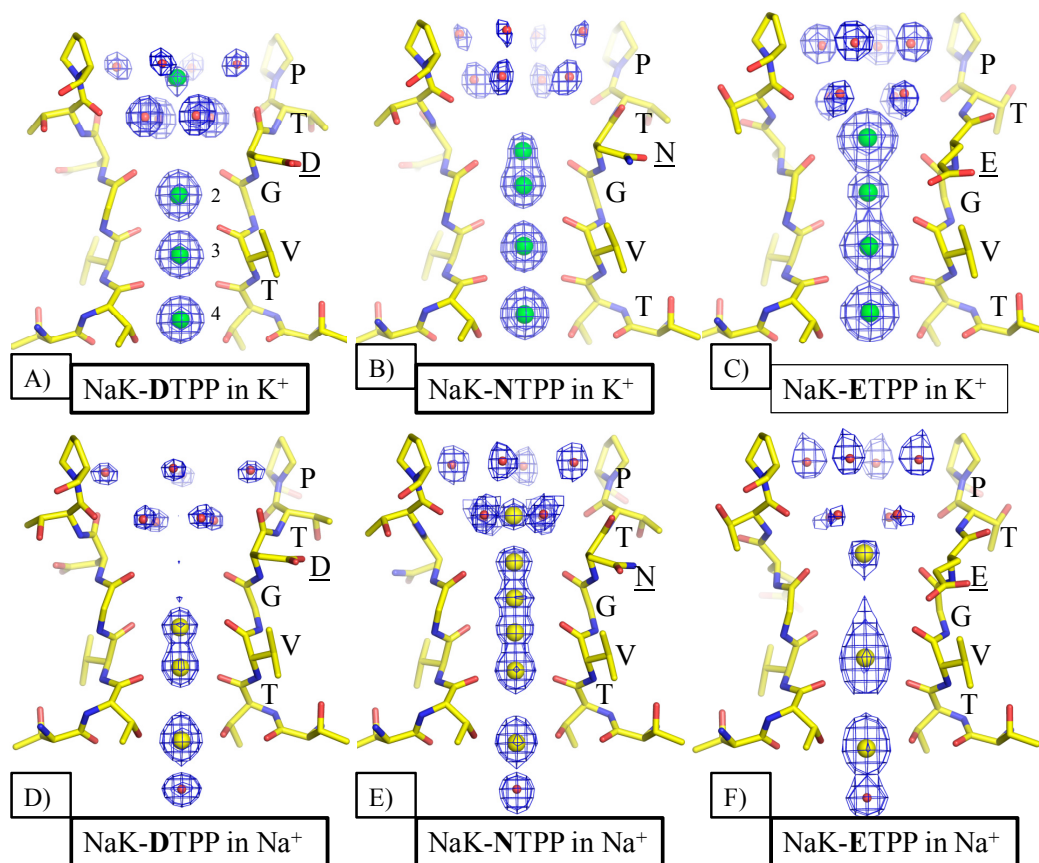


Figure 4-8 – K^+ and Na^+ binding in the selectivity filter of NaK mutants. Top panel- F_o-F_c ion omit maps at the selectivity filters of K^+ complexes of NaK-DTPP (A, 1.62 Å), NaK-NTPP (B, 1.58 Å) and NaK-ETPP (C, 1.95 Å) contoured at 4σ . Water molecules within the external funnel (red spheres) are also omitted in the map calculation. K^+ ions are represented by green spheres and ion binding sites 2, 3 & 4 are shown in comparison to structure of the KcsA K^+ channel structure. Bottom panel- F_o-F_c ion omit maps at the selectivity filters of Na^+ complexes of NaK-DTPP (D, 1.58 Å), NaK-NTPP (E, 1.62 Å) and NaK-ETPP (F, 1.95 Å) contoured at 4σ . Na^+ complex crystals were obtained by crystal soaking experiments. Na^+ ions are represented by yellow spheres.

Structures of mutants in Na^+ were determined by using K^+ complex crystals soaked in stabilization solutions containing 100mM NaCl (see methodology). No obvious structural changes were observed in the selectivity filters of all mutants after Na^+ soaking (Figure 4-9B), however Na^+ binding appears to be a bit more complicated than K^+ binding. As shown in the F_o-F_c ion omit maps of Na^+ complexes, Na^+ binding patterns in all mutants differ from the K^+ complexes (Figure 4-8). In the Na^+ complex of NaK-DTPP three strong peaks are observed at sites 3 and 4, two at the upper and lower edges of site 3 and the other on the lower edge of site 4 (Figure 4-8D). This indicates that in contrast to K^+ ions, Na^+ ions bind preferentially in a planar configuration with respect to their ligands, the backbone carbonyl oxygen atoms. In the cavity just below site 4, a water molecule, which is not observed in the K^+ complex, participate in the chelation of Na^+ ion at the lower edge of site 4. This suggests that Na^+ prefers a square planar or square-pyramidal coordination, in sharp contrast to the square-bipyramidal configuration of K^+ in either NaK or K^+ channels. A similar square pyramidal ion chelation was observed in the Na^+ complex of the wild type NaK channel (Alam and Jiang, 2009b). Some weaker electron density is also observed in the center of site 2 and at the external entrance likely arising from low occupancy Na^+ binding. The Na^+ complex of NaK-NTPP shares a similar ion binding profile as NaK-DTPP except that Na^+ binding at site 2 and the external entrance appears stronger (Figure 4-8E). In NaK-NTPP, a hydrated Na^+ ion is also

observed in the concave funnel above the external entrance, chelated by the four inner layer water molecules in the same planar manner as in the filter with Na^+ ion- ligand (water) distance of $\sim 2.4 \text{ \AA}$. This hydrated Na^+ ion is also observed in NaK-DTPP but with weaker electron density indicating a lower occupancy. In comparison, the Na^+ binding profile in NaK-ETPP is different, in particular, at site 3. As shown in the $F_o - F_c$ ion omit map of the Na^+ complex of NaK-ETPP (Figure 4-8F), the electron density at site 3 is more diffused and football shaped which cannot be assigned as a single Na^+ ion in the center and likely arises from the averaged configurations of Na^+ binding at the center and the upper and lower edges, with the central position being preferred.

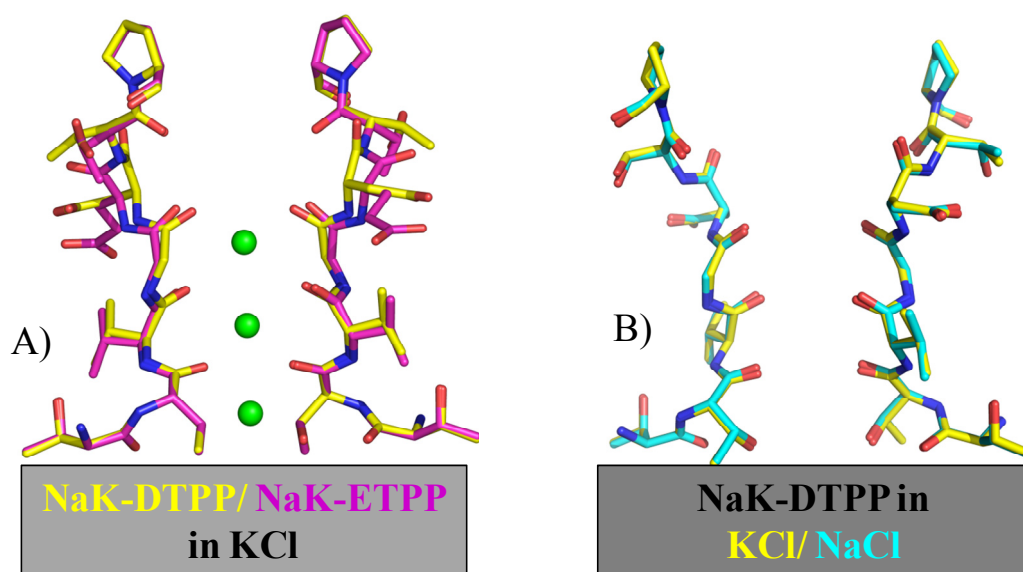


Figure 4-9 – A) Structural alignment of NaK-ETPP and NaK-DTPP. Important distinction exists especially at site 2 that may account for their different ion binding profiles. B) Structural alignment of NaK-DTPP in K and in Na.

DIVALENT CATION BINDING/BLOCKAGE

IN CNG-MIMICKING NAK MUTANTS

In CNG channels of photoreceptors and olfactory sensory neurons Ca^{2+} entry serves as a signal important for both excitation and adaptation. Ca^{2+} is a permeating blocker – it can permeate through CNG channels and subsequently block monovalent cation current, especially Na^+ , which has important physiological implications. In photoreceptors for instance this property allows for highly sensitive detection of light because Ca^{2+} blockage of Na^+ current reduces channel conductance, giving rise to low membrane potential noise. Several approaches were taken to study this property in these CNG-mimicking NaK mutants because if they are to be structural models of the former, they should exhibit this property closely. The design of the NaK mutants was also partly based on this property.

Though the detail mechanism is yet to be understood it is well established that the presence of an acidic residue at the extracellular mouth of the CNG channels is a necessary condition to exhibit calcium permeation and blockage properties. Conforming to that mostly occurring CNG channel forming A subunits (A1 – A3) carry a Glutamate residue with a selectivity filter sequence of TIGETPP. Replacing the Glutamate with Aspartate was shown to enhance Ca^{2+}

binding while replacing it with neutral residues, Asparagine or Glutamine, significantly diminish the Ca^{2+} affinity. Some less common or auxiliary CNG channels also carry an acidic residue at the equivalent position as the Glutamate. CNG channels from insects carry a Glutamate with a sequence of TIGETPT and the slightly different CNGA4 of olfactory sensory neurons, which is grouped with CNGA subunits because of its sequence homology but considered to be an auxiliary subunit, also carries an acidic residue, an Aspartate, with a sequence of TVGDTPP/L. So, NaK-ETPP is designed to mimic the filter of commonly seen CNG channels (A1, A2, A3), NaK-DTPP/S to mimic the charge-conservative Glu-to-Asp mutation of CNG channels or the less common A4 CNG channel subunit, and NaK-NTPP/S to mimic the Glu-to-Asn mutant of CNG channels to study the effect of neutralizing the negative charge on Ca^{2+} binding. These mutants were shown to form stable tetramers, maintain same overall structure with wild type NaK and behave similarly in Na^+/K^+ selectivity, though key differences exist in protein packing and ion binding profiles among these CNG mimics (previous section).

Functional analyses

The two methods described previously – radioactive uptake and liposome patch-clamping – were employed to assay the Ca^{2+} permeation and blockage property in the CNG-mimicking NaK mutants. For radioactive uptake assays the

competition assay (see methodology) (Figure 3-2B) was performed with NaK-ETPP and the modest mutants NaK-DTPS and NaK-NTPS. Note that NaK-DTPS and NaK-NTPS have virtually the same structure as NaK-DTPP and NaK-NTPP, respectively. The principle behind the competition assay is simple: when the external solution contains Ca^{2+} (at different concentrations) in addition to the radioactive test cation and tracer ion $^{86}\text{Rb}^+$, permeation by Ca^{2+} , if any, will compete with the tracer ion thereby reducing the amount of $^{86}\text{Rb}^+$ accumulation inside the liposome in a concentration dependent manner. A plot of normalized $^{86}\text{Rb}^+$ influx as a function of Ca^{2+} concentration is shown in Figure 4-10. Two important observations are clear from the figure. First, the neutral residue mutant NaK-NTPS does not show any appreciable Ca^{2+} competition while both NaK-DTPS and NaK-ETPP show strong Ca^{2+} competition implying the necessity of an acidic residue for Ca^{2+} to permeate through. Second, NaK-DTPS exhibits a slightly stronger effect than NaK-ETPP. These observations are consistent with what has been observed with eukaryotic CNG channels: Glu-to-Asp mutation enhances Ca^{2+} blocking effect while Glu-to-Asn severely reduces it.

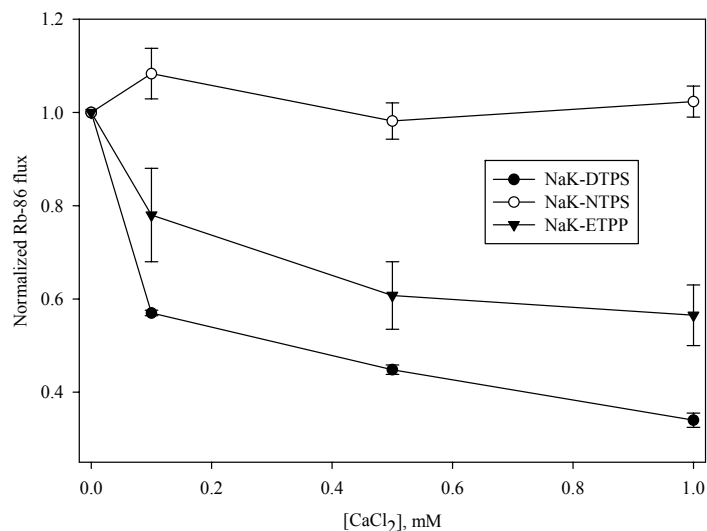


Figure 4-10 – Ca^{2+} competition in NaK mutants– the effect of increasing Ca^{2+} concentration on radioactive $^{86}\text{Rb}^{+}$ influx into proteoliposomes containing NaK-ETPP, NaK-DTPS and NaK-NTPS. Ca^{2+} increasingly impairs $^{86}\text{Rb}^{+}$ influx in NaK-DTPS and NaK-ETPP, more so in the former, but no effect in NaK-NTPS. Proteoliposomes were loaded with 450mM NaCl and contained 10 μg protein per mg lipid of composition 3PE:PG (see methodology).

The above competition assay clearly showed the effect of Ca^{2+} on the $^{86}\text{Rb}^{+}$ flux. This assay, while could be informative, is however crude by its very nature and its usefulness is limited for many reasons. For instance, it is not possible to monitor or know the directionality of the protein in the liposome. More detailed quantitative information is obtained using single channel electrophysiological methods. So, electrophysiological recordings were performed with proteoliposomes containing NaK-ETPP, NaK-DTPP and NaK-NTPP using giant liposome patch clamping, in an inside-out configuration, specifically aimed at assaying the effect of external Ca^{2+} . In this assay, various concentrations of

Ca²⁺ were added to the external side (bath solution) of the channel in addition to 150mM K⁺ (see methodology). Tetrapentyl ammonium (TPeA), an intracellular open pore blocker of NaK and K⁺ channels, was added to the bath solution to make sure that only channels with their extracellular side facing the bath solution are assayed. As shown in single channel traces (Figure 4-11), the ‘inward’ K⁺ currents in NaK-ETPP (Figure 4-11A) and NaK-DTPP (Figure 4-11B) decrease with increasing Ca²⁺ concentration whereas NaK-NTPP (Figure 4-11C) has almost no sensitivity to external Ca²⁺. Least-squares fit using the Hill equation (equation V) of unblocked current versus Ca²⁺ concentration provides the inhibition constant (*K_i*), the Ca²⁺ concentration at half maximal current. Accordingly, *K_i*s of NaK-ETPP and NaK-DTPP were calculated to be 72.4 μM and 8.1 μM at -80 mV, respectively (Figure 4-11D). This result agrees quite well with previous reports on eukaryotic CNG channels that showed a Glu-to-Asp mutation in the filter enhancing Ca²⁺ blockage while Glu-to-Asn mutation severely reducing such effect (Eismann et al., 1994; Gavazzo et al., 2000; Park and MacKinnon, 1995; Seifert et al., 1999).

$$I/I_{max} = I - \langle [Ca]^n / ([Ca]^n + K_i^n) \rangle \quad (V)$$

I- Current measured in the presence of Ca²⁺; *I_{max}*- current measured in the absence of Ca²⁺; *K_i*- inhibition coefficient and *n*- Hill coefficient.

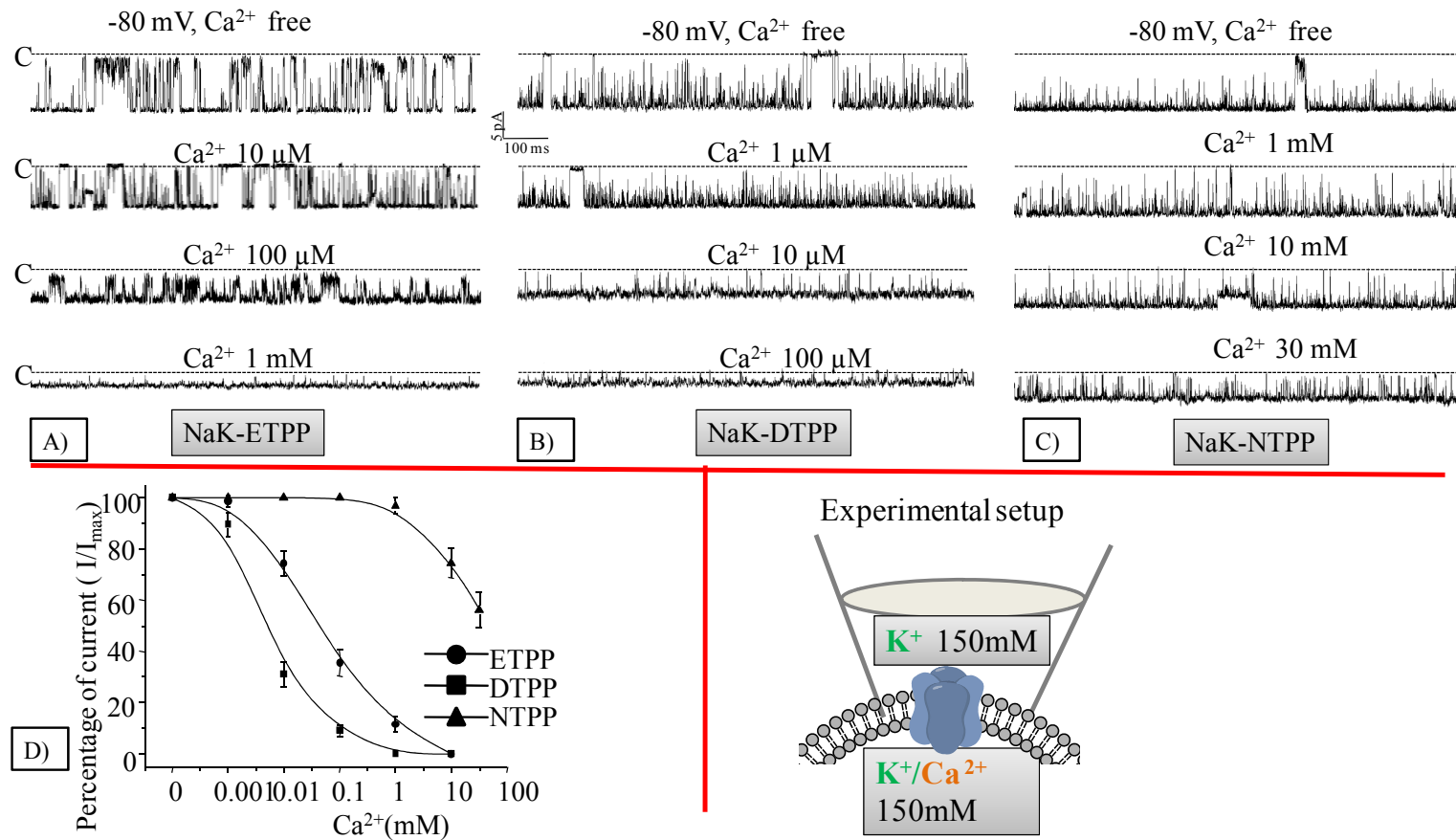


Figure 4-11 – Ca^{2+} blockage and permeation in NaK mutants. Top panel- single channel traces of NaK-ETPP (left traces), NaK-DTPP (middle traces) and NaK-NTPP (right traces) recorded at -80 mV in the presence of various concentrations of Ca^{2+} at the external side. Both pipette and bath solutions contain symmetrical 150mM KCl. The

bath solutions also contain 30 μ M tetrapentyl ammonium (TPeA) to ensure that all mutant channels in the single channel recordings have their extracellular side facing the bath solution. Bottom panel- Plot of fraction of unblocked single channel currents recorded at -80 mV as a function of external Ca^{2+} concentrations (left). Data points are mean \pm SEM from 4 measurements and are fitted to Langmuir functions with K_{is} of 72.4 μ M for NaK-ETPP and 8.1 μ M for NaK-DTPP. Experiment performed by WeiZhong Zeng.

In eukaryotic CNG channels Ca^{2+} is a permeable blocker. Same is believed to be true for NaK-ETPP and NaK-DTPP because Ca^{2+} does not completely block the current in the recordings, which indicates rapid dissociation and association of Ca^{2+} in the filter. In support of this, single channel recordings on NaK-ETPP with 100mM CaCl_2 on the internal side and 150mM KCl on the other shows a clear outward Ca^{2+} current, albeit with low conductance (Figure 4-12). Addition of tetrapentyl ammonium (TPeA), an open pore blocker for NaK and K^+ channels, leads to a complete block of the observed Ca^{2+} current in NaK-ETPP (bottom trace).

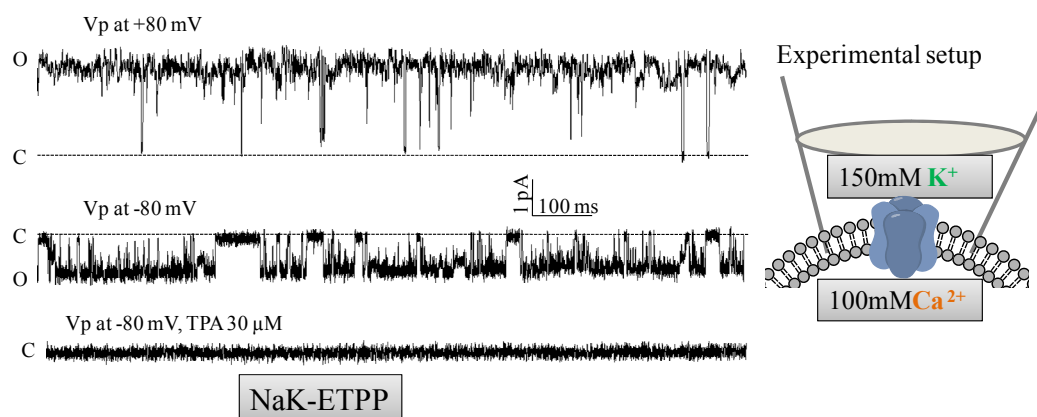


Figure 4-12 – Ca^{2+} current in NaK-ETPP. Single channel traces of NaK-ETPP recorded at +/- 80 mV with 150mM KCl in the pipette and 100mM CaCl_2 in the bath solution. The single channel in the recordings has its intracellular side facing the bath solution and can be blocked by addition of 30 μ M TPeA (bottom trace).

Structural basis of divalent cation blockage in CNG-mimicking NaK mutants

Structural analysis of mutants for their divalent cation binding was performed with respect to Ca^{2+} and Ba^{2+} . Structures of mutants in complex with Ba^{2+} were obtained from crystals of K^+ complexes soaked in 100mM KCl/10mM BaCl_2 . On the other hand, since K^+ and Ca^{2+} have the same number of electrons making it difficult to distinguish between them simply from the change in electron density, the Ca^{2+} complexes were obtained by crystal soaking in stabilization solutions containing 100mM NaCl / 25mM CaCl_2 . These $\text{Na}^+/\text{Ca}^{2+}$ soaked crystals were compared with the Na^+ soaked crystals using $F_{\text{Na/Ca-soak}} - F_{\text{Na-soak}}$ difference Fourier maps to determine whether and where Ca^{2+} binds. The structures of both sets revealed several interesting and complex features as shown in the difference maps of the mutants between soaked and native crystals (Figures 4-13 & 5-2).

Similar to wild type NaK, Ba^{2+} binding in these CNG-mimicking NaK mutants is in stark contrast to that observed in K^+ channels. In K^+ channels site 4 is the major binding site for Ba^{2+} (Jiang and MacKinnon, 2000; Lockless et al., 2007), however no Ba^{2+} binding is observed at site 4 in these NaK mutants (Figure 4-13) as well as wild type NaK (Alam and Jiang, 2009b). Differences also exist in their Ba^{2+} binding among these CNG-mimicking NaK mutants. In NaK-ETPP, Ba^{2+} only binds at the external entrance and is partially hydrated by the four inner layer water molecules, but not within the filter (Figure 4-13A). In NaK-

DTPP and NaK-NTPP, Ba^{2+} binds at both the external entrance and site 3 (Figure 4-13 B&C). However, Ba^{2+} binding at site 3 of NaK-NTPP is much weaker than that at external entrance.

Ca^{2+} binding is also slightly different among the mutants and a bit more complicated than Ba^{2+} binding. The $F_{\text{Na/Ca-soak}} - F_{\text{Na-soak}}$ difference map of NaK-ETPP indicates a single Ca^{2+} bound at site 3 (Figure 4-13D). In contrast, the difference map of NaK-DTPP reveals four major peaks along the ion conduction pathway: three at sites 2 to 4 inside the filter and one within the funnel just above the external entrance (Figure 4-13E). Which of these are due to Ca^{2+} binding or did not arise from Na^+ , which is also present in the soaking conditions? To verify this, diffraction data collected from $\text{Na}^+/\text{Ca}^{2+}$ soaked crystals at long wavelength ($\lambda = 1.5 \text{ \AA}$) was employed. At this wavelength only Ca^{2+} ions in the protein have significant anomalous scattering (Merritt). The anomalous difference Fourier map calculated under this condition revealed three peaks at the same positions as the top three observed in the $F_{\text{Na/Ca-soak}} - F_{\text{Na-soak}}$ difference map confirming Ca^{2+} binding at sites 2, 3 and above the external entrance (Figure 4-13G). In the control experiment, the anomalous difference Fourier map from the Na^+ soaked NaK-DTPP crystal does not show anomalous scattering in the filter (Figure 4-13H). The fourth peak in the $F_{\text{Na/Ca-soak}} - F_{\text{Na-soak}}$ difference map of NaK-DTPP is thus likely due to the redistribution of Na^+ at site 4 upon Ca^{2+} binding.

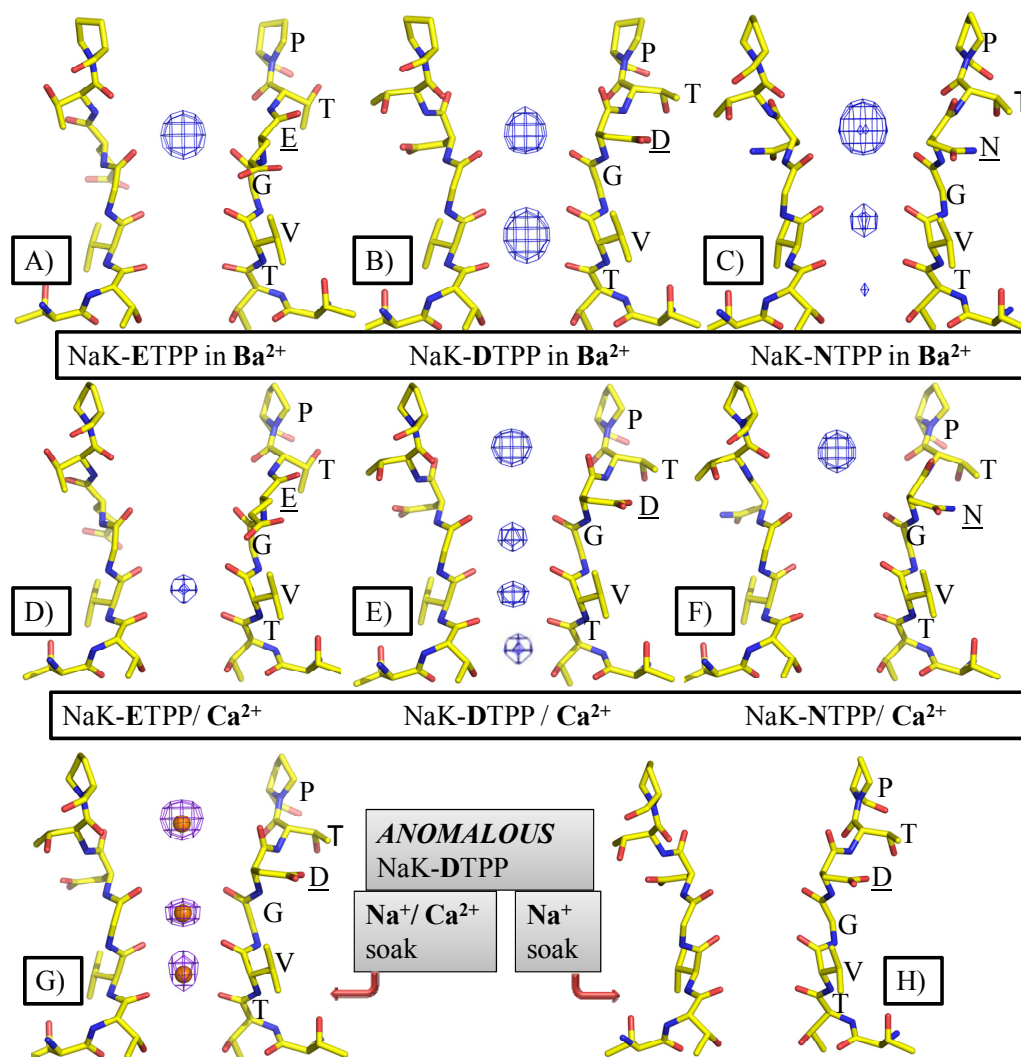


Figure 4-13 – Divalent cation binding in the selectivity filter of NaK mutants. Top panel shows $F_{\text{soak}}-F_{\text{reference}}$ difference Fourier maps between K⁺ complex crystals (reference) and crystals soaked in the presence of 10mM BaCl₂ (soak). Maps are countered at 10 σ with resolution of 2.0 Å for NaK-ETPP, 1.9 Å for NaK-DTPP and 1.9 Å for NaK-NTPP. Middle panel presents $F_{\text{Na/Ca-soak}}-F_{\text{Na-soak}}$ difference Fourier maps between mutant crystals soaked in stabilization solutions containing 100mM NaCl (Na-soak as reference crystals) and in solutions containing both 100mM NaCl and 25mM CaCl₂ (Na/Ca-soak). Maps are countered at 8 σ with resolution of 2.0 Å for NaK-ETPP, 1.8 Å for NaK-DTPP and 1.8 Å for NaK-NTPP. Bottom panel shows anomalous difference Fourier map (red mesh, at 1.9 Å and contoured at 5 σ) of Ca²⁺ and/or Na⁺ soaked NaK-DTPP crystal indicates the positions of bound Ca²⁺ ions (orange spheres). The data was collected using X-ray beam at 1.5Å wavelength to maximize the Ca²⁺ anomalous signal.

The $F_{\text{Na/Ca-soak}} - F_{\text{Na-soak}}$ difference map for NaK-NTPP shows a single electron density peak within the funnel at the same position as the external peak observed in NaK-DTPP, (Figure 4-13E) indicating that, compared to NaK-DTPP, Ca^{2+} does not bind inside the selectivity filter of NaK-NTPP but external Ca^{2+} binding is retained. Unlike external Ba^{2+} binding which occurs at the external entrance and is partially chelated by the backbone carbonyl oxygen atoms of Gly65 (Figure 4-13A-C), the position of this externally bound Ca^{2+} in NaK-NTPP or NaK-DTPP is slightly above the external entrance, at the same position as the hydrated Na^+ ion observed in the Na^+ complexes. Refined structures from the Na/Ca soaked crystals of both mutants reveal that the external Ca^{2+} is also hydrated by the inner layer of water molecules similar to Na^+ in Na^+ complexes and has no direct interactions with the protein (Figure 4-14E-I). This external Ca^{2+} binding observed in both NaK-NTPP and NaK-DTPP is thus believed to be non-specific and simply arises from the competition between hydrated Na^+ and Ca^{2+} ions within the funnel at high Ca^{2+} concentration. This is consistent with the functional analysis described above which shows that in NaK-NTPP external Ca^{2+} causes reduction in channel current only at high concentrations.

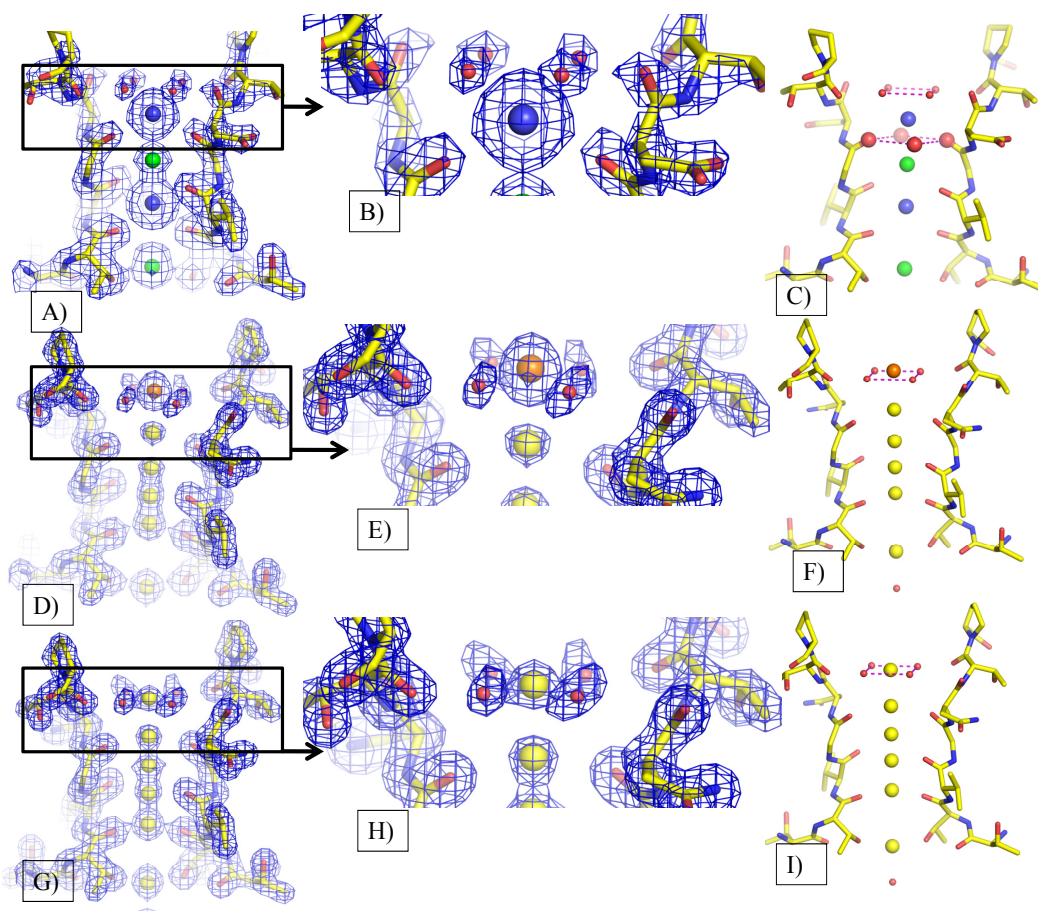


Figure 4-14 – Divalent cation binding in the extracellular entryway. Selectivity filter structures and $2fo-fc$ maps (blue mesh) of NaK-DTPP in Ba^{2+} (1.9\AA , 2σ), A-C, NaK-NTTP in Ca^{2+} (1.62\AA , 2σ), D-F and NaK-NTTP in Na^{+} (1.62\AA , 2σ), G-I. Ba^{2+} (blue spheres) binds close to the entrance directly chelated by backbone carbonyl groups of Gly65 (A-C). On the other hand, Ca^{2+} (orange spheres) binds slightly above the entrance (D-F) and is not directly chelated by backbone carbonyl groups but rather only by water ligands, similar to Na^{+} (yellow spheres) binding (G-I) in the extracellular entryway. Big and small red spheres represent oxygen and water, respectively. Green spheres are K^{+} ions.

TESTING THE VIABILITY OF CNG-MIMICKING NAK MUTANTS

CNG-mimicking NaK mutants exhibit many hallmarks of eukaryotic CNG channels. Can the structures then be used as accurate models for eukaryotic CNG channel selectivity filters? Several experiments were performed to validate the viability of the mutants as structural models for eukaryotic CNG channels. A simple structural based mutagenesis study was performed both on NaK-ETPP and bovine retinal CNG channel (CNGA1) using the structure of NaK-ETPP as a model. In the NaK-ETPP structure, the carboxylate group of Glu66 forms a hydrogen bond directly with the hydroxyl group of Thr60 from a neighboring subunit (Figure 4-6B). Interestingly, CNG channels have an extremely conserved Threonine residue at a position equivalent to Thr60 of NaK (Figure 3-1). Is this interaction between the acidic residue carboxylate group and Threonine's hydroxyl group of NaK a necessary structural/packing interaction in CNG channels and in NaK-ETPP? Structure based mutagenesis was performed to test whether such an interaction exists in eukaryotic CNG channels and cross validate with NaK-ETPP. First, mutations were introduced to the bovine retinal CNGA1 channel at positions equivalent to Thr60 and Glu66 of NaK-ETPP. Specifically, Thr357 and/or Glu363 of the bovine retinal CNGA1 channel were mutated to affect the H-bonding interaction, if any. A single T357E mutation failed to yield functional channels. However, a double exchange mutation E363T/T357E

resulted in a functional channel that conducts monovalent cations just like wild type channel, but is no longer blocked by external Ca^{2+} (Figure 4-15). Second, a similar E66T/T60E exchange double mutation on NaK-ETPP yielded a channel that was strikingly similar to the swap mutation of CNGA1: the channel conducts Na^+ and K^+ just like NaK-ETPP but is no longer sensitive to external Ca^{2+} blockage (Figure 4-16). These results confirm the direct interaction between the Glu363 and Thr357 in CNG channels and also demonstrate the importance of the exact position of the glutamate side chain in Ca^{2+} binding. The almost identical behavior also validates NaK-ETPP as a viable structural model for CNG channels.

Additional point mutations aimed at modifying the H-bond on NaK-ETPP resulted either in non-expression (T60A and T60S) or a channel with different kinetics (T60V). The NaK-ETPP T60V mutant, despite similar expression profile and I/V curve as NaK-ETPP, exhibited different single channel kinetics (Figure 4-17): the current became much smaller and closed durations longer than in NaK-ETPP. However, similar to NaK-ETPP, it exhibits Ca^{2+} blockage properties, albeit weaker. These data might indicate that, despite the absence of the H-bonding interaction the T60V mutant still maintains the tetrameric structure and, because the acidic residue is undisturbed, exhibits the Ca^{2+} blockage property but the structure may have rearranged to an unknown extent which may account for weaker Ca^{2+} blockage property. Crystallization attempts of these NaK-ETPP mutants were unsuccessful.

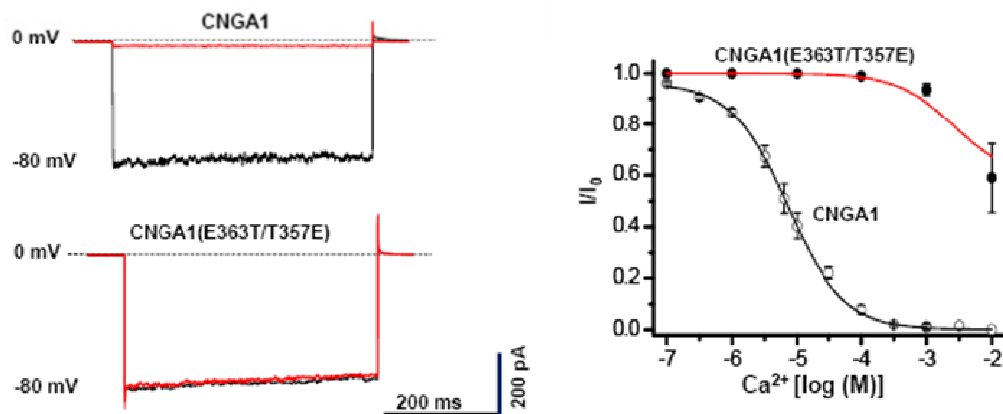


Figure 4-15– Structure based mutagenesis of bovine CNGA1 channel. Macroscopic currents of wild type bovine retinal CNGA1 (top) and its E363T/T357E swapped mutation (bottom) recorded at -80mV in the presence (red traces) and absence (black traces) of 100μM extracellular Ca²⁺. Channels were activated by 1mM cGMP in pipette solution. Shown in the right is plot of fraction of unblocked inward currents (I/I_0) at -80 mV as a function of external Ca²⁺ concentrations. Data points are mean \pm SEM from 5 measurements and are fitted to Langmuir functions with K_i of 7.1μM for wild type CNGA1. (Experiment done by Yang Li).

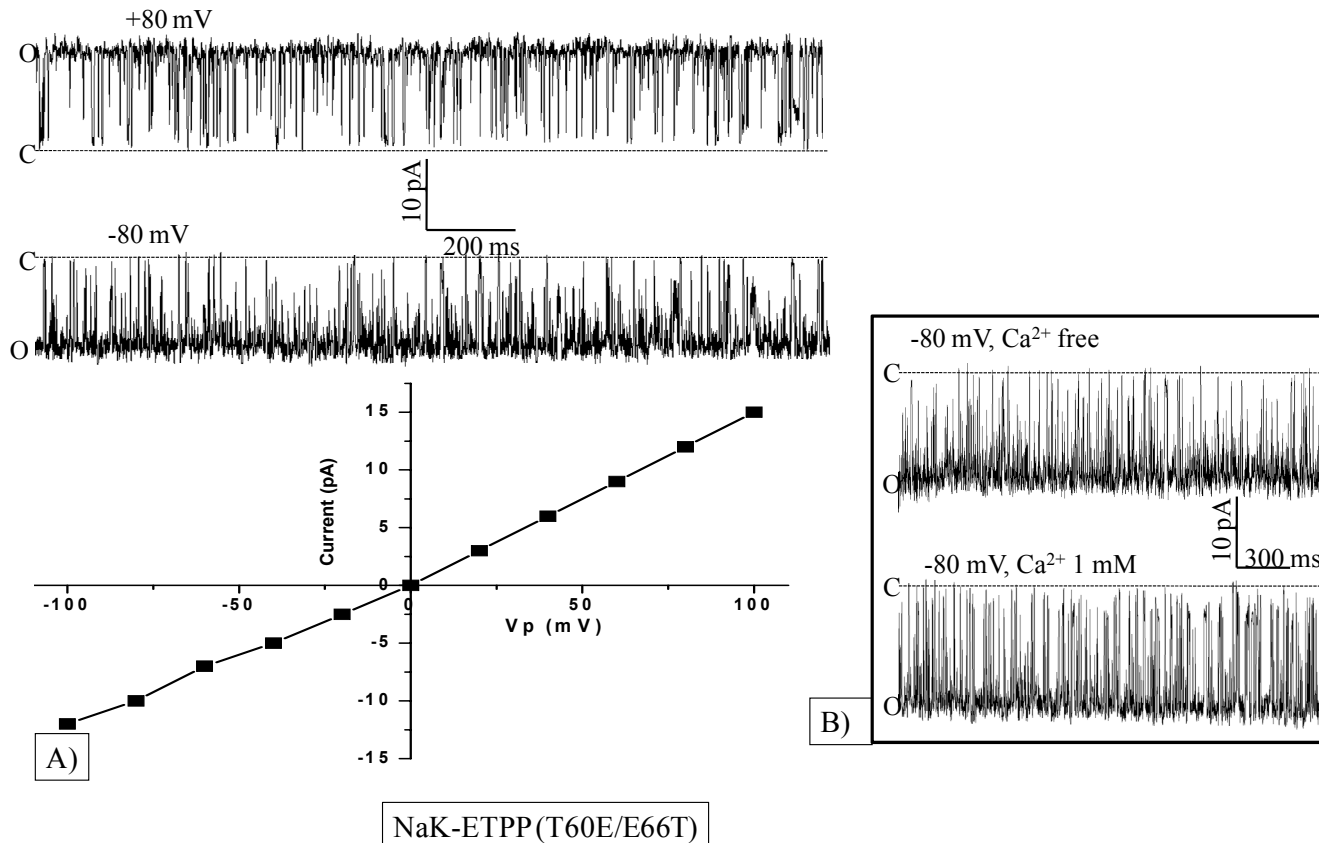


Figure 4-16 – Structure based mutagenesis of NaK-ETPP. Shown in (A) is single channel traces (top) of NaK-ETPP(T60E/E66T) swapped mutation recorded at ± 80 mV with 150 mM NaCl in the pipette and 150 mM KCl in the bath solution and its corresponding I/V curve (bottom). In (B) is its Ca^{2+} blockage test- addition of 1 mM Ca^{2+} at extracellular side (bath solution) has no effect on single channel conductance at -80 mV. Experiment performed by WeiZhong Zeng.

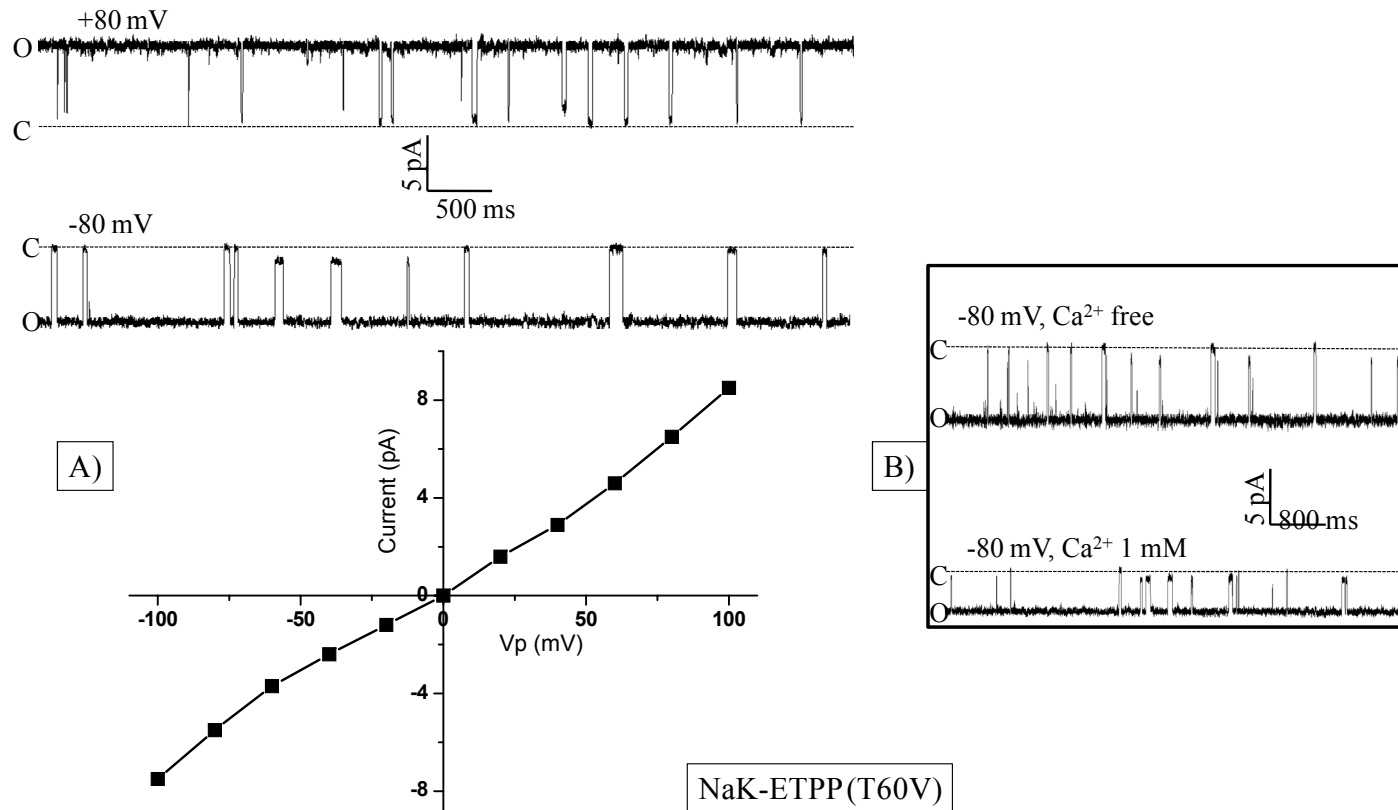


Figure 4-17- Structure based mutagenesis of NaK-ETPP. Single channel traces of NaK-ETPP(T60V) mutation recorded at ± 80 mV (A- top) with 150 mM NaCl in the pipette and 150 mM KCl in the bath solution and its I-V curve (bottom). Addition of 1 mM Ca^{2+} at extracellular side (bath solution) at -80 mV (B) reduced the current though not as strong as in NaK-ETPP. Experiment performed by WeiZhong Zeng.

Another key feature observed in all CNG-mimicking NaK mutants is that Tyr55 in the pore helix appears to be an important player in protein packing around the selectivity filter. Its hydroxyl end forms short range hydrogen bonds in all three mutants: with the backbone carbonyl oxygen of Glu66 in NaK-ETPP, with the carboxylate group of Glu66 in NaK-DTPP and the amide group of Asn66 in NaK-NTPP. These interactions are thought to be important in stabilizing the selectivity filter. This tyrosine is also absolutely conserved in CNG channels (Figure 3-1) and probably plays a similar role as in the mutants. Indeed, when the equivalent Tyr (Tyr352) in CNGA1 was replaced with Phe no obvious current was observed at a voltage range between +/- 100 mV, further cross-validating the similarity of the mutants to CNG channels. In agreement with this, a recent study of the same CNGA1 channel reported that replacing Tyr352 with Ala renders the channel conductance strongly voltage dependent resulting from voltage-dependent conformational changes at the filter (Martinez-Francois et al., 2009) even at saturating cGMP concentrations. Note that CNGA1, despite carrying the voltage sensor domain, is not gated by voltage but rather by cGMP binding. Furthermore, interaction between Tyr352 and Glu363 (equivalent to Tyr55 and Glu66 in NaK-ETPP) has been implicated in the same study, consistent with our structural observation. These results argue for the validity of the NaK mutants as accurate models for CNG channels selectivity filters.

CHAPTER FIVE

Discussion

Ion channels can be considered as one of the most critical groups of proteins upon which life depends. They are characterized by selective permeation of one or a group of ions and a method of gating. The gating mechanism usually underlies their variation among channels that transport the same or similar ion(s). Their biological function however generally depends on the ion(s) they transport and the extent of ion selectivity the channels exhibit. The extent of selectivity varies from ion channels that can discriminate between similar ions to those that discriminate cations over anions but not as well among cations. An example of the former are the voltage-gated K^+ channels that can discriminate from the very similar Na^+ ion and cyclic nucleotide-gated channels are good example of the later group because almost all common cations can permeate these channels but not anions. Understanding the molecular mechanism of ion selectivity and permeation properties of an ion channel is key to get insight into its biology. This however requires high resolution structural information, which has been a major impediment. Recent mechanistic advances in K^+ channel biology were a result of several high resolution structures. This is not the case with other ion channels, including cyclic nucleotide-gated channels.

Cyclic nucleotide-gated channels are a physiologically essential class of proteins whose functional significance in higher animals is generally well understood (Zagotta et al., 2003). However, detailed molecular picture, especially as it relates to their ion permeation and selectivity properties, has been lacking due to absence of high resolution structural information. The present study is thus focused on getting such structural information on ion selectivity mechanisms.

Among several possible approaches towards the stated goal, this work centered on modifying a bacterial non-selective cation channel, NaK, to contain selectivity filters identical in sequence to those found in majority of CNG channels. These mutants are amenable to high resolution structure determination and were found to share the same ion selectivity and Ca^{2+} blocking patterns with eukaryotic CNG channels. All are non-selective, permeable to Na^+ , K^+ , Ca^{2+} , as well as other group IA cations. Additionally, external Ca^{2+} blocks monovalent cation conduction, a process mediated by an acidic residue in the selectivity filter conserved in the mutants and CNG channels.

The CNG-mimicking NaK mutants crystallize in similar conditions and assume the same overall structure as the wild type open pore NaK channel. However, their selectivity filters exhibit profound differences from those of either NaK or KcsA. The mutants generally assume similar selectivity filter structures but exhibit some differences among themselves thought to arise due to variations in protein packing interactions around the selectivity filter. The first novel feature

of the mutants is the number of ion binding sites inside the selectivity filter. The mutants contain three contiguous ion binding sites equivalent to sites 2, 3 and 4 of the KcsA potassium channel structure (Figure 4-3). This is in sharp contrast to four ion binding sites of the highly K^+ selective KcsA and two ion binding sites of the non-selective NaK channels. Moreover, there is a funnel shaped extracellular entryway anchored by a highly conserved Proline and harboring two layers of waters. This region is believed to play important roles as a dehydration or rehydration zone for ions entering or exiting the selectivity filter.

Electrophysiological and radioactive data have shown that all mutants are non-selective. Single channel recordings under bi-ionic conditions resulted in a permeability ratio of one for Na^+ and K^+ ions, implying that these ions permeate the mutants equally well. This is supported by the radioactive $^{86}Rb^+$ uptake assays, which showed that most group I cations can permeate through the mutant channels. However, mutant structures in complex with Na^+ and K^+ reveal completely different ion binding profiles for these two ions. While the filter structure remains unchanged in both, K^+ ions tend to bind at the center of each site with eight carbonyl ligands creating a square-bipyramidal coordination, the same as in K^+ channels. In contrast, Na^+ clearly prefers to bind on the upper or lower edge of each site in plane with the carbonyl ligands resulting in a square planar or square-pyramidal, with an additional water ligand, coordination. This configuration would allow shorter ion-ligand distances for preferable Na^+ ion

binding. Of course, to traverse the pore, Na^+ ions may also bind at the center, in some cases even more preferably, like site 3 in NaK-ETPP. It is clear, however, that binding at the edge of each site is the dominating theme for Na^+ ions (Figures 5-1, 5-2).

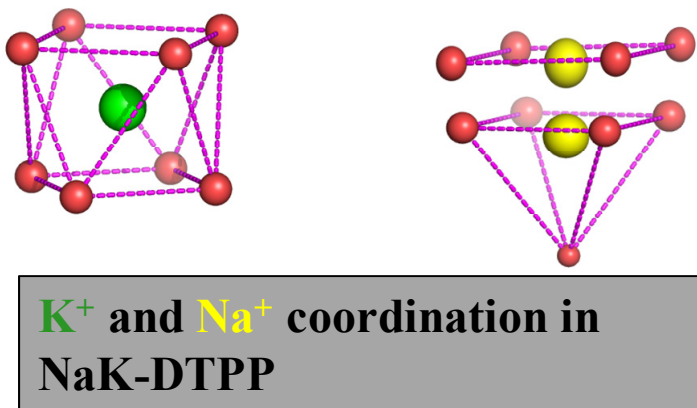


Figure 5-1 – Coordination of K^+ and Na^+ in the NaK mutants. K^+ (green sphere) coordination is similar to that in wild type NaK or K^+ channels in which eight ligands coordinate the ions in a square-bipyramidal coordination. Na^+ (yellow sphere) on the other hand prefers a square pyramidal or square planar coordination depending on the binding site, similar to wild type NaK. Big and small red spheres represent carbonyl oxygen and water ligands.

The observed monovalent cation binding behavior of the mutants is largely similar to wild-type NaK. Their selectivity filter structures are however in stark contrast to the later. The CNG-mimicking mutants have three contiguous ion binding sites and a funnel shaped extracellular entryway while wild-type NaK has two ion binding sites similar to two of those in the former, a large vestibule and an extracellular ion binding site. K^+ channels on the other hand have four

contiguous ion binding sites. Does this entail the necessity of four contiguous ion binding sites for K^+ selectivity? In Zhou's report, the KcsA channel was not crystallizable in the absence of K^+ and when crystallized under low K^+ (high Na^+) conditions its selectivity filter collapsed maintaining only two of the four ion binding sites resulting in the non-conductive conformation (Zhou et al., 2001). The authors argued that the channel maintains the conductive conformation in K^+ but not in Na^+ , and hence the selectivity. In contrast to KcsA, wild-type NaK and CNG mimicking mutants are crystallizable in Na^+ -only buffers even though for uniformity purposes K^+ crystals soaked in Na^+ solutions were used in the study. Na^+ coordination in wild-type NaK and CNG mimicking mutants is similar, despite having very different selectivity filter structures. Na^+ coordination is however different from K^+ coordination. Na^+ preferentially forms square planar or square-pyramidal coordination with four and five ligands, respectively, while K^+ coordination commonly uses eight ligands for a square-bipyramidal coordination either in K selective channels such as KcsA or the non-selective channel NaK and mutants. Does this difference in preferred coordination account for the selectivity patterns observed? Some studies suggest that the number of coordinating ligands does determine preference for one ion over another, K^+ preferring usually eight and Na^+ preferring four, five or six coordination numbers.

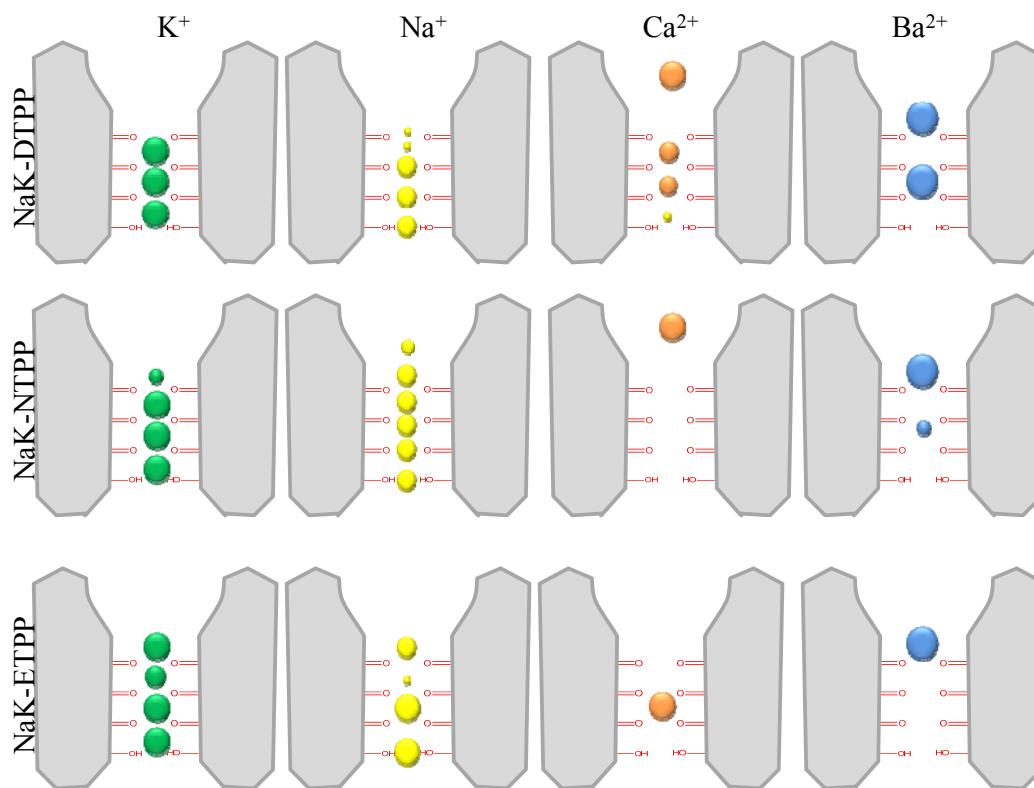


Figure 5-2- Summary of mono- and divalent cation binding in the selectivity filters of NaK mutants. Bound ions are shown as colored spheres (green for K^+ , yellow for Na^+ , orange for Ca^{2+} and blue for Ba^{2+}) with different sizes representing ion occupancy differences at each site. Note that Ca^{2+} ions observed within the external entryways of NaK-DTPP and NaK-NTPP are in a hydrated state

The CNG-mimicking NaK mutants exhibit divalent cation binding properties similar to wild-type NaK in some ways but distinctly different from K^+ channels. In K^+ channels Ba^{2+} primarily binds at site 4, however no bound Ba^{2+} was observed at site 4 in the mutant structures but instead was predominantly at the extracellular entryway coordinated by carbonyl groups of Gly65 and water ligands and at site 3 (Figure 5-2). There is slight variation among the mutants

themselves, especially the absence of electron density at site 3 of NaK-ETPP. Since there are no obvious structural variations between the ion binding sites 3 & 4 of K⁺ channels and NaK mutants, minor electrostatic differences might have contributed to the observed differences.

Ca²⁺ permeation and associated blockage of monovalent cation current is central to proper CNG channel function and the CNG-mimicking NaK mutant structures, combined with single channel recordings and radioactive tracer uptake assays, clearly demonstrate the essential role of the conserved acidic residue in Ca²⁺ binding. Strong Ca²⁺ binding is exhibited by NaK-ETPP, which mimics majority of CNG channel selectivity filters. Ca²⁺ binding is abolished in the neutral residue mutant NaK-NTPP while it is enhanced roughly 10 fold higher in the charge conservative mutant NaK-DTPP, reminiscent of Glu-to-Asn and Glu-to-Asp mutations in CNG channels, respectively. However, the structures reveal that, contrary to conventional models, the Ca²⁺ ion in the filter is exclusively chelated by backbone carbonyl oxygen atoms and not directly by the acidic side chain. In these CNG-mimicking mutants, particularly in NaK-ETPP, the side chain of the acidic residue is oriented tangential to the ion conduction pathway and buried underneath the external surface of the protein. It does not seem to make any direct contact with main chain atoms of the selectivity filter.

How then, is Ca²⁺ specificity in the NaK mutants achieved? Careful examination of the environment surrounding the acidic residue reveals some

important details that may play a role in this phenomenon. First, the side chain carboxylate of the acidic residue in the CNG-mimicking mutants is buried in a fairly hydrophobic environment shielded from the ion conduction pathway by the main chain atoms of the selectivity filter residues (Figure 4-7E). This low dielectric environment may enhance the electrostatic interaction between the negative charge and the cation in the filter which, combined with the presence of four such carboxylate groups in a channel tetramer, may help stabilize the doubly charged Ca^{2+} ion. The second possibility is that the presence of negative charges in close proximity may perturb the charge distribution along the backbone of the filter residues, making certain carbonyl oxygen atoms more electronegative and more suited for Ca^{2+} binding. Both mechanisms are not mutually exclusive and could work in an additive or synergistic manner.

The apparently greater Ca^{2+} affinity upon a Glu-to-Asp mutation in CNG channels as well as in NaK-DTPP compared to NaK-ETPP even though both preserve the essential acidic residue/negative charge can also be explained through detailed structural analysis. The multiple Ca^{2+} binding (at sites 2 and 3) in NaK-DTPP filter, is believed to result from the position of the carboxylate group of Asp66 and the presence of two water molecules, contributing to the different Ca^{2+} binding affinity. The 1st water molecule (W1 in Figure 4-6A) is located at the equivalent position as the charge center of the Glu66 carboxylate in NaK-ETPP and mediates the interaction between Asp66 and Thr60. Polarized by the

negative charge of Asp66, this water molecule could play the same role as the carboxylate of Glu66, rendering Ca^{2+} binding at site 3. The 2nd water molecule (W2 in Figure 4-6A) resides in close proximity to the backbone of the filter, making a hydrogen bonding interaction with the backbone amide of Asp66. Furthermore, the carboxylate group of Asp66 is positioned in a way that one of its oxygen atoms forms a hydrogen bond with its own backbone amide nitrogen. Both interactions could stabilize the double bonded resonance form of the peptide bond between Gly65 and Asp66, making the Gly65 carbonyl oxygen more negatively charged and suitable for Ca^{2+} chelation at site 2 in NaK-DTPP.

The structures of CNG-mimicking NaK mutants also provide a plausible explanation for the pH dependent Ca^{2+} blockage and channel conductance in CNG or Ca^{2+} channels. In vertebrate CNG channels lower pH has been shown to weaken Ca^{2+} binding and decrease channel conductance due to the protonation of the conserved glutamate carboxyl side chain in the filter with an apparent pKa of 7.6, much higher than that of a solvent exposed glutamate, which has a pKa of 4.3 (Root and MacKinnon, 1994; Seifert et al., 1999). A similar protonation induced conductance change was observed in L-type voltage-gated Ca^{2+} channels in which proton binding to an extracellular site with an apparent pKa of 7.5 resulted in a threefold decrease of channel conductance (Prod'homme et al., 1987). Such pKa shifts of acidic side chains in proteins are not uncommon and may be justified by the side chain being confined in a fairly hydrophobic micro environment, similar

to observations in our mutant structures (Mehler et al., 2002; Schutz and Warshel, 2001). Studies of catfish olfactory CNG channels have pointed to the four conserved glutamates in a channel tetramer forming two identical non-interacting protonation sites (Root and MacKinnon, 1994). Although L-type voltage-gated Ca^{2+} channels have four glutamates at presumably similar positions as those of CNG channels, only one protonation site was proposed for the L-type Ca^{2+} channel (Prod'homme et al., 1987). The CNG-mimicking NaK-mutant structures, however, would predict four such independent sites, one at every glutamate side chain, instead of one or two and further analysis is needed to reconcile this discrepancy.

In summary, results on CNG-mimicking NaK mutants provide an accurate picture of how Ca^{2+} binds in the selectivity filter as well as the position of conserved acidic residues mediating it. In light of other striking similarities between the two groups, the NaK mutant structures are thought to present the most accurate pictures to date of CNG channel pores, complementing long standing electrophysiological studies and providing novel structural insights into CNG channel biology. Although further study is needed to work out exact details of Ca^{2+} binding mechanisms, the Ca^{2+} binding mechanism observed in the NaK mutants is believed to be the same as that in CNG channels. A similar mechanism may also apply to voltage-gated Ca^{2+} channels whose Ca^{2+} binding mechanism has been suggested to be similar to CNG channels (Kaupp and Seifert, 2002;

Zagotta and Siegelbaum, 1996), utilizing the four conserved glutamate residues in the filter, one from each homologous domain, to confer Ca^{2+} specificity (Ellinor et al., 1995; Tang et al., 1993; Yang et al., 1993). These high resolution structures also open the door for computational simulations aimed at providing a more theoretical explanation for Ca^{2+} binding in tetrameric cation channels.

CHAPTER SIX

Future directions

Even though the most well characterized CNG channels are those from vertebrate photoreceptors and olfactory sensory neurons, many more similar channels have been identified in other cell types and also in many lower organisms (Kaupp and Seifert, 2002). In *D. melanogaster* two genes that encode for CNG channels have been cloned and characterized (Baumann et al., 1994; Miyazu et al., 2000). These channels, though generally similar to their vertebrate counterparts, display deviations on some key properties. The first *Drosophila* CNG channel identified by Kaupp group was shown to exhibit linear macro- or microscopic I-V relationships in contrast to those of vertebrate CNG channels that display considerable rectification (Baumann et al., 1994). The most striking deviation however occurs in their divalent cation blockage or permeation properties. A plot of I/I_{\max} versus divalent cation concentration showed that for the *Drosophila* channel the concentration of half-maximal current inhibition (the inhibition constant, K_i) increased more than 50 fold both in Ca^{2+} and Mg^{2+} compared to the bovine rod CNG channel (Baumann et al., 1994), indicating a more than 50 fold reduced divalent cation sensitivity. What might be the underlying reason for such distinct behavior of the *Drosophila* CNG channel? Examination of the selectivity filter sequences of CNG channels from several

Drosophila species and other insects show that the Glutamate residue responsible for divalent cation blockage properties in vertebrate CNG channels is also conserved in these channels (Figure 3-1). However, few residues past this conserved Glutamate considerable deviations in protein sequence are noticed and this variation was invoked as the cause of the observed functional difference (Baumann et al., 1994; Seifert et al., 1999).

In the present study a NaK mutant (NaK-ETPT) that mimics the selectivity filter of *Drosophila* and/or insect CNG channels was made. NaK-ETPT exhibits very similar biochemical properties as NaK-ETPP, mutant that mimics most common vertebrate CNG channels. However, its structure exhibited a dramatic rearrangement at the top half of the selectivity filter and the extracellular entryway (Figure 6-1A, C, D). The bottom two ion binding sites in the selectivity filter remain largely similar to those of the other mutants but residues Gly65-Thr69 undergo startling rearrangement in which the main chain bulges outward and rotates almost 180°. The pyrrolidine group of Pro68 that acts as an anchor of the extracellular funnel shaped entryway in the other mutants moves outward in NaK-ETPT making it much wider (Figure 6-1B). However, several layers of water molecules are still observed in the external entryway suggesting that this region, though wider, probably serves a similar purpose as in the other mutants. The carbonyl group of Gly65 of NaK-ETPT, which forms site 2 in NaK-ETPP, undergoes almost a 180° flip orienting itself opposite the ion

conduction pathway (Figure 6-1C, D). The side chain of the acidic residue E66 also makes similar translation and rotation resulting in the carboxylate group facing the ion conduction pathway and pointing upwards to the extracellular entryway. This translation and rotation propagates to the other residues upto Thr69. As a result, packing interactions around the selectivity filter of NaK-ETPT are completely different from the other mutants. Considering the similar biochemical behavior and identical structure in the rest of the protein, how would this structural change in the selectivity filter affect its ion permeation and Ca^{2+} sensitivity? To discern this, single channel conductance, permeability ratio and Ca^{2+} permeation experiments would be necessary. This can be done the same way as the other mutants- reconstitute protein into lipid vesicles and analyze single channel behavior by liposome patch-clamping. A more thorough structural analysis is also necessary. This can also be done in exactly the same way as the other mutants – determine structure in different cations and analyze ion binding behavior. Only after this can a correlation to *Drosophila* CNG channels be made. Is a structural change responsible for the different Ca^{2+} sensitivity of *Drosophila* CNG channels?

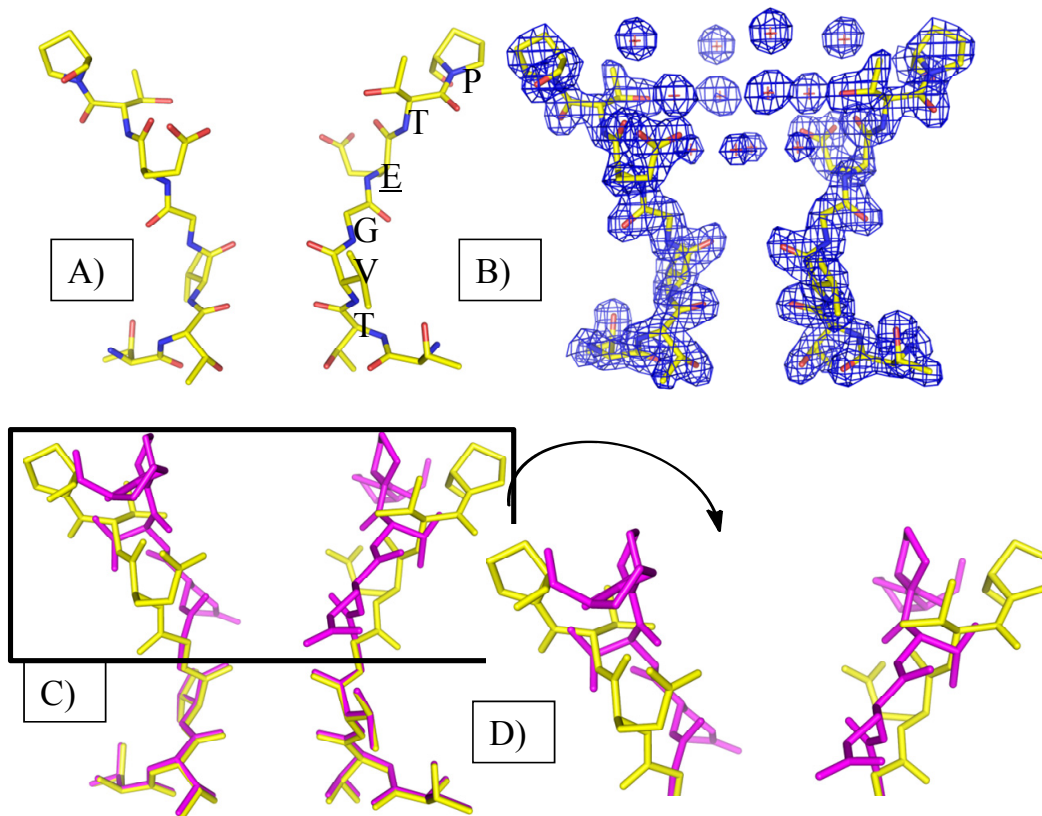


Figure 6-1 – Structure of the selectivity filter of NaK-ETPT. Shown in (A) is a stick representation of the selectivity filter; (B)- 2Fo-Fc map of the selectivity filter including water molecules (red spheres) in the extracellular entryway; (C)- structural alignment of NaK-ETPT selectivity filter (yellow) with that of NaK-ETPP (magenta) and (D) shows a slightly enlarged top-half of (C) showing the structural variation. Front and back subunits are removed for clarity purposes.

The importance of the acidic residue in Ca^{2+} permeation in vertebrate CNG channels has usually been shown by mutating it into uncharged residues, typically into Asparagine. A similar Glu-to-Asn mutation was also employed to probe the property in the present work. This mutation does remove the negative charge as intended, however its side chain is a methyl group shorter than

Glutamate. Ideally, a Glu-to-Gln mutant that only removes the charge but maintains the overall length of the side chain would be used. Studies using such mutation reported some peculiar properties. Eismann *et al* found that mutating the Glu363 of the rod photoreceptor CNG channel to Glutamine dramatically changed its properties (Eismann et al., 1994). The mutant became strongly outwardly rectifying and I-V curves for different alkali metal ions were very similar. The reason for this variation, they suggested, is structural perturbations that propagate through the entire pore region. Menini group reported almost identical results for the olfactory sensory neuron CNG channel (Gavazzo et al., 2000). A recent study on rod photoreceptor CNGA1 channel over a much wider voltage range found that the Glu-to-Gln mutant show very strong outward rectification on its macroscopic I-V curve, similar to the above two, but its single channel I-V curve did not show appreciable rectification (Martinez-Francois et al., 2009). Because these experiments involved use of saturating cGMP concentration, the results might imply a voltage-dependent gating of the Glu-to-Gln mutant. What is the underlying reason for such aberrant behavior of this mutant? Does this Glu-to-Gln mutation change the structure of the selectivity filter and would that translate into changing the conductance state of the channel? In support of this a Glu-to-Gln mutant (NaK-QTPP) of NaK-ETPP exhibited dramatic rearrangement of the selectivity filter structure (Figure 6-2). In NaK-QTPP the bottom two ion binding sites and the anchor Pro68 of the extracellular entryway remain largely

unaffected. However, the main and side chains of Gly65, Gln66 and Thr67 undergo striking conformational changes. Compared to NaK-ETPP structure, the carbonyl group of Gly65 in NaK-QTPP moves away from the ion conduction pathway creating a vestibule. The side chain of Gln66 also exhibits a dramatic leftward movement compared to the Glu66 of NaK-ETPP. The other interesting, and may be more important shift is that exhibited by the side chain of Thr67 of NaK-QTPP – it moved inwards and now faces the aqueous ion conduction pathway (Figure 6-2A). The packing interactions in NaK-QTPP are also remarkably different from those of the other NaK mutants. Can the observed structural changes of NaK-QTPP explain the observed functional variations of the Glu-to-Gln mutant of vertebrate CNG channels? Does this mutant of CNG channels represent their non-conductive or inactivated state and can NaK-QTPP represent this state? A preliminary single channel recording of NaK-QTPP proteoliposome showed that, although single channel current amplitude is only slightly reduced, the open probability is significantly lower than NaK-ETPP, and the trace exhibits several (at least three) conductance states, all of which are consistent with the observation in Glu-to-Gln mutant of vertebrate CNG channels. However, a thorough study of the NaK-QTPP mutant is necessary. Its single channel properties need to be characterized in detail, especially in relation to Ca^{2+} blockage and the different states. Its macroscopic I-V curve would also need to be analyzed if it shows strong outward rectification as observed in a similar mutation

of vertebrate CNG channels. The experiments would be essentially similar to those of the other NaK mutants. A detailed statistical analysis of the current behavior would be quite informative, such as amplitude histogram, dwell time and open probability. In addition, a detailed structural analysis would be very insightful. For that, its structure in various other cations, especially Ca^{2+} and Na^+ , will need to be determined. Ideally, this can be done similar to the other NaK mutants in this study – soaking K^+ crystals in suitable stabilization solutions, determining their structures and calculating ion-omit maps. In order to visualize Ca^{2+} more clearly X-ray diffraction data could be collected at long wavelengths to capitalize on anomalous diffraction by Ca^{2+} . Combining the structural and functional analyses would reveal important hallmarks of the mutants that may very well be correlated with vertebrate CNG channels.

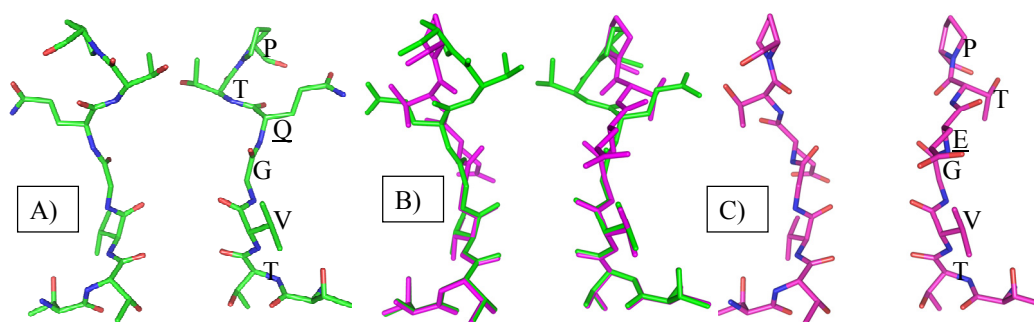


Figure 6-2 – Selectivity filter structure of NaK-QTPP (A) and its alignment with that of NaK-ETPP (B). NaK-QTPP is in green and NaK-ETPP is in magenta. Selectivity filter structure of NaK-ETPP is also shown (C) for comparison. Front and back subunits removed.

Native CNG channels from photoreceptors and olfactory sensory neurons are known to function as heterotetramers in which three A and one B subunits co-assemble to form the functional channel. Only the main channel forming A subunits have been shown to form functional homotetramers, with the exception of CNGA4, which is grouped with the A subunits because of sequence similarity. However, homotetrameric channels, despite exhibiting similar properties as native channels, do show variations from the heterotetramers, especially on their Ca^{2+} sensitivity. This can be intuitively seen from their sequences at the selectivity filter (Figure 3-1). The A subunits (A1-A3) are the main channel subunits and carry a Glutamate after the conserved T(V/I)G sequence whereas the auxiliary subunits carry either a Glycine (B1, B3) or an Aspartate (A4) at the equivalent position. Native rod and cone CNG channels comprise 3A:B subunits while those from olfactory sensory neurons assume 2A2:A4:B arrangement. In this heterotetrameric arrangement each A subunit contributes an acidic residue (A1, A2, A3 – Glutamate, A4 – Aspartate) while the B subunits contribute uncharged Glycine, but a homotetramer would have the same acidic residue from each subunit. In rod photoreceptors, the presence of the glycine residue in the heterotetramers was reported to reduce its calcium sensitivity compared to the homotetramer (Korschen et al., 1995). Moreover, native olfactory CNG channels have distinctly enhanced calcium permeation, thought to arise due to the Aspartate contributed from the A4 subunit instead of a Glutamate (Dzeja et al.,

1999). The present study relied on the homotetrameric NaK channel and the mutants thus mimic the homotetrameric CNG channels. To recapitulate the native heterotetrameric channels more closely a tandem NaK heterotetramer can be designed. The individual subunits could be separately cloned into expression vectors with suitable restriction endonucleases and designed to have short linker peptide sequences and then combined to generate the tandem tetramer. Necessity for reasonable expression and subsequent purification of a stable heterotetramer might require attempting different lengths of linker peptides and subunit sequences. To recapitulate the rod and cone CNG channels three NaK-ETPP and one NaK-GLPE sequences (see methodology) can be arranged into a tandem tetramer presumably similar to the 3A:B arrangement of the native channels. The olfactory CNG channel would be represented by a tandem tetramer created with two Na-ETPP, one NaK-DTPP and one NaK-GLPE sequences to assume the 2A2:A4:B stoichiometry.

REFERENCES

- Alam, A., and Jiang, Y. (2009a). High-resolution structure of the open NaK channel. *Nat Struct Mol Biol* *16*, 30-34.
- Alam, A., and Jiang, Y. (2009b). Structural analysis of ion selectivity in the NaK channel. *Nat Struct Mol Biol* *16*, 35-41.
- Alam, A., Shi, N., and Jiang, Y. (2007). Structural insight into Ca²⁺ specificity in tetrameric cation channels. *Proc Natl Acad Sci U S A* *104*, 15334-15339.
- Alberts, B.J., Alexander; Lewis, Julian; Raff, Martin; Roberts, Keith and Walter, Peter (2002). *Molecular Biology of the Cell* (Garland Science).
- Armstrong, C.M. (1971). Interaction of tetraethylammonium ion derivatives with the potassium channels of giant axons. *J Gen Physiol* *58*, 413-437.
- Armstrong, C.M. (2007). Life among the axons. *Annu Rev Physiol* *69*, 1-18.
- Ashcroft, F.M. (2006). From molecule to malady. *Nature* *440*, 440-447.
- AvantiPolarLipids. Avanti Polar Lipids.
- Bailey, S. (1994). The Ccp4 Suite - Programs for Protein Crystallography. *Acta Crystallogr D* *50*, 760-763.
- Baumann, A., Frings, S., Godde, M., Seifert, R., and Kaupp, U.B. (1994). Primary structure and functional expression of a *Drosophila* cyclic nucleotide-gated channel present in eyes and antennae. *EMBO J* *13*, 5040-5050.
- Bezanilla, F., and Armstrong, C.M. (1972). Negative conductance caused by entry of sodium and cesium ions into the potassium channels of squid axons. *J Gen Physiol* *60*, 588-608.
- Biel, M., and Michalakis, S. (2007). Function and dysfunction of CNG channels: insights from channelopathies and mouse models. *Mol Neurobiol* *35*, 266-277.
- Bostick, D.L., and Brooks, C.L., 3rd (2007). Selectivity in K⁺ channels is due to topological control of the permeant ion's coordinated state. *Proc Natl Acad Sci U S A* *104*, 9260-9265.
- Bradley, J., Frings, S., Yau, K.W., and Reed, R. (2001). Nomenclature for ion channel subunits. *Science* *294*, 2095-2096.
- Brunger, A.T., Adams, P.D., Clore, G.M., DeLano, W.L., Gros, P., Grosse-Kunstleve, R.W., Jiang, J.S., Kuszewski, J., Nilges, M., Pannu, N.S., *et al.* (1998). Crystallography & NMR system: A new software suite for macromolecular structure determination. *Acta Crystallogr D* *54*, 905-921.
- Camerino, D.C., Desaphy, J.F., Tricarico, D., Pierno, S., and Liantonio, A. (2008). Therapeutic approaches to ion channel diseases. *Adv Genet* *64*, 81-145.

Cheng, W.W., Enkvetchakul, D., and Nichols, C.G. (2009). KirBac1.1: it's an inward rectifying potassium channel. *J Gen Physiol* 133, 295-305.

Colamartino, G., Menini, A., and Torre, V. (1991). Blockage and permeation of divalent cations through the cyclic GMP-activated channel from tiger salamander retinal rods. *J Physiol* 440, 189-206.

Craven, K.B., and Zagotta, W.N. (2006). CNG and HCN channels: two peas, one pod. *Annu Rev Physiol* 68, 375-401.

Cuello, L.G., Romero, J.G., Cortes, D.M., and Perozo, E. (1998). pH-dependent gating in the *Streptomyces lividans* K⁺ channel. *Biochemistry* 37, 3229-3236.

deLano, W.L. (2002). The PyMOL Molecular Graphics System (San Carlos, CA, DeLano Scientific).

Doyle, D.A., Morais Cabral, J., Pfuetzner, R.A., Kuo, A., Gulbis, J.M., Cohen, S.L., Chait, B.T., and MacKinnon, R. (1998). The structure of the potassium channel: molecular basis of K⁺ conduction and selectivity. *Science* 280, 69-77.

Dryja, T.P., Finn, J.T., Peng, Y.W., McGee, T.L., Berson, E.L., and Yau, K.W. (1995). Mutations in the gene encoding the alpha subunit of the rod cGMP-gated channel in autosomal recessive retinitis pigmentosa. *Proc Natl Acad Sci U S A* 92, 10177-10181.

Dzeja, C., Hagen, V., Kaupp, U.B., and Frings, S. (1999). Ca²⁺ permeation in cyclic nucleotide-gated channels. *EMBO J* 18, 131-144.

Eisenman, G. (1962). Cation selective glass electrodes and their mode of operation. *Biophys J* 2, 259-323.

Eismann, E., Muller, F., Heinemann, S.H., and Kaupp, U.B. (1994). A single negative charge within the pore region of a cGMP-gated channel controls rectification, Ca²⁺ blockage, and ionic selectivity. *Proc Natl Acad Sci U S A* 91, 1109-1113.

Ellinor, P.T., Yang, J., Sather, W.A., Zhang, J.F., and Tsien, R.W. (1995). Ca²⁺ channel selectivity at a single locus for high-affinity Ca²⁺ interactions. *Neuron* 15, 1121-1132.

Enkvetchakul, D., Bhattacharyya, J., Jeliaskova, I., Groesbeck, D.K., Cukras, C.A., and Nichols, C.G. (2004). Functional characterization of a prokaryotic Kir channel. *J Biol Chem* 279, 47076-47080.

Fesenko, E.E., Kolesnikov, S.S., and Lyubarsky, A.L. (1985). Induction by cyclic GMP of cationic conductance in plasma membrane of retinal rod outer segment. *Nature* 313, 310-313.

Frings, S., Lynch, J.W., and Lindemann, B. (1992). Properties of cyclic nucleotide-gated channels mediating olfactory transduction. Activation, selectivity, and blockage. *J Gen Physiol* 100, 45-67.

Frings, S., Seifert, R., Godde, M., and Kaupp, U.B. (1995). Profoundly different calcium permeation and blockage determine the specific function of distinct cyclic nucleotide-gated channels. *Neuron* *15*, 169-179.

Garty, H., Rudy, B., and Karlsh, S.J. (1983). A simple and sensitive procedure for measuring isotope fluxes through ion-specific channels in heterogenous populations of membrane vesicles. *J Biol Chem* *258*, 13094-13099.

Gavazzo, P., Picco, C., Eismann, E., Kaupp, U.B., and Menini, A. (2000). A point mutation in the pore region alters gating, Ca(2+) blockage, and permeation of olfactory cyclic nucleotide-gated channels. *J Gen Physiol* *116*, 311-326.

Hamill, O.P., Marty, A., Neher, E., Sakmann, B., and Sigworth, F.J. (1981). Improved patch-clamp techniques for high-resolution current recording from cells and cell-free membrane patches. *Pflugers Arch* *391*, 85-100.

Haynes, L., and Yau, K.W. (1985). Cyclic GMP-sensitive conductance in outer segment membrane of catfish cones. *Nature* *317*, 61-64.

Heginbotham, L., Abramson, T., and MacKinnon, R. (1992). A functional connection between the pores of distantly related ion channels as revealed by mutant K⁺ channels. *Science* *258*, 1152-1155.

Heginbotham, L., Kolmakova-Partensky, L., and Miller, C. (1998). Functional reconstitution of a prokaryotic K⁺ channel. *J Gen Physiol* *111*, 741-749.

Heginbotham, L., Lu, Z., Abramson, T., and MacKinnon, R. (1994). Mutations in the K⁺ channel signature sequence. *Biophys J* *66*, 1061-1067.

Heginbotham, L., and MacKinnon, R. (1993). Conduction properties of the cloned Shaker K⁺ channel. *Biophys J* *65*, 2089-2096.

Hille, B. (1970). Ionic channels in nerve membranes. *Prog Biophys Mol Biol* *21*, 1-32.

Hille, B. (1973). Potassium channels in myelinated nerve. Selective permeability to small cations. *J Gen Physiol* *61*, 669-686.

Hille, B. (2001). *Ion Channels of Excitable Membranes*, Third edn (Massachusetts, Sinauer Associates, Inc).

Hodgkin, A.L., and Huxley, A.F. (1952a). The components of membrane conductance in the giant axon of *Loligo*. *J Physiol* *116*, 473-496.

Hodgkin, A.L., and Huxley, A.F. (1952b). Currents carried by sodium and potassium ions through the membrane of the giant axon of *Loligo*. *J Physiol* *116*, 449-472.

Hodgkin, A.L., and Huxley, A.F. (1952c). A quantitative description of membrane current and its application to conduction and excitation in nerve. *J Physiol* *117*, 500-544.

Hodgkin, A.L., Huxley, A.F., and Katz, B. (1952). Measurement of current-voltage relations in the membrane of the giant axon of *Loligo*. *J Physiol* *116*, 424-448.

Jiang, Y., Lee, A., Chen, J., Cadene, M., Chait, B.T., and MacKinnon, R. (2002). The open pore conformation of potassium channels. *Nature* *417*, 523-526.

Jiang, Y., Lee, A., Chen, J., Ruta, V., Cadene, M., Chait, B.T., and MacKinnon, R. (2003). X-ray structure of a voltage-dependent K⁺ channel. *Nature* *423*, 33-41.

Jiang, Y., and MacKinnon, R. (2000). The barium site in a potassium channel by x-ray crystallography. *J Gen Physiol* *115*, 269-272.

Jones, T.A., Zou, J.Y., Cowan, S.W., and Kjeldgaard, M. (1991). Improved Methods for Building Protein Models in Electron-Density Maps and the Location of Errors in These Models. *Acta Crystallogr A* *47*, 110-119.

Karpen, J.W., Brown, R.L., Stryer, L., and Baylor, D.A. (1993). Interactions between divalent cations and the gating machinery of cyclic GMP-activated channels in salamander retinal rods. *J Gen Physiol* *101*, 1-25.

Kaupp, U.B., Niidome, T., Tanabe, T., Terada, S., Bonigk, W., Stuhmer, W., Cook, N.J., Kangawa, K., Matsuo, H., Hirose, T., *et al.* (1989). Primary structure and functional expression from complementary DNA of the rod photoreceptor cyclic GMP-gated channel. *Nature* *342*, 762-766.

Kaupp, U.B., and Seifert, R. (2002). Cyclic nucleotide-gated ion channels. *Physiol Rev* *82*, 769-824.

Kohl, S., Baumann, B., Broghammer, M., Jagle, H., Sieving, P., Kellner, U., Spegal, R., Anastasi, M., Zrenner, E., Sharpe, L.T., *et al.* (2000). Mutations in the CNGB3 gene encoding the beta-subunit of the cone photoreceptor cGMP-gated channel are responsible for achromatopsia (ACHM3) linked to chromosome 8q21. *Hum Mol Genet* *9*, 2107-2116.

Kohl, S., Marx, T., Giddings, I., Jagle, H., Jacobson, S.G., Apfelstedt-Sylla, E., Zrenner, E., Sharpe, L.T., and Wissinger, B. (1998). Total colourblindness is caused by mutations in the gene encoding the alpha-subunit of the cone photoreceptor cGMP-gated cation channel. *Nat Genet* *19*, 257-259.

Korschen, H.G., Illing, M., Seifert, R., Sesti, F., Williams, A., Gotzes, S., Colville, C., Muller, F., Dose, A., Godde, M., *et al.* (1995). A 240 kDa protein represents the complete beta subunit of the cyclic nucleotide-gated channel from rod photoreceptor. *Neuron* *15*, 627-636.

Kung, C., and Blount, P. (2004). Channels in microbes: so many holes to fill. *Mol Microbiol* *53*, 373-380.

Kuo, A., Gulbis, J.M., Antcliff, J.F., Rahman, T., Lowe, E.D., Zimmer, J., Cuthbertson, J., Ashcroft, F.M., Ezaki, T., and Doyle, D.A. (2003). Crystal structure of the potassium channel KirBac1.1 in the closed state. *Science* *300*, 1922-1926.

Kuo, M.M., Saimi, Y., Kung, C., and Choe, S. (2007). Patch clamp and phenotypic analyses of a prokaryotic cyclic nucleotide-gated K⁺ channel using *Escherichia coli* as a host. *J Biol Chem* 282, 24294-24301.

Lockless, S.W., Zhou, M., and MacKinnon, R. (2007). Structural and thermodynamic properties of selective ion binding in a K⁺ channel. *PLoS Biol* 5, e121.

Long, S.B., Campbell, E.B., and Mackinnon, R. (2005). Crystal structure of a mammalian voltage-dependent Shaker family K⁺ channel. *Science* 309, 897-903.

Mackinnon, R., and Yellen, G. (1990). Mutations Affecting Tea Blockade and Ion Permeation in Voltage-Activated K⁺ Channels. *Science* 250, 276-279.

Martinez-Francois, J.R., Xu, Y., and Lu, Z. (2009). Mutations reveal voltage gating of CNGA1 channels in saturating cGMP. *J Gen Physiol* 134, 151-164.

MAXCHELATOR. MAXCHELATOR.

Mehler, E.L., Fuxreiter, M., Simon, I., and Garcia-Moreno, E.B. (2002). The role of hydrophobic microenvironments in modulating pK_a shifts in proteins. *Proteins* 48, 283-292.

Menini, A. (1990). Currents carried by monovalent cations through cyclic GMP-activated channels in excised patches from salamander rods. *J Physiol* 424, 167-185.

Merritt, E.A. http://skuld.bmsc.washington.edu/scatter/AS_form.html.

Miyazu, M., Tanimura, T., and Sokabe, M. (2000). Molecular cloning and characterization of a putative cyclic nucleotide-gated channel from *Drosophila melanogaster*. *Insect Mol Biol* 9, 283-292.

Morrill, J.A., and MacKinnon, R. (1999). Isolation of a single carboxyl-carboxylate proton binding site in the pore of a cyclic nucleotide-gated channel. *J Gen Physiol* 114, 71-83.

Mullins, L.J. (1959a). An analysis of conductance changes in squid axon. *J Gen Physiol* 42, 1013-1035.

Mullins, L.J. (1959b). The penetration of some cations into muscle. *J Gen Physiol* 42, 817-829.

Nakamura, T., and Gold, G.H. (1987). A cyclic nucleotide-gated conductance in olfactory receptor cilia. *Nature* 325, 442-444.

Neher, E., and Sakmann, B. (1976). Single-channel currents recorded from membrane of denervated frog muscle fibres. *Nature* 260, 799-802.

Neher, E., Sakmann, B., and Steinbach, J.H. (1978). The extracellular patch clamp: a method for resolving currents through individual open channels in biological membranes. *Pflugers Arch* 375, 219-228.

Nimigean, C.M. (2006). A radioactive uptake assay to measure ion transport across ion channel-containing liposomes. *Nat Protoc* 1, 1207-1212.

Noskov, S.Y., Berneche, S., and Roux, B. (2004). Control of ion selectivity in potassium channels by electrostatic and dynamic properties of carbonyl ligands. *Nature* *431*, 830-834.

Noskov, S.Y., and Roux, B. (2006). Ion selectivity in potassium channels. *Biophys Chem* *124*, 279-291.

Otwinowski, Z., and Minor, W. (1997). Processing of X-ray diffraction data collected in oscillation mode. *Method Enzymol* *276*, 307-326.

Park, C.S., and MacKinnon, R. (1995). Divalent cation selectivity in a cyclic nucleotide-gated ion channel. *Biochemistry* *34*, 13328-13333.

Picones, A., and Korenbrot, J.I. (1992). Permeation and interaction of monovalent cations with the cGMP-gated channel of cone photoreceptors. *J Gen Physiol* *100*, 647-673.

Pidcock, E., and Moore, G.R. (2001). Structural characteristics of protein binding sites for calcium and lanthanide ions. *J Biol Inorg Chem* *6*, 479-489.

Pifferi, S., Boccaccio, A., and Menini, A. (2006). Cyclic nucleotide-gated ion channels in sensory transduction. *FEBS Lett* *580*, 2853-2859.

Prasad, B.C., and Reed, R.R. (1999). Chemosensation: molecular mechanisms in worms and mammals. *Trends Genet* *15*, 150-153.

Prod'hom, B., Pietrobon, D., and Hess, P. (1987). Direct measurement of proton transfer rates to a group controlling the dihydropyridine-sensitive Ca²⁺ channel. *Nature* *329*, 243-246.

Root, M.J., and MacKinnon, R. (1993). Identification of an external divalent cation-binding site in the pore of a cGMP-activated channel. *Neuron* *11*, 459-466.

Root, M.J., and MacKinnon, R. (1994). Two identical noninteracting sites in an ion channel revealed by proton transfer. *Science* *265*, 1852-1856.

Schutz, C.N., and Warshel, A. (2001). What are the dielectric "constants" of proteins and how to validate electrostatic models? *Proteins* *44*, 400-417.

Seifert, R., Eismann, E., Ludwig, J., Baumann, A., and Kaupp, U.B. (1999). Molecular determinants of a Ca²⁺-binding site in the pore of cyclic nucleotide-gated channels: S5/S6 segments control affinity of intrapore glutamates. *EMBO J* *18*, 119-130.

Shammat, I.M., and Gordon, S.E. (1999). Stoichiometry and arrangement of subunits in rod cyclic nucleotide-gated channels. *Neuron* *23*, 809-819.

Shi, N., Ye, S., Alam, A., Chen, L., and Jiang, Y. (2006). Atomic structure of a Na⁺- and K⁺-conducting channel. *Nature* *440*, 570-574.

Siegel, G.J., Agranoff, Bernard W., Fisher, Stephen K., Albers, R. Wayne, and Uhler, Michael D. (1999). *Basic neurochemistry : molecular, cellular and medical aspects* Sixth edn (Philadelphia, Lippincott-Raven Publishers).

Tang, S., Mikala, G., Bahinski, A., Yatani, A., Varadi, G., and Schwartz, A. (1993). Molecular localization of ion selectivity sites within the pore of a human L-type cardiac calcium channel. *J Biol Chem* *268*, 13026-13029.

Yang, J., Ellinor, P.T., Sather, W.A., Zhang, J.F., and Tsien, R.W. (1993). Molecular determinants of Ca²⁺ selectivity and ion permeation in L-type Ca²⁺ channels. *Nature* *366*, 158-161.

Yau, K.W., and Baylor, D.A. (1989). Cyclic GMP-activated conductance of retinal photoreceptor cells. *Annu Rev Neurosci* *12*, 289-327.

Yellen, G., Jurman, M.E., Abramson, T., and Mackinnon, R. (1991). Mutations Affecting Internal Tea Blockade Identify the Probable Pore-Forming Region of a K⁺ Channel. *Science* *251*, 939-942.

Zagotta, W.N., Olivier, N.B., Black, K.D., Young, E.C., Olson, R., and Gouaux, E. (2003). Structural basis for modulation and agonist specificity of HCN pacemaker channels. *Nature* *425*, 200-205.

Zagotta, W.N., and Siegelbaum, S.A. (1996). Structure and function of cyclic nucleotide-gated channels. *Annu Rev Neurosci* *19*, 235-263.

Zheng, J., and Zagotta, W.N. (2004). Stoichiometry and assembly of olfactory cyclic nucleotide-gated channels. *Neuron* *42*, 411-421.

Zhong, H., Molday, L.L., Molday, R.S., and Yau, K.W. (2002). The heteromeric cyclic nucleotide-gated channel adopts a 3A:1B stoichiometry. *Nature* *420*, 193-198.

Zhou, Y., Morais-Cabral, J.H., Kaufman, A., and MacKinnon, R. (2001). Chemistry of ion coordination and hydration revealed by a K⁺ channel-Fab complex at 2.0 Å resolution. *Nature* *414*, 43-48.